UNIVERSIDADE DE LISBOA
FACULDADE DE CIÊNCIAS
DEPARTAMENTO DE GEOLOGIA

GENESIS OF THE BRECCIATED ROCKS FROM MID ATLANTIC RIDGE HYDROTHERMAL SYSTEMS: LUCKY STRIKE (37º20'N) AND MENEZ GWEN (37º50'N)

Isabel Maria Amaral Costa

Doutoramento em Geologia na especialidade de Metalogenia

2013

UNIVERSIDADE DE LISBOA
FACULDADE DE CIÊNCIAS
DEPARTAMENTO DE GEOLOGIA

GENESIS OF THE BRECCIATED ROCKS FROM MID ATLANTIC RIDGE HYDROTHERMAL SYSTEMS: LUCKY STRIKE (37º20'N) AND MENEZ GWEN (37º50'N)

Isabel Maria Amaral Costa

Tese orientada pelo Prof. Doutor Fernando José Arraiano de Sousa Barriga especialmente elaborada para a obtenção do grau de Doutor em Geologia na especialidade de Metalogenia

2013

To my parents and grandmother

After climbing a great hill, one only finds that there are many more hills to climb.

Nelson Mandela, sometime, somewhere in South Africa

Acknowledgements

The work presented here was only possible due to the collaboration of different people and institutions.

My first acknowledgement goes to Professor Fernando Barriga, my Ph. D supervisor. His guidance and support during the long period of this work were important to overcome the several difficulties that arose. His belief in the successful completion of this thesis and the logistic support were essential.

I also acknowledge the support of Doctor Yves Fouquet in giving me the chance to develop some of the thesis studies in “Institut Français de Recherche pour l'Exploitation de la MER” (IFREMER) and for his scientific guidance.

To “Fundação para a Ciência e a Tecnologia” (FCT) I am grateful for the financial support through a PhD scholarship (PRAXIS/BD/9408/96).

I am also indebted to the financial support of CREMINER LARSyS and to the logistic support of “Faculdade de Ciências da Universidade de Lisboa” (FCUL).

Part of the work performed in this thesis would not be possible without the collaboration of IFREMER, especially some of the laboratory analyses and the oceanographic cruises.

IFREMER is the working place of many collaborators in the present work. I start to send my gratitude to Marcel Bohn and Claire Bassoullet. I’m also grateful for the help provided by Hélène Ondreas, Daniel Bidou, Jean-Luc Charlou, Joël Knoery, Jean-Pierre Donval, Pierre Cambon, Henri Pelle and Ronan Apprioual in “Départment de Géosciences Marines”; and Daniel Desbruyères, Michel Segonzac, Alexis Khripounoff and Philippe Crassous (thanks for the work done with the Scanning Electron Microscope) in “Département Environnement Profond”.

I am enormously grateful to the crews of Nadir and Atalante oceanographic vessels, and Nautile submersible team. They all made possible my dives in the Atlantic Sea!

In the “Departamento de Geologia” of FCUL I am grateful to Jorge Relvas and António Mateus. To Miguel Miranda I thank the advices given.

The technical support in “Departamento de Geologia” of FCUL I owe to Sr. Alberto Verde, and the administrative support in the same department, I acknowledge to D. Cleta, D. Dulce and D. Maria.

All the friends I made in France are part of this work: Katell, Marco (my scuba-diving teacher and photographer!), Philippe (le voisin!), Anne-Marie (vrai copine du sejour Breton!), Emilie (la petite), Armelle, Marie-Claire, Laurent, Eric, Julliette, and many others.

Thanks to a special group of friends the support, in particular in the initial years of this work. I express my gratitude to Filipe, Pedro and Nuno for the initial incentive and help in this adventure.

To Ana Colaço thanks for your support during the stay in Brest.

Special thanks to Ágata and David for their incentive every time we were together. Thanks to Patrícia the technical help. Carlos, I thank his availability every time I needed. Thanks also to Teresa, Raquel, Ana Jesus, Álvaro and Filipa.

Isabel Costa I am grateful to your precious help and advices. Inês Cruz thanks for being my recent support

Martim forever friend, I know you are always there.

Big Mário, thanks for existing even if you are always physically distant.

I don't forget Ana, Tiago and Xoni (sorry!) that saw me (a few times) year after year with this work on my back!

To my colleagues and friends from ESTBarreiro I sincerely thank you. Especially to Professor João Vinagre and Otília, I thank you most sincerely the support and comprehension to my absence several times school activities. Joaquim, precious computer engineering, thanks for your constant help in the boring pieces of this work. Eugénia e Miguel, thanks for your lessons in ACAD. Thanks for the patience, Clara. António, thanks for the philosophical talks. Many thanks to Norberto and Anabela. Pedro and Rui, thanks for your humour!

I am very grateful to my students, particularly those that have always a new question, making me search and investigate the answer. They are the best stimulation a teacher can have!

The composers that with geniality know how to add and arrange music notes, and their performers, could never imagine how important they were to keep my mind clear and motivated!

To Carlota thanks for your loyalty and company. Jota is here sometimes warming your place and my heart. Ella, the most recent faithful company, stayed patiently near me literally all the time.

To my family, specially my parents and my grandma, I owe this work. I could never be able to acknowledge all that I owe to them. To my brother and sister in law, and specially to my nieces, Carolina and Maria, thanks for understanding my last times absence. Many thanks to the rest of my family that were always supporting me, even if I recognise that I've been very absent.

To José I don't know how to express my gratitude unless saying that he has the greatest qualities I recognize in the human being. I owe him the permanent and unconditional support in these years of common living. Thanks for your enormous patience.

Preamble

This is a long time work with many advances and setbacks since the beginning in 1997. It was hard to achieve this stage and it is far from what I wanted it to be, but I was not able to do better.

Many years have passed most of them working in subjects none related with science and I naturally withdrew myself from this target. Every time I returned it was a long journey.

During this long period of my life I have lost many. Moments with my family, with my friends, holidays, walks near the sea, gymnasium classes, music live concerts, etc.

Most of all I lost my grandma and my father.

Let me watch by the fire and remember my days
And it may be a trick of the firelight
But the flickering pages that trouble my sight
Is a book I'm afraid to write
It's the book of my days, it's the book of my life

Gordon Sumner (better known by the stage name Sting) – English musician, singer and songwriter

Abstract

The Lucky Strike and Menez Gwen hydrothermal fields are both located in the Mid-Atlantic Ridge (MAR), southwest of Azores islands, in two different ridge sections. These systems were discovered in the nineties, Lucky Strike in 1993 (Langmuir *et al.*, 1993a) and Menez Gwen in 1994 (Fouquet *et al.*, 1994).

In the first group of samples recovered it was found a type of rock distinct from the basalts and from the sulphide structures. This rock with heterogeneous appearance is a hydrothermal breccia forming consolidated plates around the sulphide deposits, and is essentially composed of basaltic fragments with a minor amount of chimneys fragments, cemented by hydrothermal precipitates where some types of amorphous silica are dominant.

The study of these discovered rocks seems to be important for a better understanding of the actual hydrothermal processes happening on the seafloor, but also for the knowledge of the formation of old sulphide deposits, some of them with economic importance like Aljustrel (in the Iberian Pyrite Belt – Portugal) or Kuroko (Hokuroko Province – Japan).

The microscopic detailed studies made in an initial phase of this thesis reveal three types of hydrothermal breccia based on the degree of alteration presented by the basalt fragments.

Several analytic methods were used to characterise in detail the breccias. Chemical elements like barium, sulphur and strontium generally considered as trace elements are present in percentage grades due to barite enrichment. Rare earth elements study reveal mixed patterns in what concern the fluid source: seawater and hydrothermal fluids. This is also confirmed by the strontium isotope ratios analysed in the altered basaltic fragments.

The hydrothermal breccias are genetically related with the circulation of low temperature hydrothermal fluids. If the system conditions are favourable to the consolidation of these rocks, they may play an important role in the protection of subseafloor hydrothermal deposits forming an impermeable cap due to the high content in siliceous material. This can explain some of the processes taking place in the early phase of formation of old sulphide deposits where equivalent siliceous material is found.

Key words: Hydrothermal breccias; Sulphide deposits; Hydrothermal fluids; Silicification.

Resumo

Os campos hidrotermais Lucky Strike e Menez Gwen estão ambos localizados na Crista Médio-Atlântica, a sudoeste das ilhas açorianas, em dois segmentos de crista adjacentes. Ambos descobertos na década de noventa, são objecto de estudos multidisciplinares desde então.

No conjunto das primeiras amostras recolhidas no Lucky Strike (primeiro local a ser descoberto) encontrava-se um tipo de rochas que se destacou pelo facto de não fazer parte do grupo dos basaltos (substrato rochoso típico na região) nem do grupo dos sulfuretos constituintes das estruturas hidrotermais lá existentes. Esta rocha com aspecto heterogéneo foi recolhida em redor das saídas hidrotermais, e a descrição petrográfica preliminar revelou uma brecha hidrotermal. A parte detrítica é constituída por fragmentos de natureza basáltica e, em menor quantidade, pedaços de chaminés inactivas e eventuais fósseis, enquanto o cimento é formado por precipitados hidrotermais resultantes da precipitação a partir de um fluido que circula difusamente por entre os fragmentos.

O estudo deste tipo de rocha então descoberta revelou-se importante não só para se compreender melhor os processos hidrotermais geradores dos inúmeros sistemas geológicos e biológicos existentes nos fundos oceânicos; mas também para o conhecimento da génese dos depósitos de sulfuretos antigos. A sua semelhança com exemplares provenientes de jazigos de sulfuretos antigos, como por exemplo Aljustrel (Faixa Piritosa Ibérica - Portugal) ou Kuroko (Província de Hokuroko - Japão), é bastante interessante.

Numa fase inicial procedeu-se à análise microscópica detalhada das amostras de modo a confirmar observações preliminares e com o objectivo de identificar caminhos analíticos a prosseguir. Foi possível, com base neste trabalho, identificar três tipos de brecha hidrotermal, com base na alteração dos seus componentes basálticos. Esta divisão não tem uma correspondência geográfica e é difícil de relacionar com a componente química dos mesmos exemplares.

Vários métodos de análise foram utilizados para caracterizar em pormenor o tipo de rocha: Espectrometria de emissão por plasma, Espectrometria de massa e Espectroscopia por fluorescência de raios-X. Estes revelaram a composição total da brecha tendo como elemento principal a sílica, geralmente enriquecida relativamente ao basalto (seu componente principal

na fracção detrítica). Elementos como o bário, o enxofre e o estrôncio, geralmente considerados elementos em traço, estão presentes, em várias amostras, em teores da ordem dos elementos maiores, devido à frequente presença de barite. Elementos de transição como o ferro, o cobre e o zinco são importantes quando a quantidade de sulfuretos, no cimento, é considerável. No caso dos elementos menores, destaca-se o estudo das Terras Raras que revelam padrões mistos relativos à origem dos fluidos a partir dos quais precipitaram os minerais hidrotermais: água do mar e fluido hidrotermal proveniente da crosta. Estes dados foram posteriormente confirmados por dados de isótopos de estrôncio que, apesar de não serem em número considerável, indicam precisamente razões isotópicas entre as da água do mar e dos fluidos hidrotermais.

O estudo pormenorizado da alteração dos componentes basálticos das brechas, a partir de dados de microssonda, permitiu identificar algumas argilas (esmectites e misturas esmectite-clorite) formadas durante o processo hidrotermal; permitiu igualmente verificar a variação composicional ao longo dos pedaços de basalto com grau de alteração intermédio, revelando variações em elementos com o silício e o alumínio. Algumas das argilas foram detectadas nos estudos de difracção de raios-X (saponite, nontronite e sauconite) que permitiram detectar igualmente a “cowlesite” e a “motukoreaite” em duas amostras distintas. A primeira é um zeólito que surge geralmente associado a basaltos oceânicos, e a segunda, mais rara, é um sulfato hidratado de alumínio e magnésio, que resulta da alteração de vidro basáltico por acção da água do mar a baixa temperatura.

A silicificação é o processo de alteração mais relevante para formação desta brecha hidrotermal. O aumento dos teores em sílica é reconhecido em vários dos procedimentos analíticos utilizados. As formas de sílica reconhecidas são maioritariamente amorfas (“sílica gel”), embora as formas cristalinas também estejam presentes – cristobalite e quartzo – mas em apenas duas amostras. A utilização do Microscópio Electrónico de Varrimento permitiu a identificação de um tipo de textura típica da “sílica gel” – microsferas em textura “favo-de-abelha”, resultante de deposição a partir de fluidos de baixa temperatura.

As brechas hidrotermais têm a sua génese directamente relacionada com a circulação de fluidos hidrotermais de baixa temperatura, sendo constituídas maioritariamente por sílica. Deste modo, se as condições do meio favorecerem a sua consolidação, poderão funcionar como protectoras dos eventuais depósitos hidrotermais existentes na subsuperfície, devido ao carácter impermeável do material silicioso. Esta constatação permite explicar alguns dos

processos vigentes na fase inicial de formação de alguns dos jazigos de sulfuretos antigos que têm associadas rochas que se podem considerar os equivalentes deste tipo de material silicioso.

TABLE OF CONTENTS

1. INTRODUCTION

Active hydrothermal fields are intensively studied since the first discovery of black smoker chimneys growing on the seafloor. All the means were mobilised, man submersible technology, sophisticated instruments that allow the observation and collection of all kinds of data from the bottom of the ocean and the funding of oceanographic institutions that were able to explore more areas of the seafloor, enabled an effort on research in this area.

Today more than five hundred hydrothermal sites are recognized on the ocean floor, on various geological settings, each with specific characteristics (Beaulieu *et al.*, 2012). These data was recently published in a complete hydrothermal vents database from the InterRidge organization and includes confirmed active (direct observations on seafloor), inferred active (water column measurements) and inactive sites grouped in a list of vent locations (see figure 1.1 for illustration).

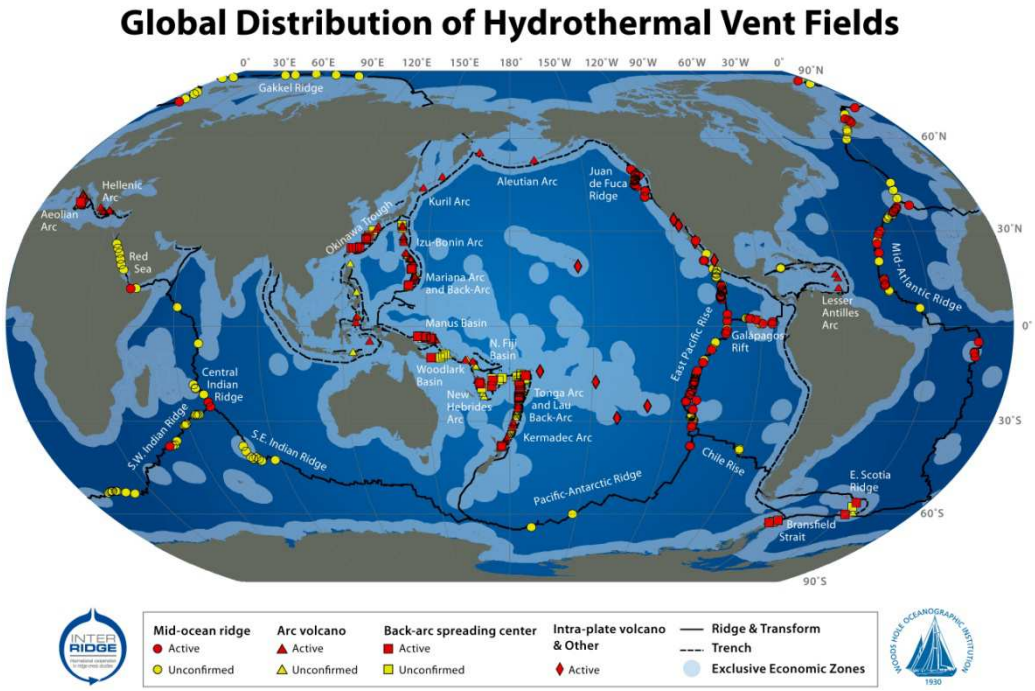

Figure 1.1 – Location of known hydrothermal activity along the global ocean (map from Beaulieu *et al.*, 2010).

These discoveries sustain that hydrothermal activity is a major process associated with the formation of ocean crust. As knowledge about these systems grows, greater is the conviction that there is much more to discover, and that the chemical composition of the oceans might be strongly influenced by hydrothermal systems.

1.1. FROM ANCIENT TO MODERN HYDROTHERMAL SYSTEMS

Seafloor mineralization is the result of hydrothermal activity at mid-ocean ridges and the existence of processes, currently active, leading to the formation of metal deposits give the opportunity to observe and study the step by step formation in real time of a volcanogenic massive sulphide (VMS) deposit. Detailed studies of mineralogy and chemistry of these old mineralised bodies indicate that the physical and chemical processes of seafloor mineralization in the early oceans were essentially the same as those observed on the modern mid-ocean ridges (Hannigton *et al.,* 1995). Some of the actual sites are large enough to be considered ore deposits and, if they were located on land, they would certainly be mined. The knowledge of the geochemical and geophysical processes associated with modern hydrothermal systems is essential to understand the formation of ancient deposits, some of them with economic significance.

Volcanogenic sulphide deposits are studied since the beginning of 20th century and may be described as mineralised bodies of massive pyritic sulphides containing various amounts of metals such as zinc, copper and lead, and generally important concentrations of silver and gold. They have strata bound and lenticular shapes and occur associated with volcanic rocks suggesting a volcanogenic origin. Studies indicate that they are formed subaqueously by episodes of fumarolic activity during periods of submarine volcanism (Horikoshi, 1969 and Schermerhorn, 1970 *in* Hutchinson, 1973). Lenses of sulphides are usually overlain by thin sedimentary strata rich in silica, iron and manganese, and underlain by altered sulphide-impregnated lavas. Near the aforementioned top zone it is common to observe breccia textures, apparently related to volcanic activity. This brecciation in the ancient deposits is very important in this work as one may be analysing the recent analogues of those breccias.

A large number of these massive sulphide bodies are considered ore deposits and exploited for base and/or precious metals. They have been recognised around the world and their distinct varieties can be separated by their compositions, ages (ranging from Archean to Tertiary) and rock association. This last feature is intimately related with the type of geotectonic setting in which the deposit was formed. Although host rocks are always volcanic their composition varies from felsic to mafic depending on the tectonic environment they are in. As it happens with modern deposits, ancient ones are found in various geotectonic environments.

Nowadays hydrothermal systems are known as the result of important interaction processes between oceanic crust and seawater such as cooling and chemical alteration. Cooling occurs in part by upward heat conduction through the lithosphere, but it also takes place due to convective circulation of cold seawater through the rock (Stein *et al.*, 1995) which in turn causes hydrothermal alteration. The flow of seawater through the crust comprises recharge – where seawater enters the crust, get warm and reacts with the rocks in its path downwards – and discharge zones – where hydrothermal fluids exits (Alt, 1995). This rapid upward flow will reach the seafloor on diffuse or focused vents as hydrothermal fluid which differs significantly in composition from seawater: it is hotter, less dense, generally acid, metal and silicon (Si) rich, magnesium (Mg) and sulphate poor (Von Damm, 1995; German & Von Damm, 2003; Tivey, 2007). Yet these chemical characteristics of the end-member fluid may vary from site to site depending on: the initial fluid composition; the composition and structure (presence of fractures and fissures) of the rock that reacts with the fluid; the depth, size and shape of the heat source (Tivey, 2007) which drives the fluid. These factors affect the temperature and pressure at which water-rock reactions take place, consequently the fluid may experience phase separation. This process occurs when a homogenous fluid is transformed into two phases with different properties in parameters such as density and chemical composition – a vapor phase depleted in chloride as well as enriched in volatile components, and a brine phase more dense and enriched in chloride – when temperature and pressure exceeds the values of the two phase curve proposed by Bischoff and Rosenbauer (1984).

1.2. HYDROTHERMAL ACTIVITY ON THE MID-ATLANTIC RIDGE

The first sulphide mineralization on the seafloor was discovered in a fast spreading ridge, the East Pacific Rise (EPR) (Corliss *et al.*, 1979; Spiess *et al.*, 1980), but there are also very important deposits in slow spreading ridges, most of them in the Mid-Atlantic Ridge (MAR). Initially, in the seventies, the reports refer to low temperature deposits like in TAG (26ºN) (Rona *et al.*, 1976; Scott *et al.*, 1974), in Fracture Zone "A" – Famous area (Arcyana, 1975; Ballard *et al.*, 1975; Hoffert *et al.*, 1980); and stockwork mineralizations, like in Romanche Fracture Zone (Bonatti *et al.*, 1976a; Bonatti *et al.*, 1976b). In the following decade, two

important sites were discovered with high temperature hydrothermal activity, TAG (26ºN), with active black smokers and massive sulphides (Rona *et al.*, 1986), and Snakepit (23ºN), the only known important sites on the slow spreading MAR, in 1988 (Thompson *et al.*, 1988). Since 1991 the MAR in the Azores area has been extensively surveyed: some cruises were made under the French-American FARA program and the European MAST-MARFLUX project. In 1992 during a FAZAR survey cruise (C. Langmuir and G. Klinkhamer, Chief scientists), a dredge recovered sulphides from the seafloor near the 37º20'N latitude, and chemical anomalies of manganese (Mn) and methane (CH_4) were detected in the water column (Charlou *et al.*, 1993) – a new site was discovered (Fazar Scientific team, 1992; Fazar, 1993). This site was named "Lucky Strike" as it was found totally by chance (Fig. 1.2). A year later six dives were carried out with the Woods Hole Oceanographic Institute submersible, ALVIN (ALVIN 93 mission), on this site where it was possible to recover rock, fluid and biological samples (Langmuir *et al.*, 1993a; Langmuir *et al.*, 1993b; Colodner *et al.*, 1993; Humphris *et al.*, 1993). In May 1994 during DIVA 1 cruise very important exploratory work was made in Lucky Strike (Fouquet *et al.*, 1994a). Geologists were able to draw a geologic map not only of the site but also of the surrounding area, based on the data recovered in 12 exploratory dives. The hydrothermal products cover a surface of about 1 km^2 indicating that an important sulphide deposit may exist in the sub-seafloor. One of the cruise objectives was to explore two other segments in the northern part of Lucky Strike segment, and as a result of this a new active site was discovered – Menez Gwen (37º50'N) (Fig. 1.2). Sampling of rocks, hydrothermal fluid and bottom water was carried out in both sites using the submersible NAUTILE, from IFREMER. Detailed petrographic and geochemical studies were made in all types of rock samples collected (Costa, 1995 and Costa *et al.*, 1997).

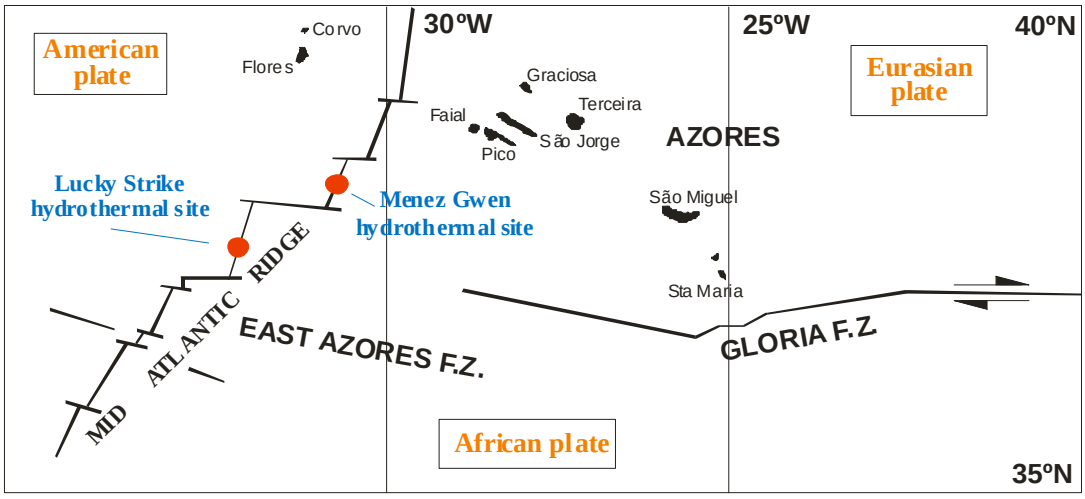

Figure 1.2 – Location of Lucky Strike and Menez Gwen in Mid-Atlantic Ridge near the Azores islands.

1.3. PREVIOUS WORK ON SEAFLOOR HYDROTHERMAL BRECCIAS

Hydrothermal breccias associated to modern mineralized systems are not so frequent, or at least are not reported. Besides this fact there are two sites in the Pacific Ocean floor where this type of rocks were sampled and studied.

The first indication of a hydrothermal deposit consisting of silica and barite with volcanic fragments was reported on the Lau basin back-arc system (northeast of Australia) by Bertine and Keene (1975). The samples collected in Peggy Ridge are described as unusual submarine rocks consisting of barite, opal, and volcanic detritus. Actually they are breccias of hyaloclastites (vitreous tholeiitic basalts) and fragments of some minerals (palagonite, plagioclase, some augite and authigenic clay minerals and barite) cemented by opal. Both the opal and barite show evidence of having been deposited under higher temperatures than that of seawater, which suggest that they were precipitated from hydrothermal solutions.

Another hydrothermal field where this type of rock is described and documented (Zierenberg *et al.*, 1995) is at the off-axis Sea Cliff site in Gorda Ridge. Here the crusts are formed by extensive alteration of basaltic hyaloclastite with initial formation of Mg-rich smectite and in a later stage deposition of amorphous silica. Temperatures of alteration range from near 100ºC to 220ºC. Some of the basaltic fragments have their original texture preserved but mostly replaced by alteration products.

Both of the occurrences described above are in different geological settings when compared with the MAR, however the Sea Cliff rocks presents several similarities with the rocks studied here, specially the types of alteration products and the preservation of original textures in some of the basaltic clasts.

1.4. PURPOSES OF THIS WORK

A specific type of rock was first collected from Lucky Strike and Menez Gwen hydrothermal sites, during the already mentioned two cruises (ALVIN 93 and DIVA 1). It

seems to cover a broad area around the hydrothermal vents where diffuse venting dominates. It is a kind of hydrothermal breccia that appears on the seafloor with a plate or slab morphology. At is first detailed on board description, during DIVA 1 cruise, a crew scientist, Meg Tivey, termed it as “slab”. Since then the use of this non scientific designation, even in several scientific publications, is frequent. We also adopted this appropriate word in this work.

The *slab* is a very heterogeneous rock, with predominant volcanic fragments cemented by hydrothermal precipitates, including sulphides, amorphous silica and barite. These interstitial precipitates are responsible for the breccia consolidation decreasing its permeability. These conditions favour the precipitation of sulphides in the sub-surface forming a potential VMS deposit. The study of this rock and the modern sites where they were found, especially Lucky Strike, can bring us important information about the genesis of some similar ancient sulphide deposits.

In July 1997 another oceanographic cruise – FLORES – took place in the Atlantic near the Azorean region. The propose was to locate a possible active hydrothermal field hosted in ultramafic rocks, in AMAR segment, and return to the Lucky Strike and Menez Gwen sites to study the evolution of the hydrothermal processes observed some years before (Fouquet *et al.*, 1997). A group of *slab* samples was collected and is studied in this work. Two subsequent missions were carried out in the summer of 1998: PICO for biological studies in the Lucky Strike and Menez Gwen areas, including recovery of some monitoring material deployed in previous cruises (Desbruyeres et équipe scientifique PICO, 1998); and SALDANHA for geological exploration of the FAMOUS segment and recover of some material in Menez Gwen (Barriga *et al.*, 1998).

The aim of this work is to study in detail the composition and the genesis of the *slab* rocks, and extrapolate this information to the ancient massive sulphide deposits and their associated hydrothermal sediments, which are very similar to modern *slab*, trying to compare ancient and modern processes.

Chapter 1 is a general introduction to this study.

Chapter 2 describes the geological setting of the two sites in the Mid-Atlantic Ridge.

Chapter 3 is a detailed description of the geology of both hydrothermal sites with the geological maps.

Chapter 4 describes the sampling and analytical methods.

Chapter 5 characterizes the mineralogy and geochemistry of the basaltic rocks in the region as basaltic fragments are dominant in the detrital fraction of the *slab*.

Chapter 6 is dedicated to the characterization of the hydrothermal breccias with detail petrography, mineralogy and geochemical analyses (whole rock and rare earth elements geochemistry).

Chapter 7 describes the hydrothermal alteration of the basaltic fragments using mass-balance methods, strontium isotopes data and scanning electron microscope data to illustrate an important silicification process.

Chapter 8 presents the discussion and conclusions for the model of formation of the hydrothermal breccias and provides an association with ancient hydrothermal deposits in what seems to be old hydrothermal breccias found in a similar position around the vents.

2. GEOTECTONIC SETTING

2.1. MID-ATLANTIC RIDGE AND THE AZORES PLATFORM

The hydrothermal sites studied here are located in the Azorean volcanic Platform, which is a topographic anomaly well defined in the MAR above the 2000m isobath, situated at the boundary of African, Eurasian and American plates - the usually called "Azores Triple Junction" (ATJ). The platform is defined between 40ºN and 37º30'N in the MAR axis, and is asymmetric in relation to this mid-ocean ridge, with a favoured development to the east (Fig. 2.1). Gravity and basalt geochemistry anomalies concur with the referred bathymetric anomaly. Here the oceanic crust presents a thickening of 60% in relation to a normal crust (Searle, 1976) and the basalts are enriched in relation to the normal mid-ocean basalts. They have a remarkable enrichment in barium, which is responsible for the abundance of barite on both hydrothermal fields.

The MAR in this region exhibits some specific characteristics both because of the tectonic plate triple junction (ATJ) and of the presence of the Azores hotspot. Each of the three ridge sections shows contrasting tectonic and volcanic characteristics, resulting from their different geometries and relationship to the spreading direction.

The presence of the hotspot may modify the thermal structure of the lithosphere in a way that the morphology of the MAR resembles that of a fast-spreading ridge, exhibiting axial highs instead of the typical well developed median valley, although a minor valley (200m depth) still persists.

According to Luís et al. (1994), during the last 10 Ma, the Azores behaved initially as an independent block in relation to the neighboring plates, and the triple junction moved northwards. After that, some 2.45 Ma ago, the Azorean platform moved together with the Eurasian plate to the present position in the vicinity of the north Azores Fracture Zone (Fig. 2). This process occurred after an important episode of enhanced magmatism that took place in upper Miocene times (Cannat et al., 1999), due to a melting anomaly originated in the hotspot, and played a significant role in the enlargement of the Azorean platform.

Luís et al. (1994) calculated a present full spreading rate of the ridge in this portion of the MAR of 2,4 cm/year along an azimuth of 100º. The rate value suffered some variation related with the above-mentioned lost of independent motion of the Azores platform.

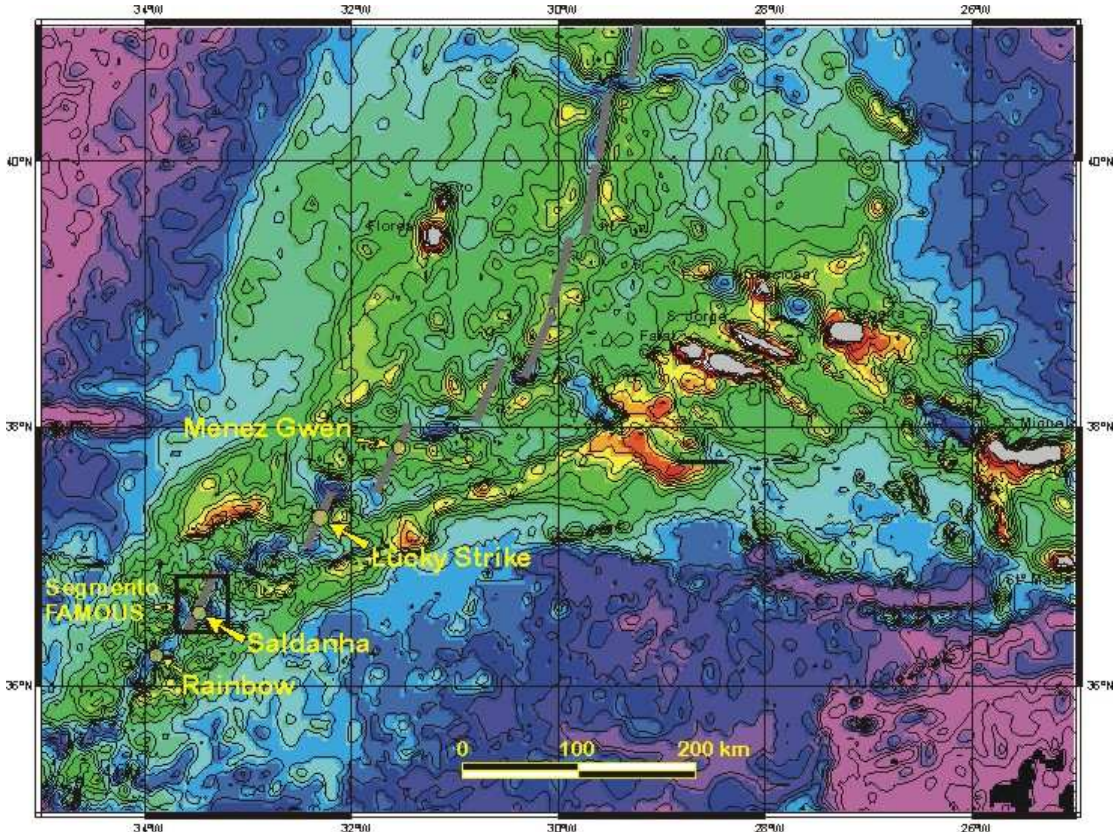

Figure 2.1 – Azorean Plateau and the related location of the ridge segments in this part of the Mid Atlantic Ridge.

For the present work the south-western arm of the triple junction is of particular interest because it is where Lucky Strike and Menez Gwen hydrothermal fields are located. The MAR here is segmented by three important discontinuities – Kurchatov Fracture Zone (40ºN), Pico offset (38ºN) and Oceanographer Fracture Zone (35º30'N) – that constrains two ridge sections: Kurchatov to Pico (KP) and Pico to Oceanographer (PO). Each section comprises a succession of second-order ridge segments linked by a series of left-lateral non-transform offsets (Parson, et al., 2000) (Figure 2.1).

2.2. THE LUCKY STRIKE SEGMENT

The Lucky Strike segment is one of the second-order segments of the PO section, located between latitudes 37ºN and 37º35'N. It has a well developed rift valley, with rectilinear and

sub parallel axial valley walls, characterized by large fault scarps (Parson, *et al.*, 2000) – a typical morphology of a slow spreading ridge.

This segment is the deepest (1700 m) of the two segments described in this work. It has a 60 km long and 15 km wide rift valley (1570 m to 3650 m water depth). This structure is divided in two parts by a North-South depression (Figure 2.2). West side of the graben there is an elongated ridge formed by volcanic centres, oblique to the main direction of the MAR. The eastern flank of this ridge is cut by a normal fault system installed after the formation of the volcanic relieves. The central part of the rift is occupied by a 1268 km central volcano whose summit consists of three, predominantly scoriaceous breccia cones surrounding a restricted area of layered volcaniclastic deposits localized near the centre of a 1 km wide and 100 m deep caldera. The three volcanic cones are at water depths ranging from 1600 to 1749m (Ondréas *et al.*, 1997). In the depression surrounded by these three volcanoes there is a lava lake (Fouquet *et al.*, 1995a). The hydrothermal vents that form the Lucky Strike field are located around this lava lake. This volcanic structure and some local faults spatially control the distribution of the vents.

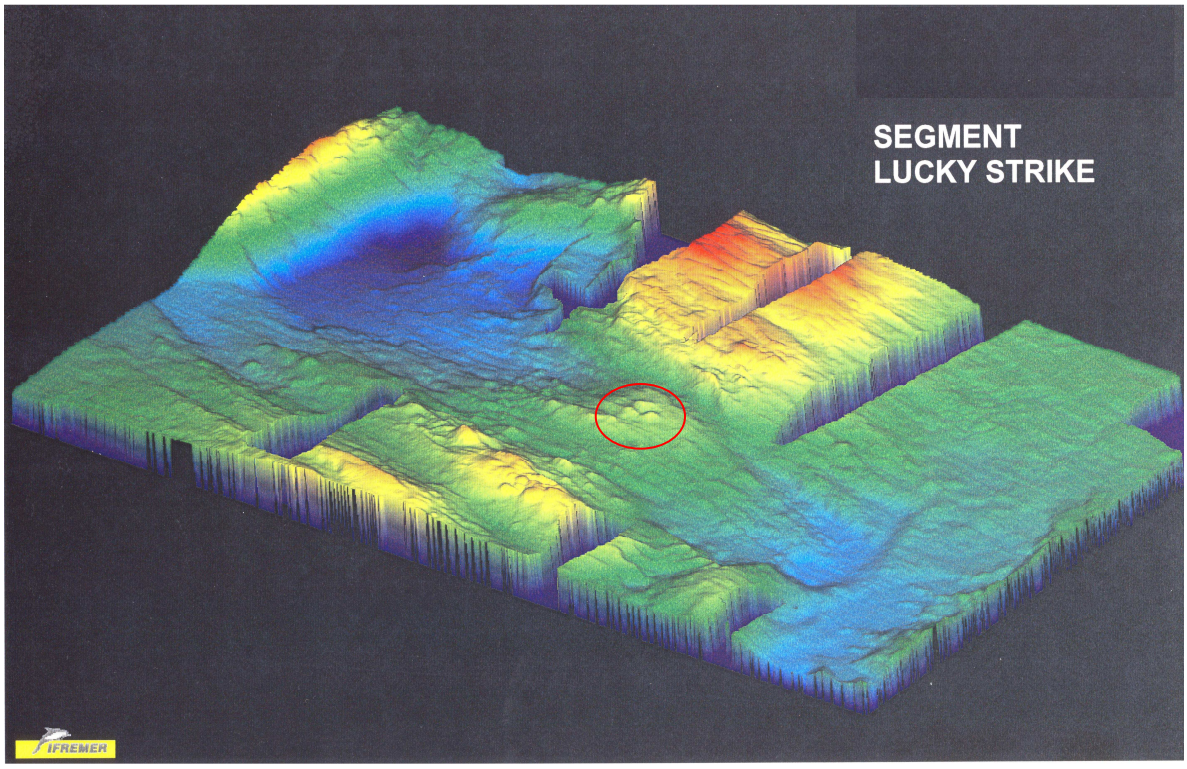

Figure 2.2 – Schematic overview of Lucky Strike segment. Encircled in red are the three volcanic cones surrounding the lava lake central depression.

Based on the interpretation of side-scan sonar images it is possible to say that the segment extremities are sedimented, but the central part is generally poorly sedimented showing high reflectivity corresponding to fresh basaltic rocks (Ondréas *et al.*, 1997). Closely spaced faults or fissures, forming a fabric, can be observed almost everywhere in the surface of the rift valley (Parson, *et al.*, 2000).

2.3. THE MENEZ GWEN SEGMENT

The Menez Gwen site is located on the volcanic segment immediately north of the Lucky Strike segment, between the latitudes 37º35'N and 38º00'N. It is the southern most second-order segment of the KP section. It has a particular morphology for a slow spreading ridge: absence of a central rift valley (Fouquet *et al.*, 1994b).

The main volcanic system is a central volcano with circular shape, with depths ranging from nearly 700 m to 1050 m and a diameter of 17km, which is cut on the top by an axial graben 6 km long, 2 km wide and nearly 300 m deep. A new small volcano – 600m wide and 120m high - is growing on the northern end of this graben and the hydrothermal site is in the west flank of this volcano, near the top at a water depth of 800m (Figure 2.3). The graben bottom is composed of relatively fresh to very fresh lava. In the deepest part there is a lava lake 1400m long and 400m wide (Fouquet *et al.*, 1998a).

The central part of the segment, in the axial valley floor, is characterised by fissured lava flows. Sonar data from the central volcanic edifice show an irregular reflectivity pattern, not typical of ridge areas (Parson, *et al.*, 2000). Submersible observations (Fouquet *et al.*, 1995 and Ondréas *et al.*, 1997) confirm that the exposed flanks of the volcanic system are composed of a series of bedded pyroclastics, presumably deposited as a result of the shallow water depth during eruption. The same observations helped in evaluating the segment evolution: firstly, there was the emplacement of massive lava flows (bottom of the valley), secondly the emplacement of volcanic ejecta (flanks of the volcanic system), followed by opening of the axial graben, and finally the latest eruption episode with pillow lava, lobate lava and the lava lake. Here, a cycle between explosive and effusive volcanic activity is identifiable (Ondréas *et al.*, 1997).

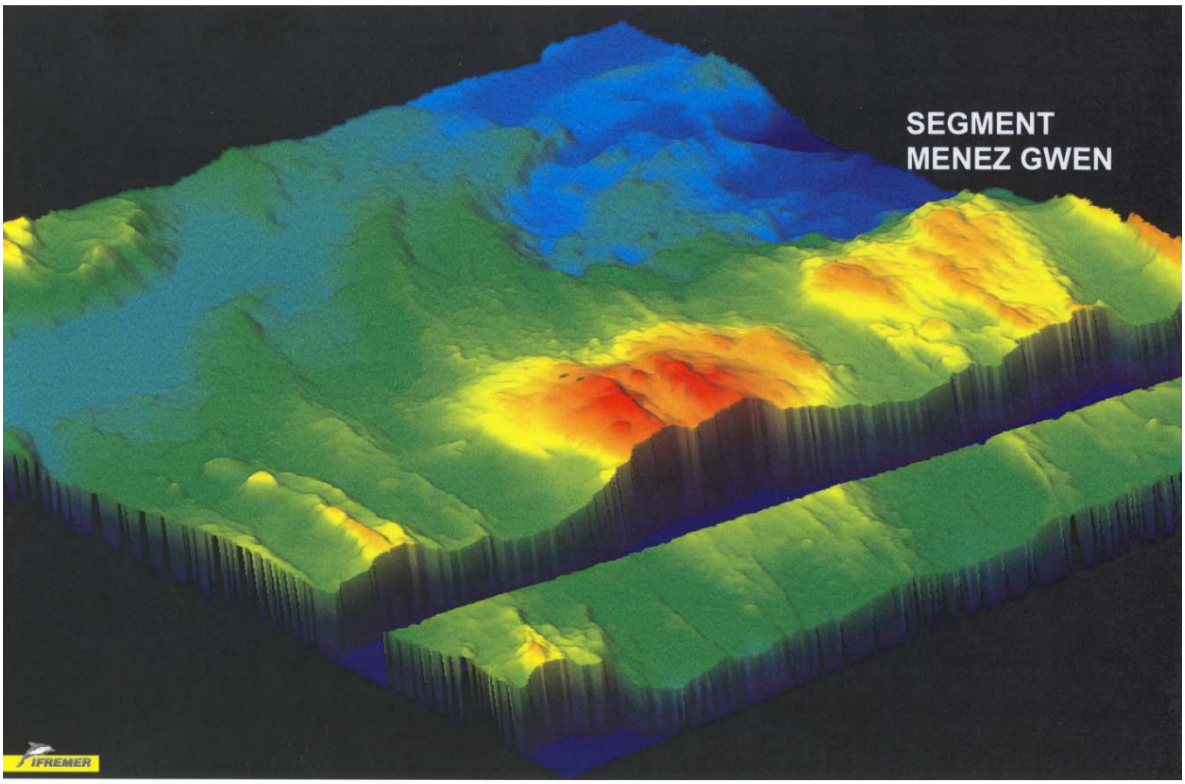

Figure 2.3 – Schematic overview of Menez Gwen segment.

3. GEOLOGY OF THE HYDROTHERMAL FIELDS

3.1. GEOLOGICAL MAPPING

Lucky Strike and Menez Gwen are two active hydrothermal sites intensively explored since their discovery. Direct observations of both systems led to their geologic description with the construction of a geologic map for each hydrothermal site (geologic maps in pages ahead). The scale for both maps is approximately 1:10 000.

Based on data from several cruises on both sites and using the cartographic information from many dives it was possible to reconstruct reliably the geology of these sites. Most of the geologic data came from DIVA1 (Équipe scientifique DIVA 1, 1994) and FLORES (Équipe scientifique FLORES, 1997) missions, with some complementary information from DIVA2 (Desbruyeres *et al.*, 1998). The submersible bottom tracks collectively cover most of the hydrothermal field areas. The zones with no direct cartographic information were filled by the interpretation of other data, including sonar maps (Fouquet *et al.*, 1995b).

The most important hydrothermal active vents were named during the dive after their discovery or after the dive by the scientific team. The names of the vents followed several criteria: name of the diving scientist, chimney form, etc. Each of these vent names is referred to in both geologic maps.

3.2. LUCKY STRIKE

The Lucky Strike hydrothermal field is the more important of the two sites studied in this work. The hydrothermal vents (active or inactive) are distributed around the lava lake in the depression formed between the three volcanic tops. The site is at latitudes ranging from 37º17’15’’N to 37º17’45’’N, and longitudes from 32º16’15’’W to 32º17’15’’W – an extension of nearly 1 km^2.

The three volcanic elevations are mainly composed of non-consolidated highly vesicular volcanic breccia – Volcanic Breccia Formation. Fragments of pillow lavas, lava tubes, scoriaceous lava and other lavic structures can be observed in several sizes. The volcanic breccia appears to have been produced *in situ* by autobrecciation, but there is also a thermoclastic component that results from the rapid cooling of the lava in contact with the

cold seawater – cooling-contraction fragmentation. Another cause, less important, is the tectonic movements associated with the active spreading ridge.

Pillow lavas are abundant in some areas, with their characteristic morphology (Figure 3.1a), very fresh and without any cover of pelagic sediment – forming the Pillow Lava Formation.

Some massive lava flows were observed during the dives, but they are not shown due to the used cartographic scale. They are very well exposed especially in fault scarps or fissures, where in some parts it is possible to observe the typical columnar joints formed during cooling (Figure 3.1b).

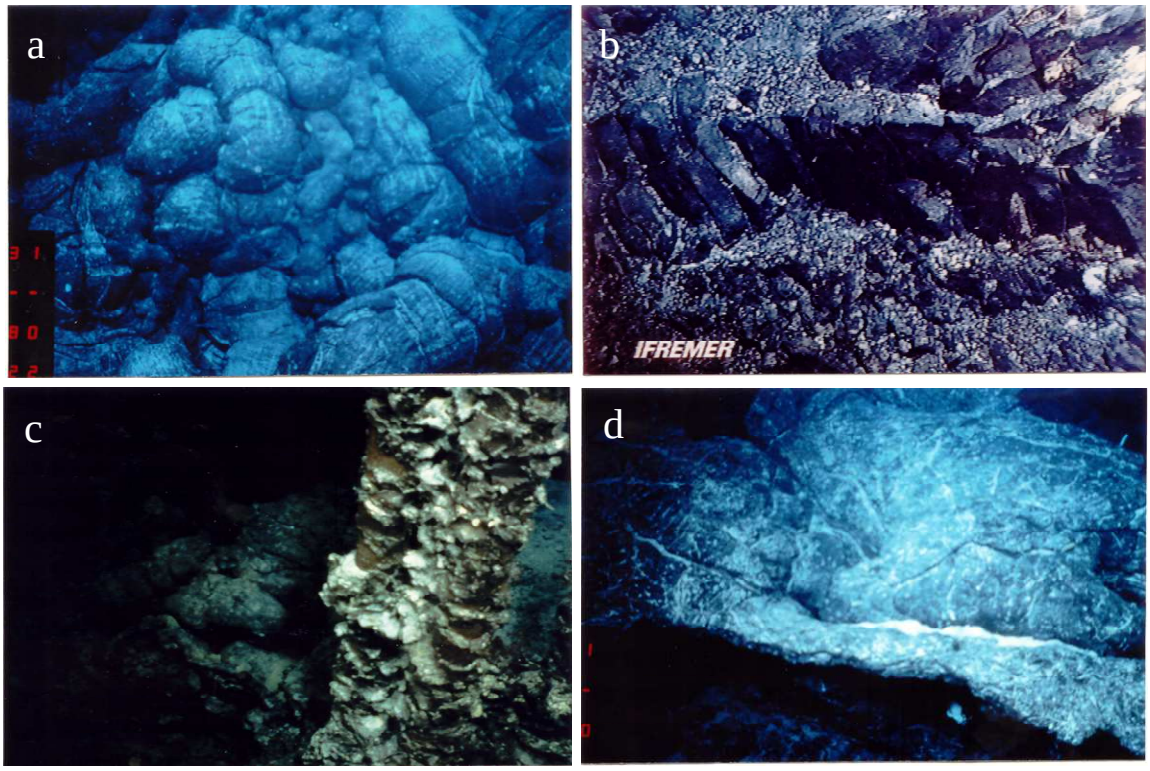

Figure 3.1 – Several volcanic geologic features in the seafloor near hydrothermal active sites. (**a**) Pillow lava and lava tubes; (**b**) Columnar joints in massive lava flows; (**c**) Lava lake pillar; (**d**) Fresh lobated in the lava lake roof. (Photos from IFREMER)

The Lava Lake is a very interesting structure formed by several types of very fresh lava – we name it the Lava Lake formation. It was the first discovery in a slow spreading ridge, although it was already known in East Pacific Rise (Francheteau *et al.*, 1979). It has a circular shape with a 300m diameter and up to 6m in depth. During the investigations made by the

exploratory dives it was possible to establish that the lava lake in Lucky Strike is made of very fresh basaltic glass, with low vesicularity, forming different lava structures: draped and scoriaceous lavas, pillars of lava connected to each other by centimetric lavic layers (Figure 3.1c), and the top layer is made of lobate lavas (Figure 3.1d).

The formation process of this kind of volcanic structure is not yet clear. Francheteau *et al.* (1979) refers a hypothesis that has some incompatibilities with the observations carried at Lucky Strike. An alternative explanation is proposed in Costa (1995) but has also some inconsistencies, albeit different from the former.

The massive sulphides, also mapped, are concentrated northwest and east of the central lava lake, zones where the active sites are also predominant. Mostly they correspond to broken inactive chimneys (Figure 3.2b) formed during previous hydrothermal episodes. In certain places it is still possible to observe conserved relics of old chimneys structures, but in other places other fragments may be a part of some massive sulphide deposits, exposed on the seafloor and fragmented due to tectonic movements. All the collected samples exhibit an extremely advanced alteration state explained by the ceasing of the hydrothermal activity, allowing the rapid oxidation of the sulphides by the contact with cold seawater.

Hydrothermal *"slab"* is the term used to refer the hydrothermal plates found and most sampled near the sulphide deposits. This rock is the object of study in this work and is part of what we called the Hydrothermal Breccia Formation. It outcrops in the central area surrounding the lava lake as flat sometimes layered deposits, and is intimately related with the hydrothermal vents (active or inactive). Chimneys and spires resulting from direct high temperature discharge are growing through this breccia formation and it is common to observe a diffuse low temperature flow coming through the cracks and fissures. Some volcaniclastic deposits (that we can call non consolidated breccia) are also included in the Hydrothermal Breccia formation.

Active vents surround the lava lake, as it was already mentioned, with the most active venting on the western side. The hydrothermal discharge occurs both focalised, with high temperature active black smokers (up to 324ºC) (Figure 3.2c), and diffuse, with low temperature flow depositing amorphous silica that becomes part of the *slab*. Among the active structures there are some spires that can reach 20m high.

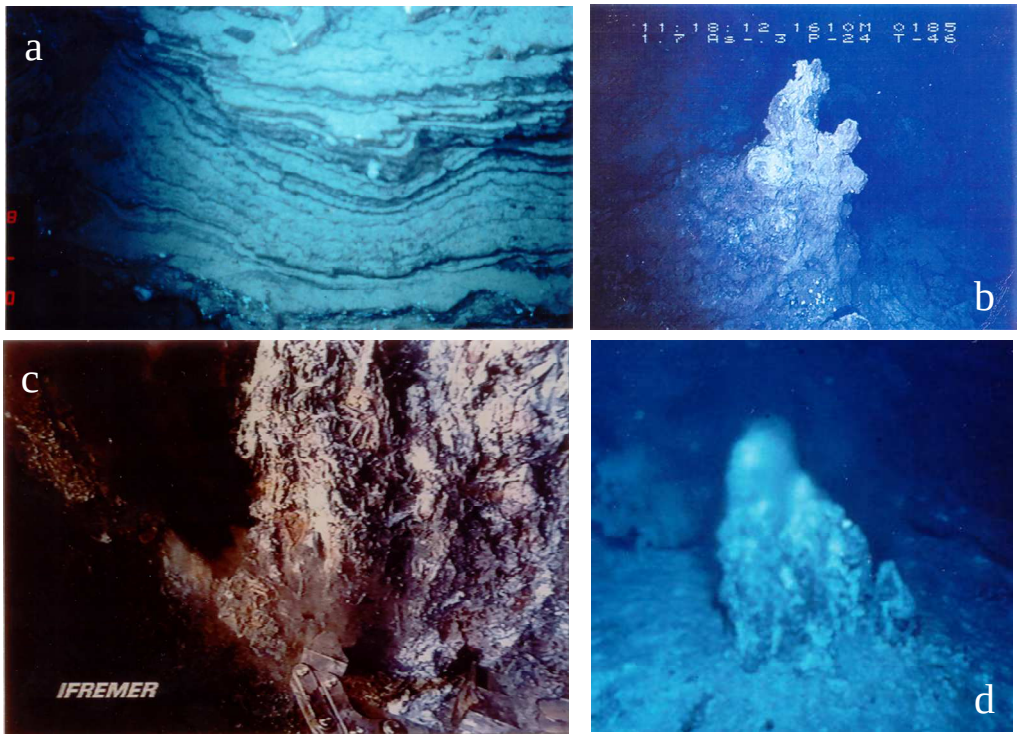

Figure 3.2 – Bottom photos from IFREMER: (**a**) Aspects of Volcaniclastic Deposits Formation; (**b**) Ancient chimney: (**c**) Black-smoker; (**d**) White smoker chimney (Menez Gwen).

Pelagic sediment occurs rarely in the active sites region, as a very thin deposit. It has some importance only in the depression that corresponds to the central graben.

The most important tectonic structures observed in the area are normal faults oriented parallel to the MAR, where one can observe several features, as vertical striations on the fault plane or fault breccias, indicating the tensional character of the tectonic regime. Fissures are also detected reaching some tens of meters in depth. In some cases, these tectonic structures control the location of some vents and a good example of this is the chimney alignment on the east side of the depression. Anyway, the entire Lucky Strike region is extremely fractured, with high permeability favouring fluid venting.

3.3. MENEZ GWEN

The Menez Gwen site was discovered after Lucky Strike during the DIVA1 mission (Équipe scientifique DIVA 1, 1994) and is located at latitudes ranging from 37º50'12''N to 37º50'36''N, and longitudes from 31º31'00''W to 31º31'36''W.

"Menez Gwen" is a name from Brittany that means "White Hill", fitting perfectly with its appearance: a little mountain covered with snow, composed mostly by anhydrite with important amounts of barite (Figure 3.2d).

For the discovery of Menez Gwen it was very important the use of a new strategy of exploration where both CH_4 and H_2S concentrations were measured in the seawater samples collected near the bottom (Fouquet *et al.*, 1994b). High concentrations of these compounds were found in the fluids collected during the dives before the discovery of the site.

This hydrothermal field seems to be a young site, with only one hydrothermal episode in the beginning of its activity. Two facts support this hypothesis: there was no detected anomaly in the fluid composition, between 200 and 300m above the seafloor, in a cruise held two years before the site discovery;

Volcanic breccia and pillow lavas are the dominant rocks in the Menez Gwen hydrothermal field, forming two units similar to those of Lucky Strike, named respectively, Volcanic Breccia Formation and Pillow Lava Formation. There is also a bedded unit of volcanic sediments, composed mainly of piroclasts, found in the east and west sides of the graben – Volcaniclastic Deposits Formation (Figure 3.2a). The axial valley is filled with massive flows, corresponding to an effusive volcanic episode, where we can observe prismatic joints – Massive Lava Formation, and it is also recognizable a 1400 m long, 400 m wide and up to 8 m deep lava lake at its deepest point (1045 m) (Fouquet et al., 1995b).

Pelagic sediment is present as in the Lucky Strike segment and there is also a lava lake with the same morphologic characteristics but slightly larger. This lava lake is situated in the central graben in the south part of the segment (not shown in the map presented in page 21)

Small anhydrite chimneys (Figure 3.2d), venting white smoke, controlled by an important N-S fault compose the active site. The maximum temperature measured was 281ºC (Équipe scientifique DIVA 1, 1994). Sulphides are very rare in the chimney structures but frequent in *slab* rocks.

Some authors (Haymon, 1983 & Lyndon, 1988) defend that anhydrite form in the initial stage of the hydrothermal field construction. Here in Menez Gwen, a very young system, it was possible to observe the formation of anhydrite chimneys "*in situ*". In Lucky Strike hydrothermal field, much more evolved than this one, anhydrite is a minor mineral indicating its dissolution or replacement by sulphides.

4. SAMPLING AND METHODS

"Perfection is lots of little things done well"

Marco Pierre White – English kitchen chef

4.1. SAMPLING

The samples studied were mostly collected using deep-diving manned submersibles. These vehicles are compact and depend on research vessels for maintenance and preparation for dives, as well as for transport of the submersible, associated equipment and operators to the site to be investigated. Sampling with submersibles in deep ocean environments has some important constrains related with the dive time, the accessibility of the submarine to the outcrop and the restricted visibility from the device. However, for the samples needed in this study, the use of these vehicles had many advantages, because the area of the hydrothermal fields is reduced compared with the ocean floor, making possible a representative sampling knowing exactly where the sample come from.

ALVIN operated by the American Woods Hole Oceanographic Institution, and NAUTILE owned by IFREMER, were the submersibles used to collect the samples. Each submersible track was prepared before and during the expeditions based in bathymetric maps (structure and morphology) and in sonar images (differences in acoustic facies).

Dredging was the other sampling method used to acquire some of the rock specimens. This is a much less expensive process, generally with limitations regarding the precise location of the sample, currently used with much success in collecting mid-ocean ridge basalts (MORB), as their chemical composition varies only in a regional scale. In the MOMAR area (Rainbow site) there have been operations combining dredging and submersible operations, with great success (Seahma cruise, 2002).

A set of 90 samples – 58 from Lucky Strike and 32 from Menez Gwen - was collected and used in this work. Some of the samples were studied in a previous work (Costa, 1995). All the samples are plotted in the geologic maps of both hydrothermal fields, and listed in Appendix 2, where other information (references, type of sample, location, analytical processes) related to each one is also mentioned. These samples were collected during six oceanographic missions, ALVIN 93, DIVA 1, DIVA 2, FLORES, PICO and SALDANHA, already cited in the text.

Upon arrival on board, samples are dried, described macroscopically under the binocular microscope, some sliced, and photographed to keep a record of all the collected material. On land, photos and slides are repeated in better conditions, before any analytical procedure.

To better understand the formation of the *slab* rocks, other type of samples were also described and studied in this work – the basalts. Basalts are the main component in the detrital fraction of the *slabs*, where it is possible to observe fresh basaltic fragments, without any alteration, and also pieces showing several stages of alteration.

4.2. METHODS

Most of the *slab* and basalt samples collected in Lucky Strike and Menez Gwen were cut in slices and examined and described under the binocular microscope. After an initial selection, polished thin sections were carried for petrographic studies in both transmitted and reflected light. Preparation of thin sections was a particularly delicate procedure, since most of the samples are very fragile and friable, including the vesicular basalts. The polishing procedure had to be fine tuned, otherwise the sample in the thin section could easily be lost. Around 130 polished thin sections were made and studied under transmitted and reflected light on petrographic microscopes (IFREMER and Geology Department in University of Lisbon).

The preliminary macroscopic and microscopic observations led to a selection for geochemical studies, starting with whole-rock chemical analyses. 45 samples among the *slabs* and the basalts were analysed for major and trace elements, including Rare Earth Elements (REE). Some of the *slabs* had to be divided in two parts (A and B or I and II) and analysed separately due to its heterogeneity. This characteristic is typical in the brecciated rocks studied here; therefore detailed descriptions of the powdered materials were carried prior to crushing, in order to guarantee a petrographic control.

The preparation of the powders for analysis was made avoiding contact with metal, using the following procedure: (1) samples were cut in thin slices (around 0,5 cm thick) with a diamond-saw; (2) each piece was cleaned from possible metal contamination under a diamond grinding wheel, and then washed and dried; (3) this material was fragmented by hammering in

enclosed thick paper packages; (4) the resulting fragments were finally ground by agate and tungsten-carbide mills (possible contamination was considered not relevant).

Whole-rock chemical analyses were performed at ACTLABS (Activation Laboratories, Ltd - Canada) for most samples. A few samples were analysed in another Canadian laboratory – BONDAR-CLEGG (Inchcape Testing Services) - including 6 of the samples analysed by ACTLABS, to compare the results provided by both laboratories. These results are acceptable taking into account the heterogeneity of the *slab* samples but, in general, the values considered in the study are those from ACTLABS, despite the difference in the precision of the analyses reported below.

The precision of the major element analyses as an error of $\pm$7.7%, and of the minor element analyses the error is $\pm$7%, for ACTLABS, and from $\pm$5% for major and minor element analyses in BONDAR-CLEGG. The difference is explained due to the duplication of a single sample of the same rock. For ACTLABS it was porphyritic basalt from Lucky Strike exhibiting an incipient alteration, and for BONDAR-CLEGG it was typical fresh Atlantic basalt collected in an island far away from the sites, usually used as a pattern.

The analyses of FeO, H_2O^- and H_2O^+ for FLORES samples were conducted in the Faculty of Sciences of University of Lisbon, using X-ray fluorescence (XRF) technique.

Three laboratories were used to obtain the suite of the whole rock analyses, so most of the elements were analysed by more than one method (see Table 1). Each value was carefully examined for each sample and the method which led to the most reasonable value was selected. For most major elements the best method seems to be Fusion-ICP (Inductively Coupled Plasma Emission Spectrometry), and for minor elements, including REE, the most reliable was ICP-MS (Inductively Coupled Plasma – Mass Spectrometry). See Appendix 3 for analyses of Lucky Strike and Menez Gwen hydrothermal breccias and basalts.

For the presentation and treatment of the whole rock data a procedure used by Relvas (2000, p23-25) was followed. The *slab* samples have important amounts of hydrothermal components, so the correspondent analytical data cannot be treated and presented as usual silicate rocks. Considerable amounts of some sulphides and especially barite are present in some samples. Hence, several elements that occur in trace amounts in rocks are here major elements.

Table 1 – Analytical processes used in this work to determine the whole rock composition of the samples. Detection limits (d.l.) are shown for the selected technique.

Oxide/ Element	Method	d.l. (%)	Element	Method	d.l. (ppm)	Element	Method	d.l. (ppm)	Element	Method	d.l. (ppm)
SiO_2	Fusion-ICP	0.01	Li	Fusion-ICP	2.00	Cd	INAA	5.00	Dy	ICP-MS	0.01
$Al2O_3$	Fusion-ICP	0.01	Rb	ICP-MS INAA XRF	0.10 2.00	Hg	INAA	1.00	Ho	ICP-MS	0.01
FeO	Tritration XRF	0.1	Cs	ICP-MS INAA	0.10	Ga	ICP-MS DCP	10.00	Er	ICP-MS	0.01
MnO	Fusion-ICP	0.01	Be	Fusion-ICP	1.00	In	ICP-MS DCP	0.20 10.00	Tm	ICP-MS	0.005
MgO	Fusion-ICP	0.01	Sr	Fusion-ICP ICP-MS INAA XRF	0.10 1.00	Tl	ICP-MS	0.01	Yb	ICP-MS INAA	0.01 0.20
CaO	Fusion-ICP	0.01	Sc	INAA Fusion-ICP ICP-MS	0.10 1.00	Ge	ICP-MS DCP ICP-MS	1.00 10.00 1.00	Lu	ICP-MS INAA	0.002 0.05
Na_2O	Fusion-ICP	0.01	Y	Fusion-ICP XRF	1.00	Sn	INAA Fusion-ICP	100.00 20.00			
K_2O	Fusion-ICP	0.01	Zr	Fusion-ICP ICP-MS	0.10	Sb	INAA ICP-MS	0.10 0.10	Element	Method	d.l. (ppb)
TiO_2	Fusion-ICP	0.01	Hf	ICP-MS INAA	0.05 1.00	Bi	ICP-MS Fusion-ICP	0.05 5.00	Ir	INAA	5.00
P_2O_5	Fusion-ICP	0.01	Th	ICP-MS INAA	0.005 0.20	Se	INAA	5.00	Au	INAA	2.00
$Fe_{(Tot)}$	INAA Fusion-ICP	0.01 0.01	V	Fusion-ICP ICP-MS	1.00	Te	INAA	10.00			
Ba	INAA Fusion-ICP ICP-MS	0.005 0.01 0.0001	Nb	ICP-MS XRF	0.10 2.00	Br	INAA	0.50			
Cu	ICP-MS Fusion-ICP	0.0005 0.0001	Ta	ICP-MS INAA	0.005 0.50	La	ICP-MS INAA	0.01 0.50			
Zn	ICP-MS INAA Fusion-ICP	0.0002 0.005 0.0002	Cr	INAA ICP-MS	5.00 1.00	Ce	ICP-MS INAA	0.01 3.00			
Pb	ICP-MS Fusion-ICP	1.00 0.0002	Mo	INAA ICP-MS	1.00 0.10	Pr	ICP-MS	0.005			
As	INAA ICP-MS	0.00005 0.0001	W	INAA ICP-MS	1.00 0.01	Nd	ICP-MS INAA	0.01 5.00			
S (Tot)	LECO	0.02	U	ICP-MS INAA	0.005 0.5	Sm	ICP-MS INAA	0.01 0.10			
CO_2	LECO	0.009	Co	INAA ICP-MS AA	1.00 0.10 1.00	Eu	ICP-MS INAA	0.005 0.20			
H_2O^-	Fusion-ICP Gravimetric XRF	0.01	Ni	ICP-MS INAA AA	1.00 20.00 1.00	Gd	ICP-MS	0.01			
H_20^+	Fusion-ICP Gravimetric XRF	0.01	Ag	INAA ICP-MS AA	5.00 0.50 0.10	Tb	ICP-MS INAA	0.01 0.50			

Most of the analyses were conducted in ACTLABS (Activation Laboratories, Ltd - Canada); some were carried out in BONDAR-CLEGG (Inchcape Testing Services - Canada); and XRF analyses of FeO, H_2O^- and H_20^+ were produced in the Faculty of Sciences - University of Lisbon.

Li, Cd and Te were analysed only in BONDAR-CLEGG. XRF analyses of Rb, Sr, Y and Nb are from BONDAR-CLEGG. AA and DCP analyses were performed just in BONDAR-CLEGG. INAA, Fusion-ICP and LECO were made in both ACTLABS and BONDAR-CLEGG.

Methods: AA – Atomic Absorption; DCP – Direct Current Plasma; Fusion-ICP - Inductively Coupled Plasma by fusion; ICP-MS - Inductively Coupled Plasma – Mass Spectrometry; INAA - Instrumental Neutron Activation Analysis; LECO - Light Elements Combustion (infrared spectrometry); XRF – X-ray Fluorescence spectroscopy.

In the series of the analysed *slab* samples, 17 have sulphur concentrations above 5% (12 more than 10%). Cu and Zn may attain 6% and 16%, respectively. Mineralogy shows that the copper and zinc minerals are sulphides, so computations must consider that sulphur is shared by other sulphides apart from pyrite. Sulphur is also a component to be considered in barite, as Ba concentrations may go up to 30%. If a comparison between the LOI percentages and the sum of the volatiles, analysed separately, is made, it is clear that S was incompletely volatilised in the *slabs* rich in sulphides and barite. As a consequence, the frequent difficulties with the bulk-rock totals cannot be completely solved in such samples.

Observing the *slab* samples analyses, besides the common major elements, other elements like BaO (may attain up to nearly 36%), sulphide-forming metals as Fe, Cu and Zn, and the volatiles, have to be added to the list of major elements. Water has great relevance among the volatiles, which is easily explained by the youth of the studied samples. The arsenic is not an important element here (no arsenopyrite was observed in the in the samples of the hydrothermal deposit), albeit it was analysed and detected in minor amounts in some *slab* samples. Thus it will not be considered in the original expression from Relvas (2000).

Iron is shared by sulphides (both pyrite and chalcopyrite) the basaltic fragments and the iron oxides/hydroxides that compose the *slabs*. Using the aforementioned procedure it is possible to calculate the iron content of the sulphides using a norm-like calculation, and hence to find the remaining iron of the basalt and the oxides. It is assumed that all copper is in chalcopyrite, all zinc is in sphalerite, all lead is in galena (very rare in the samples), all arsenic is in arsenopyrite (petrographically not detected), and all barium is in barite. Other assumptions are that the sulphur is shared by the sulphides and barite, there are no other important phases carrying S and that sphalerite and galena are iron free. Thus, an expression can be deduced relating the concentrations of S, Cu, Zn, Pb, As and Ba, with the amount of Fe (as an element):

$$Fe_{(sulphides)} = 0{,}8709761\ S_{(Tot)} + 0{,}0000001\ Cu - 0{,}4270952\ Zn - 0{,}1347657\ Pb - 0{,}2033312\ Ba \qquad (1)$$

The remaining iron with respect to the analysed $Fe_{(Tot)}$ was obtained by the difference and assumed to be part of the basaltic fragments and oxides/hydroxides.

The whole rock data for basalt samples is presented with the format that was used for the *slab* samples, according to the above-described procedure.

X-ray diffraction analysis (XRD) was used to determine some of the mineralogy (specially the clay minerals) in the altered basaltic fragments, and to confirm some of the observed petrographic minerals. When it was possible, the fragments were mechanically separated from the *slab*. However, it was not possible to guarantee complete lack of contamination of the surrounding matrix, so detailed descriptions of the separated material were made prior to crushing. In cases where it was difficult to get the basaltic pieces from the rock, the whole rock powder was used for diffraction.

The analyses were performed at the Department of Marine Geosciences of IFREMER (Brest), using a difractometer (software; analytical conditions – graphite crystal monochromator for CuKα radiation, 350 kV, 250 mA, continuous scan for $5^o<2\theta<70^o$, 2θ step = 0.05^o at 2s intervals) and at the XRD laboratory of the Department of Chemistry of the Faculty of Sciences of University of Lisbon, using a Phillips PW 1710 diffractometer (software PC-APD V 3.6; analytical conditions – graphite crystal monochromator for CuKα radiation, 40 kV, 30 mA, continuous scan for $2^o<2\theta<70^o$, 2θ step = 0.02^o at 1.25s intervals; for glicolated samples - 50 kV, 40 mA, continuous scan for $2^o<2\theta<10^o$, 2θ step = 0.02^o at 1.25s intervals).

For the samples analysed in Lisbon, the fragments mechanically separated were crushed and then mixed with distilled water to make a solution. This mixture was left in a thin glass plate to dry in order to allow the orientation of the clay minerals during the drying, so that the minerals can be better identified by the diffractometer. The difficulties in differentiating the clay minerals in some samples required a more accurate method: treatment with glycerol - an alcohol that occupies the interlayer spaces of same clays enhancing the diffraction peaks. The samples already analysed were used for this special treatment.

Data analysis and interpretation was made using "DiffracPlus EVA" search-match software in IFREMER, and "XRDIdentify" (© Carlos Carvalho) in Lisbon.

Microprobe analyses were extensively used for studying the components of the *slabs*, especially the basaltic fragments. Most of the data regards quantitative chemical microanalyses. Thirty samples, 50 thin sections were studied, giving more than 1000 points of compositions among the basaltic pieces (fresh and altered), the fibrous vesicular material, the *slab* matrix, the sulphides, the barite, the plagioclase, the quartz, the pyroxene and the chromite. Most of the analyses were performed at the Department of Marine Geosciences of IFREMER (Brest), using a CAMECA model CAMEBAX SX 50 microprobe (analytical conditions: 15 kV, 15 nA, 20s intervals for Ba and S, and 6s for major oxides; 15 kV, 30 nA, 10s intervals for metals). Additional data were obtained in the University of Lisbon (Faculty of Science, Geology Department, Centre of Geology) with a JEOL JCXA 733 microprobe (analytical conditions: 15 kV, 25 nA, 20s intervals for major oxides).

Strontium isotope analyses were performed at the Department of Marine Geosciences of IFREMER (Brest), using a Mass Spectrometer MAT 262 equipped with collectors. The

samples were selected for analysing altered basaltic fragments (8 *slab* samples) and barite (4 *slab* samples). These components were separated and hand-picked from the rock in a slow process which couldn't avoid contamination with other sample components than the required fragments. Afterwards these were prepared during a several stage chemical process that precedes the use of the Mass Spectrometer.

Polished thin sections and pieces of a few samples were used for textural and some qualitative chemical analyses (EDAX - Energy Dispersive X-ray Analyses), using a PHILIPS Scanning Electron Microscope (SEM) equipped with an Energy Dispersive X-ray Spectrometer (EDS), at the Department of Deep Environment of IFREMER (Brest). Before observation, samples were coated with a thin film of gold to enable conduction of the electron beam. Several magnifications were used, according to the features observed. Although it was not an extensive study, the results regarding the amorphous silica texture of the *slab* matrix were found to be rather important in clarifying the previous petrographic microscopic identification of this material.

5. BASALTIC ROCKS

5.1. INTRODUCTION

The study of the *slab* rocks requires the knowledge of related basaltic rocks, as these are one of the main components in the breccia's detrital fraction. Therefore, a preliminary analysis of the volcanic rocks from Lucky Strike and Menez Gwen sites was made, in order to compare them with the *slab* fragments.

An initial study of the petrographic and mineralogical features of the basalt was complemented with a few bulk rock analyses. Some of these were useful for mass balance calculations in the basalt samples, which could then be compared with the mass balance results for the *slab* basaltic fragments (see chapter 7).

The geochemical results for these basalts collected in the enriched zone of the Azores were somehow expected and the information from the altered samples was very useful to understand the altered basaltic fragments of the hydrothermal breccias.

5.2. PETROGRAPHY AND MINERALOGY

Basalts are the dominant host rocks in both hydrothermal fields, distributed by the several volcanic formations defined in chapter 3 (Geology of the Hydrothermal Fields). With respect to texture it is possible to recognise several types of basaltic rocks in hand sample analysis: vitreous (glassy), aphanitic, porphyritic and pyroclastic (volcano-sedimentar tuff).

Most of the samples are relatively fresh, but some depict alteration in variable degrees. All types of samples were considered here. A group of 16 samples out of 28 recovered were selected for detailed petrographic studies.

Samples of completely fresh glassy basalts are exclusively from the lava lakes or the Lava Lake Formation. The outer part of the sample has a glassy texture, and the inner part is vesicular but also with a glassy appearance (Figure 5.1a). In thin section these basalts have a spherulitic texture made of small needle shape crystals of pyroxene or feldspar. Spherulites are formed from high temperature devitrification of natural glass. The spherulitic morphology observed is axiolitic and in "bow-tie", seldom spherical (Mcphie *et al.*, 1993) (Fig. 5.2). In

general, the fresh basalt samples have a thin external crust of iron and manganese oxides (Fig 5.1).

Figure 5.1 – Fresh basalts hand sample photos from Lucky Strike and Menez Gwen. (**a**) Vitreous basalt sampled in a dredge with external coating of iron oxides; (**b**) Aphanitic, compact, extremely fine grained crystalline basalt from Lucky Strike; (**c**) Vesicular porphyritic basalt from Menez Gwen, where the plagioclase phenocrysts are dominant; (**d**) Vesicular porphyritic basalt from Lucky Strike, already depicting some alteration, with big plagioclase phenocrysts. Note the external thin layer of iron and manganese oxides in all the samples.

The aphanitic, non porphyritic basalts were collected just at Lucky Strike, in the Pillow Lava Formation and exhibit typical petrographic characteristics with low vesicularity and an external coating of iron and manganese oxides (Figure 5.1b).

Basaltic samples from Volcanic Breccia Formation, in both hydrothermal fields, have a porphyritic texture with predominant plagioclase phenocrysts (bytownite – see microprobe data in Appendix IV), and pyroxene and olivine in minor amounts (Figures 5.1c/d). The plagioclase crystals are generally up to 1 cm in length size (2 cm in some Lucky Strike samples), and may exhibit some alteration. Fluid inclusions are observed in some of them. Vesicularity is a textural feature of these samples. Low to high vesicularity is present, growing from the margins to the core of the pillow lava. The vesicles are generally small (less than 1 millimetre in diameter, exceptionally 2 millimetres) and, if the basalt is not altered, are rarely filled with iron oxides or amorphous silica.

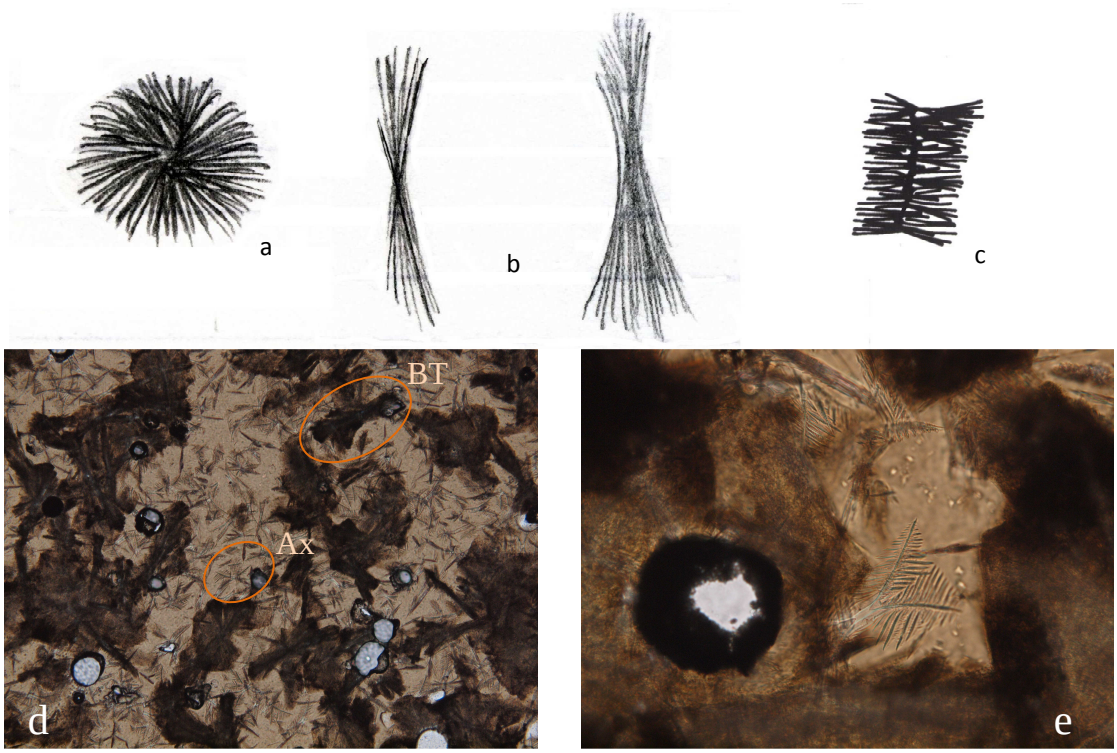

Figure 5.2 – Spherulitic textures. (**a**) Spherical spherulite, (**b**) Spherulite in "bow-tie" and (**c**) Axiolitic spherulitic (adapted from Mcphie *et al.*, 1993); (**d**) Photomicrograph of spherulites in "bow-tie" (BT) and axiolitic (Ax) in a fresh basaltic glass from Lucky Strike; (**e**) Detail of a dendritic spherulite.

In general, the basalt is highly vesicular when it is formed at low depths. Vesicularity is a characteristic that increases with decreasing depth. The chemical composition may also interfere with this property. The more alkaline the magma is, the bigger is its content in water in the vapour phase, and the vesicularity increases (Moore, 1970). Therefore, these basalts have a chemical composition that is closer to the alkaline basalts from the Azores region, as it is shown ahead.

The altered basalts, common to Menez Gwen and Lucky Strike, are mostly porphyritic. They depict different degrees of alteration, from low to very highly altered (Figure 5.3) as a consequence of hydrothermal circulation in some parts of the Volcanic Breccia Formation. The observations in thin section reveal altered plagioclase phenocrysts and vesicular filling increasing with the intensity of alteration. Vesicles are filled by manganese and iron oxides, hydrothermal precipitates (silica) and aluminium and manganese alteration products (Figures 5.3c/d). Some sulphides are observed in vesicles from basalts collected near *slab* samples (pyrite, pyrite spheres, marcassite).

Highly altered basalts are very friable and brownish or orange in colour because of abundant iron oxides/hydroxides, which are dominant in the aphanitic groundmass (Figure 5.3d). Other components of the altered material in these samples are clay minerals (some smectites – see chapter 7) and a mineral discovered in the seventies (Robinson and Flower, 1977 *in* Zamarreño *et al.*, 1989) – motukoreaite (aluminum-magnesium hydrosulfate) – was detected by XRD analyses in one of the much altered samples from Menez Gwen (see chapter 7 for detailed XRD patterns description).

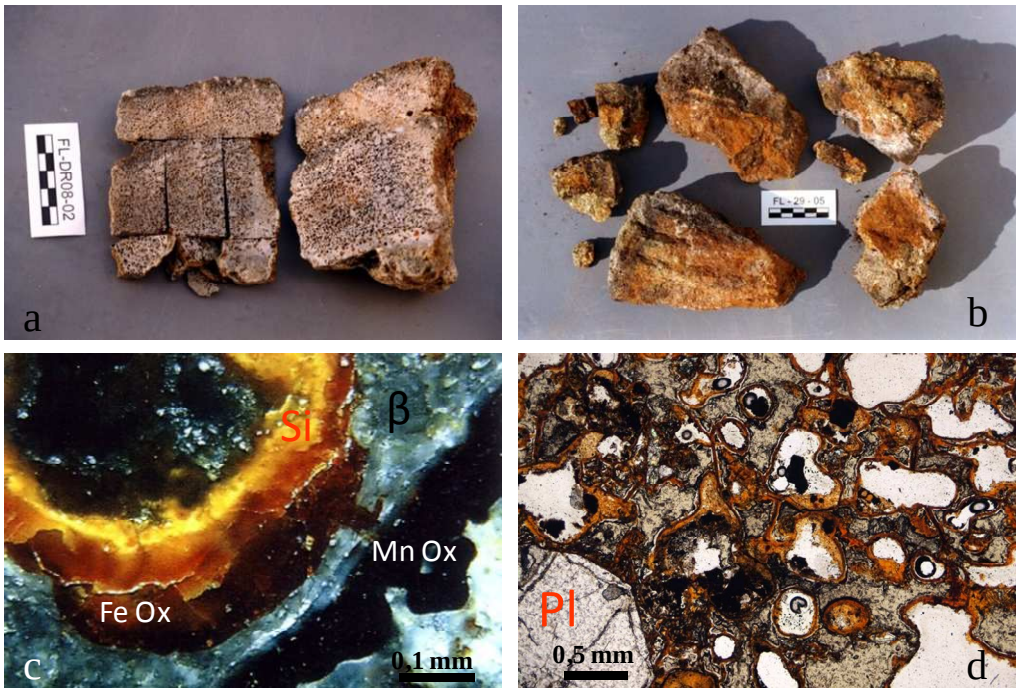

Figure 5.3 – Altered basalts from studied sites. (**a**) Hand sample photo of basalt exhibiting medium degree of alteration sampled in a dredge; (**b**) Hand sample photo of basalt (pillow lava) exhibiting high degree of alteration; (**c**) Photomicrograph (reflected light) of vesicular porphyritic basalt from Lucky Strike with iron oxides (Fe Ox), manganese oxides (Mn Ox), and silica (Si) filling the vesicles; (**d**) Photomicrograph (transmitted light) of the same sample as in (c) where it is clearly seen the iron oxides filling the vesicles and remaining plagioclase phenocryst (Pl).

Some basalts are very poorly consolidated (Figure 5.4a), as can be confirmed under the microscope: many pieces of altered vesicular (scoriaceous) basalt with some isolated phenocrysts (less altered) loosely aggregated by a siliceous cement (fig 5.4b) or, as in one sample, a calcium carbonate component (pelagic sediment with foraminifers). These are certainly part of the volcaniclastic deposits described by Eissen *et al.* (2003) and also referred by Fouquet *et al.* (1998a). Other samples, in a prior degree of alteration can also exhibit this

fragmented texture, where the pieces of vesicular basalt are still vitreous and the cement is also amorphous silica.

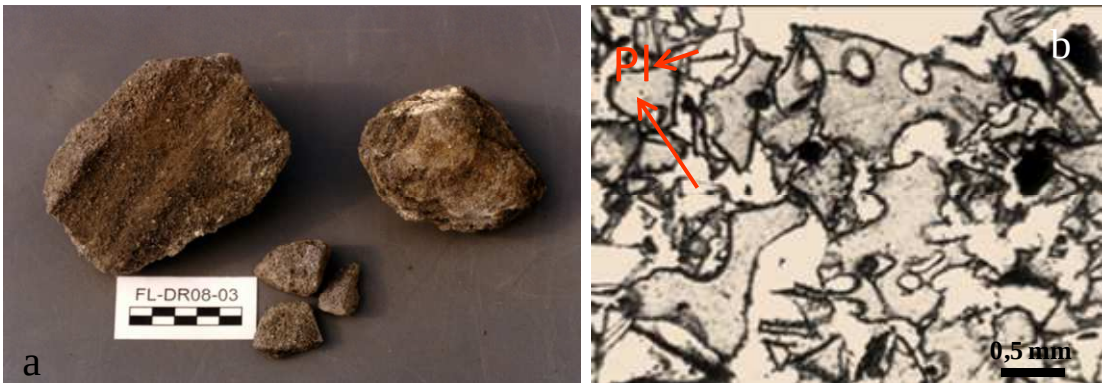

Figure 5.4 – Altered basalt very poorly consolidated – part of volcaniclastic deposits – from Lucky Strike. (**a**) Hand sample photo from a dredged sample with brown colour and very friable; (**b**) Photomicrograph (black&white) from same sample with loose pieces of volcanic glass and isolated plagioclase phenocrysts (Pl).

Sometimes, mixed with the dominant yellow pieces of altered basalt there are fragments of non-vesicular fresh basaltic glass. This can be explained by a difference in the chemical composition of these two types of basaltic samples. The non-vesicular fragments probably represent different portions of broken pillow margins that were fragmented by the rising of juvenile magma, rich in volatiles (vesicular basaltic samples), during the more violent seafloor eruptions (Fouquet et al., 1998a).

5.3. GEOCHEMICAL DATA

The depth and chemistry of the Lucky Strike and Menez Gwen ridge segments are influenced by the Azores hot spot and consequently the basalts have high concentrations in several major and trace elements, namely Ba, Pb, the light rare earth elements (REE), K, Cs, and Rb (Langmuir *et al.*, 1997; Dosso *et al.*, 1999; Donnelly *et al.*, 2004). These authors recognize three groups of basaltic rocks with variable enrichments, but all with incompatible elements patterns situated between those of Enriched - Mid Ocean Ridge Basalts (E-MORB) and those of the Oceanic Island Basalts (OIB).

The same type of interpretation was attempted with our data, using spider-diagrams for plotting the patterns of the incompatible elements normalized to N-MORB, in spite of our small group of samples. The results are very similar to those referred above (Figure 5.5a).

Lucky Strike and Menez Gwen basalts fall in the area defined from OIB and E-MORB patterns, so probably they are P-MORB (Plume - Mid Ocean Ridge Basalts), although it is possible to recognize some differences between them. Lucky Strike basalts are closer to the E-MORB values, and those from Menez Gwen approach OIB, especially on the left-hand side of the diagram where there is a clear enrichment in more incompatible elements. This is easily explained if we consider the shorter distance from Menez Gwen to the Azorean Plateau.

More recently Marques *et al.* (2009) corroborate these heterogeneities in the enriched basalts from both sites in what concerns incompatible trace element composition and ratios. Although the porphyric and more vesicular basalts from Lucky Strike (not analysed in this strudy) can approach the results of those from Menez Gwen, non vesicular basalts from Lucky Strike Lava lake Formation less enriched in incompatible elements have concentrations within the E-MORB field (Figure 5.6).

Data from the altered basaltic samples were also plotted in a spider-diagram (Figure 5.5b) showing patterns similar to those from hydrothermally altered basalts, with strong positive anomalies in Ba, U and Pb. Ba and Sr anomalies are very pronounced, as these elements exist in high concentration in the fresh basalts, influenced by the proximity of the Azores mantle plume. If Nb/Sm versus Zr/Rb ratio is considered (Figure 5.6) the altered basalts do not show a so clear pattern even if most of them are generally more enriched in incompatible elements than the fresh ones.

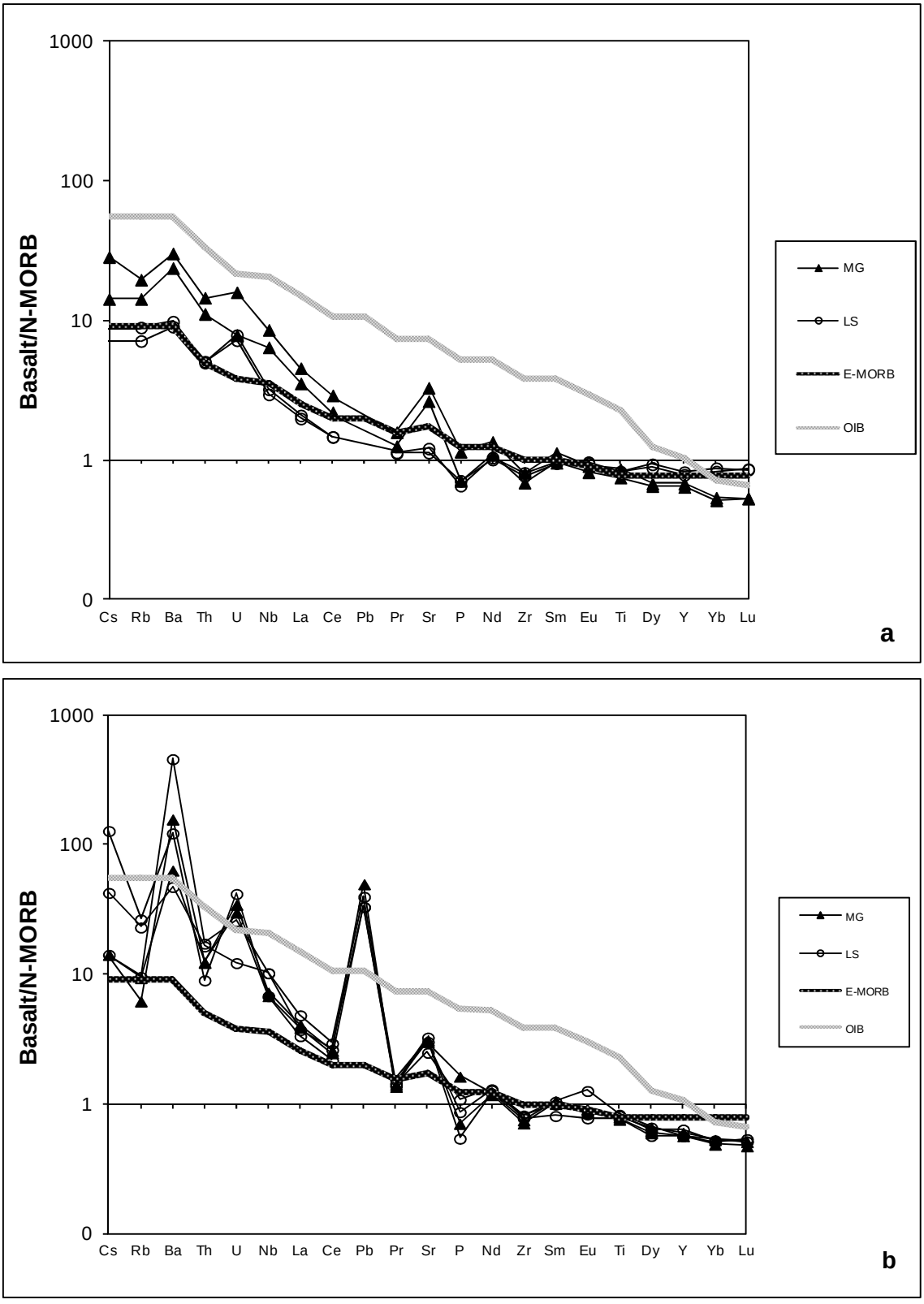

Figure 5.5 – N-MORB normalized compositions of Lucky Strike (circles) and Menez Gwen (triangles) basalts. (**a**) Fresh basalts; and (**b**) Altered basalts. Normalisation after Sun & McDonough (1989)

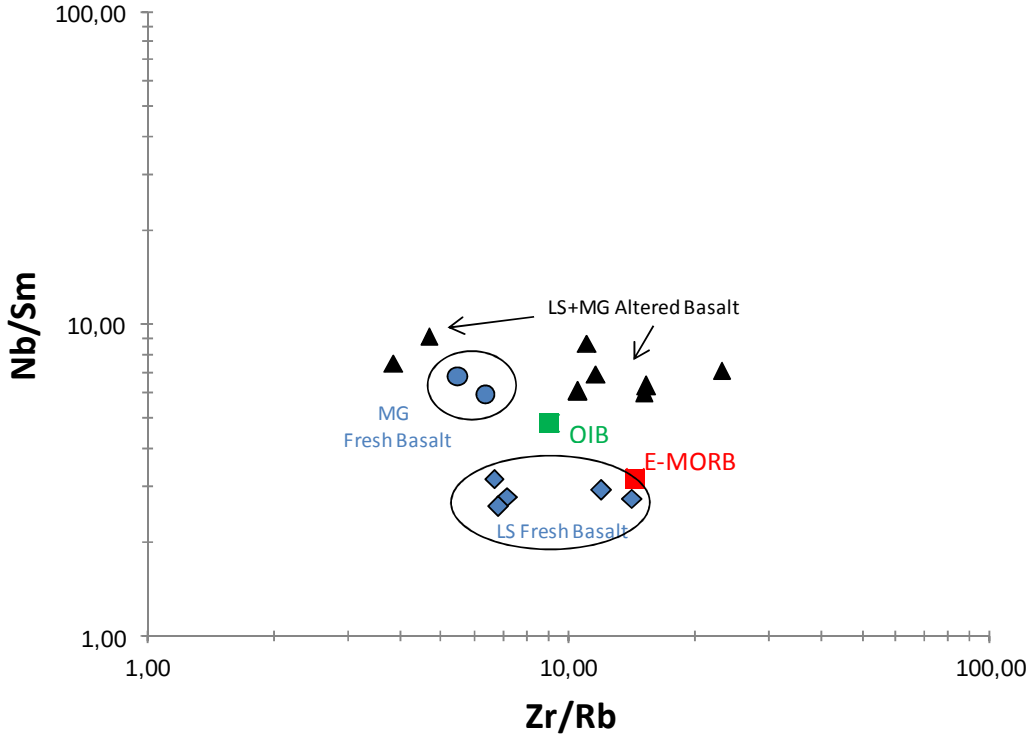

Figure 5.6 – Nb/Sm versus Zr/Rb ratios in the basalts from Lucky Strike (LS) and Menez Gwen (MG). LS fresh basalts (lozenges) - non vesicular and sampled in Lava Lake Formation. MG fresh basalts (circles) - porphyric and vesicular (similar to the samples analysed by Marques *et al.*, 2009). LS+MG altered basalt (triangles). Reference values (E-MORB and OIB) in squares (Sun & McDonough, 1989)

6. BRECCIATED ROCKS FROM LUCKY STRIKE AND MENEZ GWEN

6.1. INTRODUCTION

The hydrothermal breccias are part of big plates situated around the vents (active or inactive) (Figure 6.1), but also observed away from the focused venting hydrothermal sites. These plates have variable thickness and are fractured. The fractures may be filled with biologic specimens (mainly chemosynthetic bacteria and mussels) (Figure 6.1b) suggesting discharge of diffuse fluid flow.

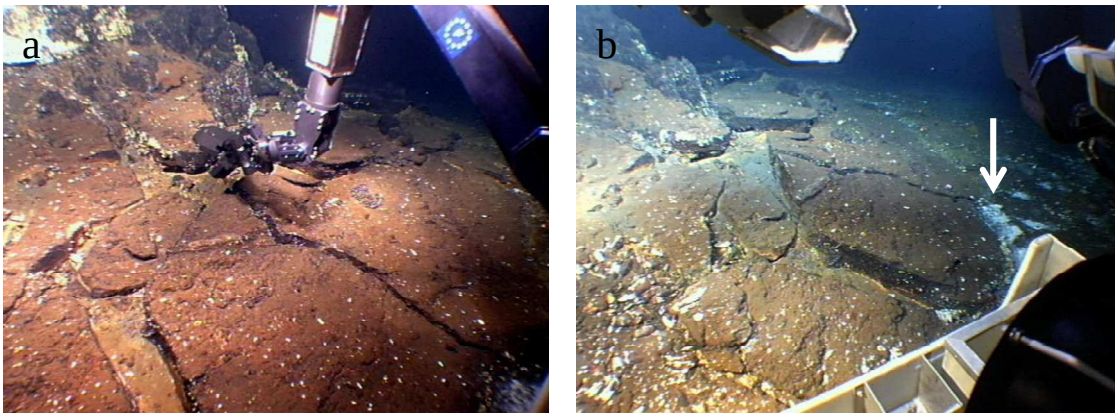

Figure 6.1 – Fractured plates of hydrothermal breccias in Lucky Strike area (photos collected from IFREMER ROV Victor during VICTOR PREMIERE mission, 1998): (**a**) Sampling plates of hydrothermal breccias near an active vent; (**b**) White microbial material (arrow) filling the fractures of the *slab*. (Scale: manipulator arm "mouth" length 40 cm).

This kind of rock shows a very heterogeneous texture, like a breccia with several different elements. These are mostly basaltic fragments and in minor amounts chimney fragments, cemented by hydrothermal precipitates (Figure 6.2). Some pelagic sediment – carbonates and foraminifer fossils – might also be present, but it is rare. The cement is rare in cases of poorly consolidated material. It is often observed an external coating, variable in thickness, of iron and manganese oxides and amorphous silica in the samples.

In this chapter, the mineralogical and petrographic characteristics as well as geochemical data of the *slabs* are reported.

Textural and mineralogical properties of these rocks were described based on macro and microscopic detailed observations of the samples. A suite of 58 samples was considered to represent the sites studied. The description is organised to present the most frequent fragments

observed - the basaltic fragments - and its heterogeneous textures depending on the degrees of alteration; and the cement composed by hydrothermal precipitates.

As a result of this detailed petrographic analysis it is possible to identify several types of *slab* referred forward. In fact this differentiation has no remarkable consequences for the conclusions of the present work although it is useful to group samples with similar textures.

6.2. PETROGRAPHY AND MINERALOGY

6.2.1. TYPES OF HYDROTHERMAL BRECCIAS

The observations and analyses of the Lucky Strike hydrothermal field *slabs* showed three different groups with increasing alteration directly related with the amount of hydrothermal precipitates (especially sulphides) in the cement, which are function of the circulating fluids that alter the fragments.

In Menez Gwen the *slabs* have in general important contents in hydrothermal minerals (barite is more important than in Lucky Strike samples), and the basaltic pieces are much altered, so there is only one type of sample.

The first group of *slabs* is composed of fresh and vesicular basalt glass fragments poorly indurated with amorphous silica. Most of these samples were collected in the east part of the hydrothermal field.

The other type considered has some altered basaltic fragments mixed with glassy pieces well cemented by silica and other hydrothermal precipitates.

Finally, there is a group of samples where the fragments of basalt generally present a considerable degree of alteration, and are associated with sulphides, indicating circulation of higher temperature fluids.

The spatial relation between the three types of Lucky Strike *slabs* is not clear. The much altered ones are widespread in the hydrothermal field but always (as expected) near the vents.

The second group seems to be concentrated in the west part, near "Bairro Alto" zone, while the first type is mainly from the east part of the field. These observations are possibly casual, maybe influenced by the heterogeneous location of the different types of basaltic fragments (hyaloclastites or pieces of basalt from the Volcanic Breccia Formation), or on the other hand a result of a non systematic sample collection in the zone (hydrothermal field and surrounding region).

6.2.2. BASALT FRAGMENTS

The basaltic elements are dominant in relation to other kind of components, in such a way that the rock granularity changes with the size of the fragments (some have more than a couple of centimetres as major length). For both hydrothermal sites, the fresh fragments are glassy and rarely crystallized (Figure 6.2d), although it is possible to observe some vesicular pieces semi-crystallized, perhaps because of devitrification of natural glass described for the basalt samples in chapter 5. Other basaltic pieces exhibit different degrees of alteration.

It is frequent to observe phenocrysts in the fragments (Figure 6.2c) but also isolated in the groundmass: plagioclase (prevailing phenocrysts, as in the basaltic samples) - bytownite (An_{87-88}); olivine – forsterite ($Fo_{89,5}$); and pyroxene - augite (see Appendix 4 for microprobe analyses of these minerals).

The vesicularity is a textural characteristic of most of the basalt pieces observed, which may indicate that, for both hydrothermal fields, they are fragments of the surrounding Volcanic Breccia Formation. The vesicles have a regular shape, rounded to oval, and in contrast with the samples of this formation, are partially filled with hydrothermal precipitates, particularly the much altered basaltic fragments (Figure 6.2e/f). (See next section – "Hydrothermal precipitates")

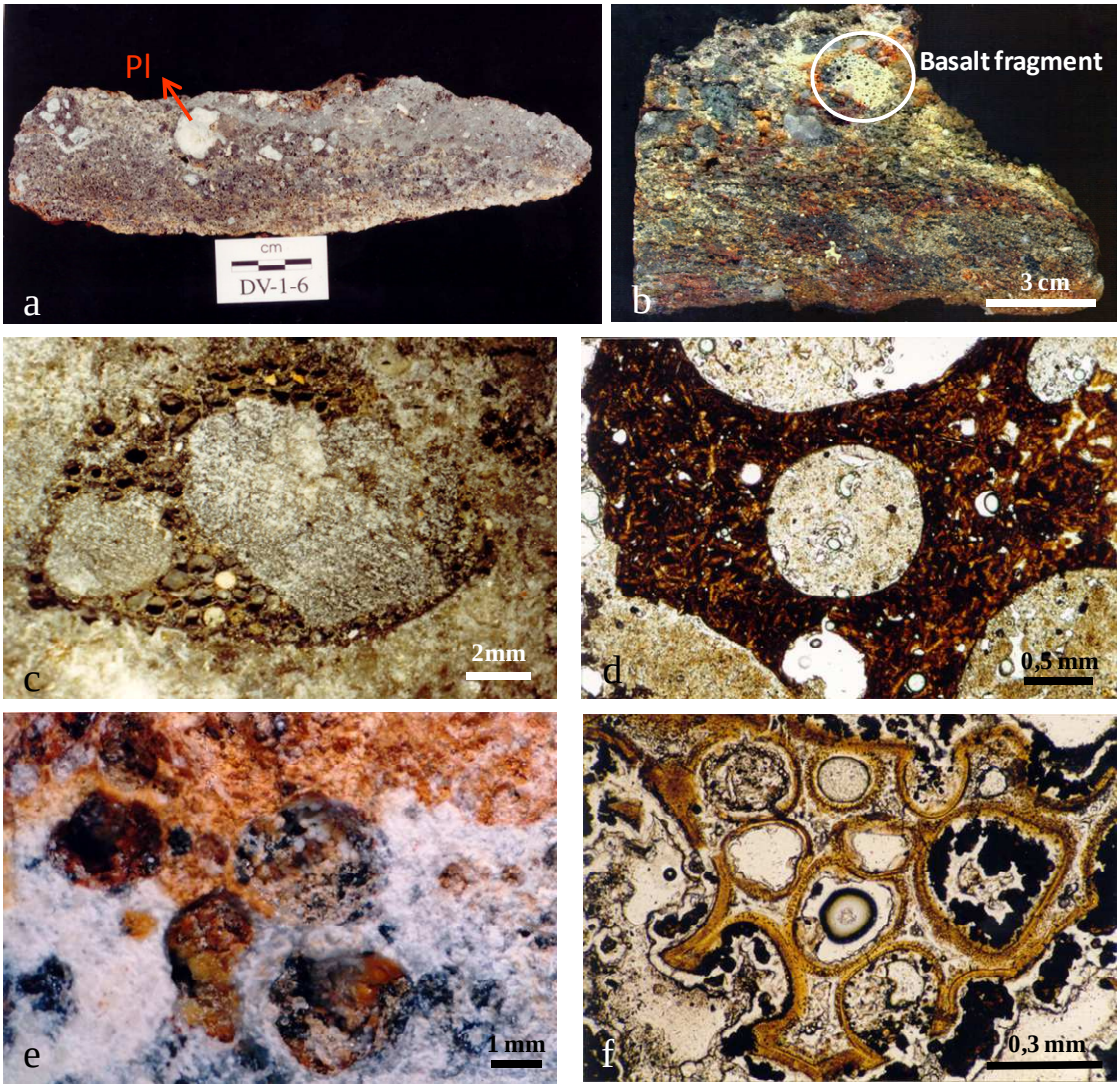

Figure 6.2 – Hydrothermal breccias and its components. (**a**) and (**b**) Two *slab* hand samples, the first more consolidated with greater amounts of hydrothermal precipitates, including some sulphides, and plagioclase phenocrysts (Pl); the second one is poorly indurate with altered basaltic fragments easily identified; (**c**) Fresh basaltic fragment with two plagioclase phenocrysts (binocular microscope photo); (**d**) Photomicrograph of a fresh crystallized basaltic fragment; (**e**) Round vesicles in a very altered filled with iron oxides, amorphous silica (white) and sphalerite (black) (binocular microscope photo); (**f**) Vesicles filled with amorphous silica (transparent) and sphalerite in a altered basaltic fragment.

The glassy nature of most fragments may indicate other origin than the Volcanic Breccia Formation. The fragments are probably formed *"in situ"* as a result of an explosive eruption originating a hyaloclastite deposit. This hypothesis stated by other authors (Fouquet *et al.*, 1998a and Humphris *et al.*, 2002) is confirmed by our observations. However, we propose that the *slab* fragments have a mixed source: pieces of basalt from the Volcanic Breccia Formation fragmented and shortly transported together with local formed hyaloclastites. A possible explanation for this is proposed further on, in chapter 8, and is related with the presence of basaltic fragments exhibiting different degrees of alteration, in the same sample.

In polished thin sections some of the fresh basaltic clasts have inclusions of chromite with a brown-reddish colour in plane-polarized light (Figure 6.3a). It's an iron magnesio-chromite from the chromite series, determined by microprobe analyses (Appendix 4). The occurrence of this type of mineral may be explained by the eventual existence in the studied regions of the olivine basalts and/or picritic basalts, studied by Hekinian *et al.* (1976) for the FAMOUS area. These authors observed spinel as inclusions in the larger crystals of olivine or as micro-phenocrysts in the glassy groundmass of the basalts. Albeit this type of basalt wasn't collected during the cruises where our samples came from, the contents in Cr and Al of our spinels are typical of basalts related to the oceanic ridge system (Kamenetsky, *et al.*, 2001).

The basalt fragments may exhibit different stages of hydrothermal alteration, from fresh up to completely altered. Therefore, we identify pieces of fresh basaltic glass, with typical MAR basaltic chemical composition (Figure 6.3b). Others depict some alteration in the border, where the contents in silica have increased (Figure 6.3c). And, in extreme cases of high degree of alteration, it is possible to observe a complete replacement by pure silica (usually amorphous), not only in the border but also inside the fragment (Figure 6.3d).

The altered basaltic clasts, besides the phenochysts, are predominantly composed of amorphous silica and clay minerals (some of these identified only by X-ray diffraction analysis). In plane-polarized light, most of these fragments are yellow brownish. Often is observed an alteration rim of amorphous silica surrounding the basaltic clasts (Figure 6.3d).

All types of basaltic fragments were analysed in the microprobe. The main alteration products are Si, Al and Ti. Titanium can be concentrated in an amorphous material named leucoxene. This is a high TiO_2 alteration product of ilmenite or basaltic glass which lacks defined crystal structure and its chemical composition is far too variable to be expressed as a chemical formula. Usually leucoxene consists of hydrated titanium oxide. It is easily recognized because it displays very bright white internal reflection in both plane polarized and cross-polarized light (Figure 6.3e).

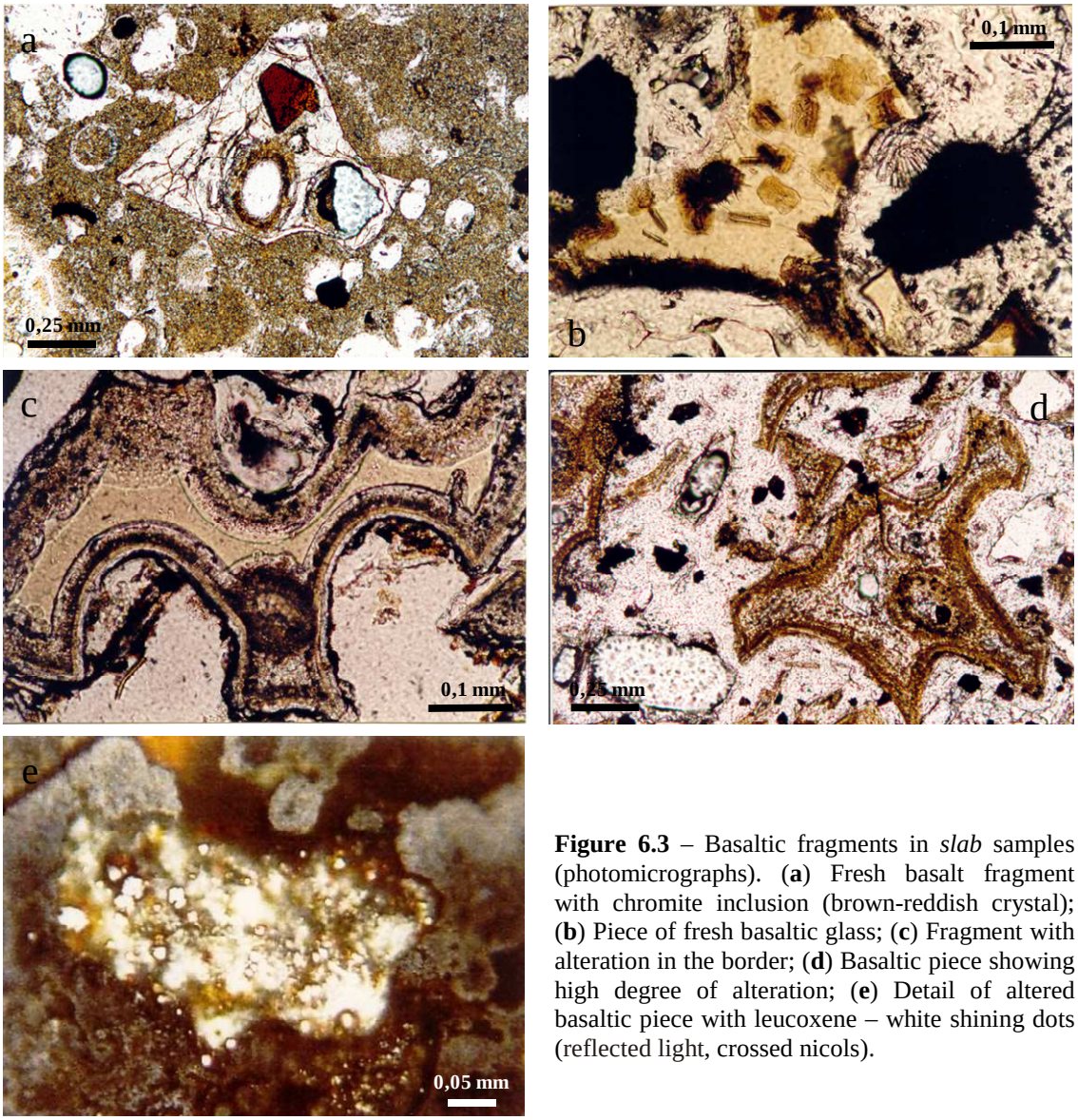

Figure 6.3 – Basaltic fragments in *slab* samples (photomicrographs). (**a**) Fresh basalt fragment with chromite inclusion (brown-reddish crystal); (**b**) Piece of fresh basaltic glass; (**c**) Fragment with alteration in the border; (**d**) Basaltic piece showing high degree of alteration; (**e**) Detail of altered basaltic piece with leucoxene – white shining dots (reflected light, crossed nicols).

Results of the microprobe data in basalt fragments and detailed interpretation are given further on in this work.

6.2.3. HYDROTHERMAL PRECIPITATES

Hydrothermal precipitates compose the matrix of the *slab* rocks, which is generally present. Mainly amorphous silica deposited during low temperature hydrothermal activity as a late stage product. Other components are sulphides, barite, iron and manganese oxides and rare carbonates. Anhydrite, an important mineral in chimney structures, is rare or absent in *slabs*. All the precipitates can be observed in macroscopic and microscopic scales.

SULPHIDES

Authigenic sulphides are disseminated in the rock or concentrated in basalt vesicles. Marcasite and sphalerite are abundant, but chalcopyrite and pyrite are also observed. Some are already altered, presenting a rim of iron oxides.

Pyrite appears frequently in the contact glass fragment/amorphous silica in spheroid aggregates – pyrite spheres or framboids (Figure 6.4a) – giving the appearance of being part of the fragment (Figure 6.4c). These structures are typical of low temperature hydrothermal activity, probably transported by the hydrothermal fluid responsible for the alteration of the fragment borders. Some of them are yet totally replaced by iron oxides (Figure 6.4b).

Melnikovite is a fine grain amorphous material with the chemical composition of pyrite/marcasite, which also exists in the hydrothermal breccias. It is a sulphide gel of pyrite or marcasite, with a collomorphic (or botryoidal) texture. Melnikovite is part of lower-temperature varieties of iron sulphides and may occur in sedimentary and low-grade metamorphic rocks as well as in low-temperature hydrothermal assemblages. The observed melnikovite is usually associated with big crystals of marcasite which are found randomly in the cement of some samples (Figure 6.4d).

Chalcopyrite is observed in massive sulphide fragments (broken chimneys) and dispersed in the breccia cement. In some samples with chalcopyrite, some alteration minerals resulting from the oxidation of this sulphide are identified (Figure 6.4f): copper sulphides - covellite and digenite – and an iron/copper sulphide – bornite. This seems to be formed after covellite; perhaps taking the iron left over from the replacement of chalcopyrite by covellite. Digenite are rare and is always observed near bornite and chalcopyrite.

Also resulting from seawater alteration of the chalcopyrite there is another mineral, formed in the surface of the slab structures, which is atacamite. It’s a copper chlorite, very frequent in the outer part of the black smoker chimneys (Costa, I, 1995), easily observed from the submarine because of its bright green colour. Atacamite appears less frequently in association with slabs, but it can be observed in hand samples.

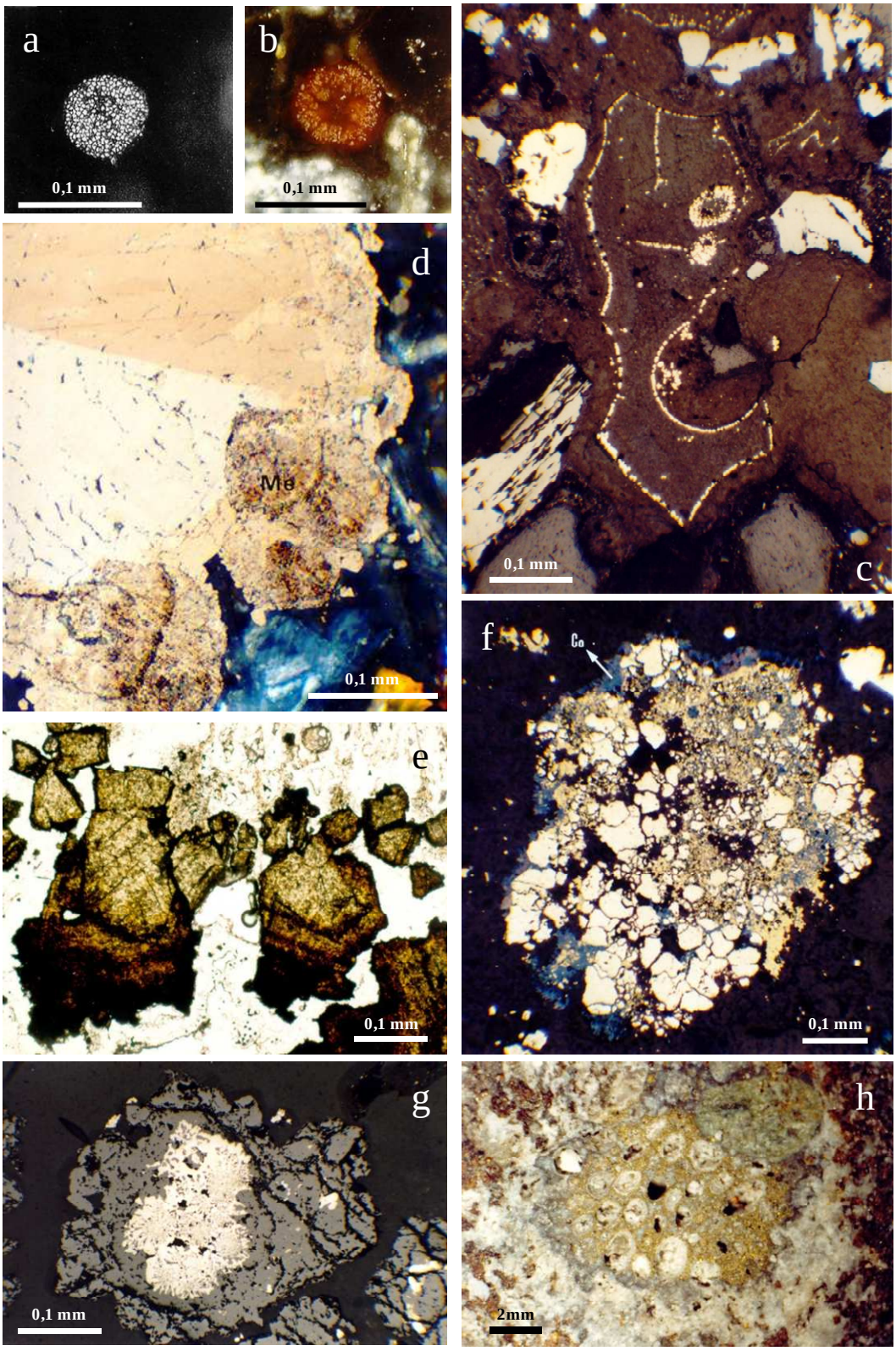

Figure 6.4 – Sulphides in *slab* samples (photomicrographs). (**a**) Pyrite framboid (reflected light); (**b**) Altered pyrite framboid (reflected light) replaced by iron oxides; (**c**) Pyrite lining the border of a basaltic fragment (reflected light); (**d**) Development of melnikovite (Me) botryoidal aggregates around marcasite crystals (reflected light, crossed nicols); (**e**) Sphalerite zoned crystals develop in a *slab* vein (transmitted light); (**f**) Piece of massive sulphides composed of pyrite and chalcopyrite with a alteration rim of covellite (Co) (reflected light); (**g**) Marcasite enveloped by later sphalerite (reflected light); (**h**) Vesicular basalt fragment replaced by sulphides; note the siliceous grey-white material in the border of the fragment; vesicles filled by amorphous silica (binocular microscope photo).

Sphalerite is transparent, with a yellow to light-brown colour. Some crystals are optically zoned, although the microprobe analyses do not reveal this feature. The zinc sulphide appears in crystalline aggregates with a collomorphic texture (Figure 6.4e), sometimes growing on barite tabular crystals (Figure 6.5a).

The light colour in sphalerite indicates low content in iron, and in this case it is possible that the sulphur fugacity is high so that an important amount of H_2S is formed. This possibility sustains also another petrographic textural feature where we observe that pyrite (or marcasite) is formed before the other sulphides (chalcopyrite and sphalerite) taking most of the iron from the fluid (Figure 6.5g).

In some polished thin sections of *slabs* inter-grows between sphalerite and chalcopyrite are observed. This can be explained by the formation of both sulphides at the same time, from a fluid with copper in excess.

The sulphides filling the vesicles and fractures are usually covered by amorphous silica. Sulphides can rarely be observed as clasts among the analysed *slab* samples (Figure 6.4f). They are part of chimney fragments with variable sizes (in one sample there are pieces with 4 cm diameter). These pieces result from chimney desegregation, transportation (with a maximum distance of a few meters), deposition and consolidation in the hydrothermal breccias. Some of the chimney fragments have an alteration rim composed of iron oxides, formed during transport.

Sulphides were also reported in a *slab* sample collected in Lucky Strike area near “Tour Eiffel” active chimney. Interesting and unexpected replacement textures of vesicular basaltic fragments with clarifying relic textures were described (Figure 6.4h). This feature was not observed in any other analysed sample. As most of the altered basaltic fragments have higher contents in silica and in extreme cases are entirely replaced by silica, the question is: are the sulphides later replacements of silica or took directly the place of the basalt? Petrographic observations seem to indicate the later hypothesis as the outer part of the fragment is composed by silica showing a possible replacement by silica after sulphides.

BARITE

Barite is another cement element which precipitates after most of the sulphides (except sphalerite) as a result of hydrothermal fluid and seawater interaction.

In some samples, barite exists in considerable amounts and it is easily observed in hand sample descriptions. In thin sections, clusters of tabular crystals are typical in the groundmass, but in cavities and fractures barite forms large prismatic crystals (Figure 6.5a).

It is an abundant mineral species also in the active structures of the Lucky Strike and Menez Gwen hydrothermal sites consequence of the high content in Ba in the host basalts.

OXIDES

Iron and manganese oxides/hydroxides cover most of the external part of the *slab* samples. They are easily observed in hand samples.

In thin section, iron oxides are pale yellow to dark red (Figure 6.5b) and the manganese oxides may exhibit collomorphic textures. Hematite and goethite are sometimes recognized, but in general the oxides are composed of amorphous material.

Most of the oxides associated with hydrothermal fields result from the alteration of sulphides, but they also may have a primary origin, precipitating directly from low temperature hydrothermal fluid as it happens with the silica. These two materials (in the amorphous state) are usually associated in the outer edges of the samples.

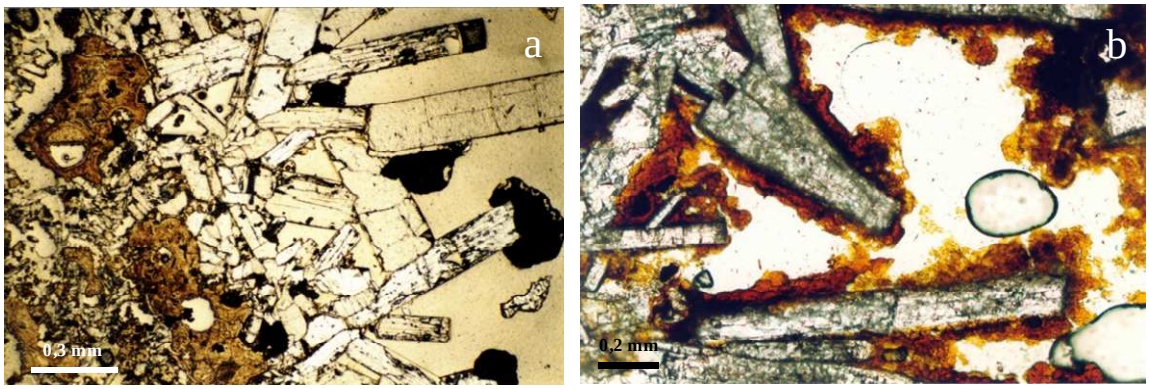

Figure 6.5 – Barite in *slab* samples (photomicrographs). (**a**) Barite crystals in a cavity of a *slab* sample; sphalerite (black crystals) is lining barite; two altered basaltic fragments are present (light brown) (**b**) Iron oxides surrounding barite crystals.

SILICA

Silica is ubiquitous in the hydrothermal breccias! It is the dominant material in the cement. It is observed in the inner parts of the basalt fragments, filling the void space (lining the vesicles and filling it), surrounding other hydrothermal, and in the outer part of the samples as a surface coating.

Macroscopic observation indicates grey to white colours for this siliceous material (Figure 6.6a/b) that is often identified optically as opal – transparent and colourless. The opal lines the intergranular cavities and cement clasts depicting a botryoidal or colloform texture (Figure 6.6c).

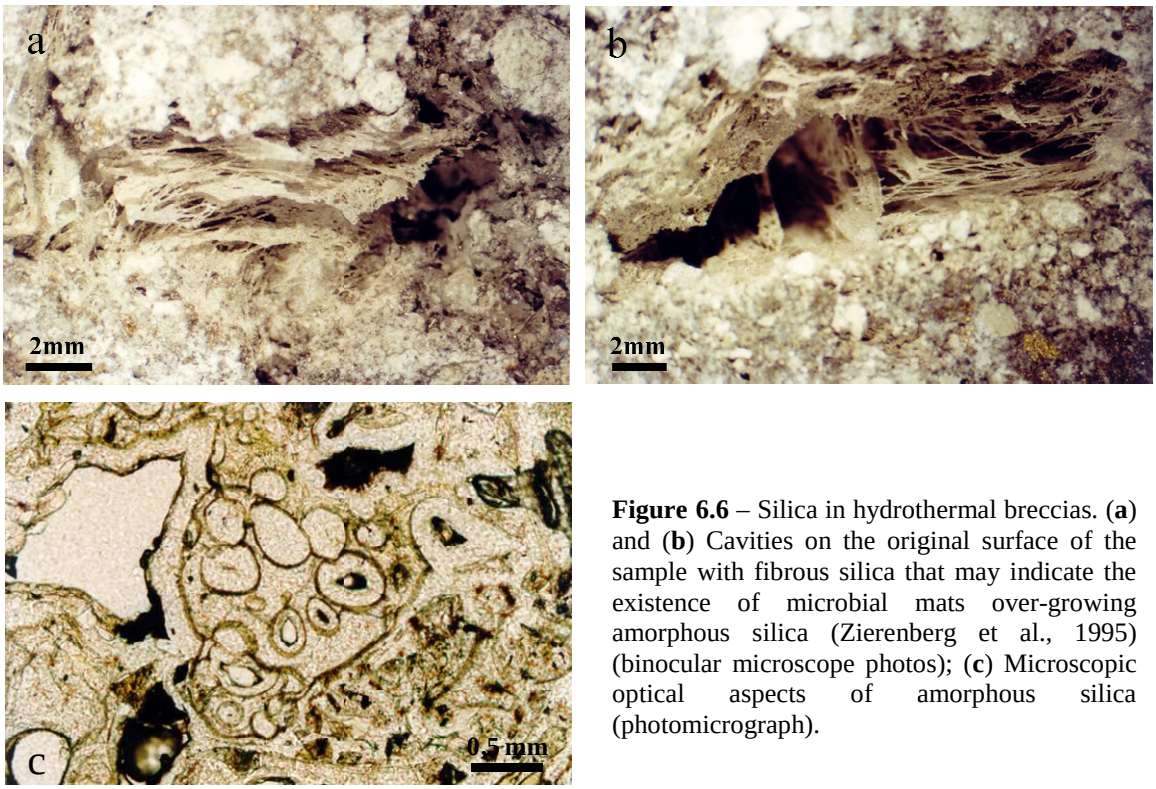

Figure 6.6 – Silica in hydrothermal breccias. (**a**) and (**b**) Cavities on the original surface of the sample with fibrous silica that may indicate the existence of microbial mats over-growing amorphous silica (Zierenberg et al., 1995) (binocular microscope photos); (**c**) Microscopic optical aspects of amorphous silica (photomicrograph).

Silica is an important component of the basaltic fragments in the hydrothermal breccia as a result of a process of Silicification, so it will be described in detail further on chapter 7.

6.3. GEOCHEMICAL DATA

This section is dedicated to the study of the whole rock geochemical analyses of the hydrothermal breccias. A relation with the basalt data is made, as basaltic fragments are the main components of the *slabs*. Representative chemical analyses for *slab* samples, and also for fresh and altered basalts are presented in Appendix 3.

Rare Earth Elements are also analysed in this part of the study.

Other data related with X-ray Diffraction, Microprobe analyses and strontium isotopes in the basaltic pieces will be study in chapter 7.

6.3.1. WHOLE ROCK CHEMICAL DATA

The *slab* samples are very heterogeneous, so the whole rock analysis has the contribution of their several components. In table 6.1 there are some of the representative chemical analyses of the *slabs*, and two fresh basalts. In what concerns the hydrothermal crusts, we select specimens from each one of the groups defined in section 6.2.1. After a brief study it is possible to conclude that the separation in 3 groups can only be made on a petrographic basis. Nevertheless, in the chemical numbers there is a difference in the Al_2O_3 content between the samples of Group II and III, and the Group I, explained by the high content in fresh basaltic fragments in this last group.

Silica is generally the most important component, due to the contribution from both the basaltic fragments and the matrix. Thus, in comparison with fresh basalts the hydrothermal slabs are generally enriched in SiO_2, BaO, S and in water (Table 6.1). The increase in sulphur is due to sulphides and/or barite. This mineral is present in considerable amounts in both of the studied hydrothermal fields, even in the chimney structures, which can be explained by extraction from the host basalts, which are rich in barium (e. g. L Dosso, p. com.). Sulphide-dominated slabs can be rich in transition metals as iron, copper, zinc or (in minor amounts) lead, and in this case these are considered major elements in the hydrothermal crusts. Al_2O_3, TiO_2, MgO are depleted in relation to the fresh basalts.

Table 6.1 – Whole rock analyses of selected *slab* samples and two fresh basalts from Lucky Strike. Group I, Group II and Group III are related with the types of *slab* defined on 6.4.

Sample Ref.	ALV2608-3-3B	DV-4-10	FL-18-09	FL-DR-05 B	FL-29-06	ALV2608-4-1B	DV-8-4	FL-DR-04-02A	FL-DR-04-02B	DV-3-2	FL-DR-08-04	DV2-05B	FL-DR-04-V1
Sample Type	Slab - Group I					Slab – Group II				Slab – Group III		Fresh Bas.	Fresh Glass
Weight percent													
SiO2	61.78	46.04	73.88	57.80	59.08	65.22	32.23	78.10	53.40	74.94	31.41	50.91	51.22
Al2O3	13.31	18.22	7.24	13.85	12.22	10.17	1.38	3.28	2.00	3.50	1.31	14.97	14.37
Fe2O3(Cal)	0.65	1.38	0.41	0.54	0.83	1.98		0.00		0.65			1.15
FeO	3.30	4.50	2.07	5.09	3.38	2.60	0.96	1.31	1.26	0.60	1.49	8.94	8.47
MnO	0.07	0.29	0.08	0.10	0.08	0.09	<0,01	0.01	<0,01	0.05	<0,01	0.21	0.18
MgO	4.53	6.41	2.31	5.98	4.12	4.08	0.06	0.81	0.21	1.03	0.08	9.20	8.22
CaO	7.89	11.7	4.25	11.01	7.31	7.40	0.02	1.37	0.29	1.62	0.05	11.86	12.51
Na2O	1.41	2.52	1.06	1.83	1.86	1.65	0.07	0.48	0.32	0.72	0.35	1.64	2.22
K2O	0.37	0.53	0.28	0.38	0.51	0.43	0.13	0.20	0.18	0.18	0.04	0.20	0.19
TiO2	0.72	1.20	0.47	0.87	0.82	0.69	0.11	0.19	0.13	0.22	0.35	1.30	1.04
P2O5	0.11	0.25	0.06	0.16	0.13	0.15	0.09	0.05	0.04	0.03	0.03	0.10	0.12
BaO(Cal)	0.46	0.09	1.02	0.04	1.15	0.13	1.79	4.25	13.17	5.92	24.90	0.02	0.01
Fe(sulph)(Nor)	0.27	0.22	0.20	0.06	0.12	0.19	24.53	0.61	4.94	0.50	4.43	0.08	0.08
Cu	0.02	0.03	0.02	0.02	0.04	0.02	5.10	0.07	0.35	0.05	2.43	0.01	0.01
Zn	0.02	0.01	0.02	0.01	0.01	0.00	0.35	0.88	3.82	0.36	9.59	0.01	0.01
Pb	0.00	0.00	0.00	0.00	0.00	0.00	0.01	0.02	0.01	0.16	0.00	0.00	0.00
As	0.00	0.00	0.00	0.00	0.00	0.00	0.02	0.01	0.01	0.01	0.06	0.00	0.90
S(sulph)(Cal)	0.17	0.24	0.24	0.07	0.15	0.18	27.77	1.13	7.55	-1.08	9.79	0.09	0.10
S(barite)(Cal)	0.24	0.04	0.21	0.01	0.24	0.07	0.93	0.89	2.75	3.09	5.21	0.01	0.00
CO2	< 0,009	0.06	0.07	0.07	0.18	0.08	0.06	0.12	<0,05	<0,009	0.07	0.05	0.18
H2O-	1.25	3.57	2.30	0.85	2.72	1.79	1.30	2.29	1.12	2.16	0.67	0.03	Not Analysed
H20+	0.54	1.94	2.54	0.57	3.88	0.29	0.90	2.94	4.35	0.50	2.80	<0,01	Not Analysed
TOTAL	**97.11**	**99.25**	**98.73**	**99.31**	**98.84**	**97.23**	**97.80**	**99.01**	**95.90**	**95.21**	**95.06**	**99.62**	**100.97**
Fe(Tot)	3.29	4.69	2.09	4.39	3.33	3.60	23.40	1.63	4.84	1.42	2.98	6.24	7.47
S (Tot)	0.41	0.28	0.45	0.08	0.39	0.25	28.70	2.02	10.30	2.01	15.00	0.10	0.10
Razão Fe	0.46	0.44	0.46	0.48	0.45	0.37	-1.95	0.50	1.11	0.34	-3.92	0.53	0.47
Parts per million													
Rb	7.99	14.00	7.80	12.00	9.60	8.68	4.00	7.00	5.60	4.44	5.10	6.00	5.00
Cs	0.19	<0,50	0.30	0.10	0.10	0.19	0.54	0.20	0.10	0.17	0.40	<0,50	<0,10
Sr	346.00	201.00	239.00	207.00	357.00	193.00	154.00	355.00	941.00	1019.00	1660.00	102.00	109.00
Ba (%)	0.41	0.08	0.92	0.03	1.03	0.12	1.60	3.81	11.80	5.30	22.30	0.01	0.01
Sc	25.00	30.80	14.00	28.00	24.00	21.00	2.10	6.40	4.60	7.10	3.20	40.40	40.40
Y	11.80	14.00	6.80	15.00	13.00	12.60	3.00	3.30	2.70	3.70	3.10	21.00	23.00
Zr	40.00	52.00	35.00	65.00	52.00	39.00	<5,00	14.00	11.00	16.00	26.00	40.00	60.00
Hf	1.19	1.00	0.90	1.60	1.40	1.01	0.18	1.00	2.70	0.80	3.50	2.00	1.70
Th	1.07	1.20	0.89	1.39	1.10	1.10	0.10	0.52	0.29	0.35	0.48	0.70	0.61
V	140.00	129.00	87.00	170.00	138.00	131.00	<2,00	126.00	75.00	69.00	167.00	180.00	278.00
Nb	11.84	17.00	8.00	17.00	15.00	11.96	1.88	5.40	3.70	3.72	6.40	8.00	7.50
Ta	0.80	1.10	0.36	0.95	0.74	0.83	0.395	0.47	0.33	<0,5	<0,01	0.60	0.50
Cr	510.00	660.00	250.00	390.00	320.00	360.00	<20,00	83.00	59.00	90.00	140.00	84.00	79.00
Mo	62.00	9.00	2.70	1.70	2.40	<1,00	64.00	18.00	25.00	11.00	14.00	<1,00	<1,00
W	<1,00	<1,00	180.00	2.80	17.00	<1,00	<1,00	260.00	231.00	<1,00	96.00	<1,00	338.00
U	0.85	1.10	1.46	0.61	3.07	2.87	6.40	4.98	4.72	5.71	23.00	0.20	0.37
Co	22.00	24.00	35.00	26.00	19.00	19.00	194.00	62.00	95.00	5.00	22.00	40.00	77.00
Ni	44.00	71.00	39.00	72.00	52.00	53.00	7.00	22.00	16.00	9.00	26.00	70.00	69.00
Ag	< 5,00	0.40	0.60	1.80	<0,50	< 5,00	14.70	40.00	67.00	34.00	32.00	0.20	<0,50
Au (ppb)	11.00	<2,00	21.00	<2,00	14.00	< 5,00	247.00	78.00	298.00	176.00	74.00	<2,00	<2,00
Hg	2.00		<1,00	<1,00	<1,00	2.00		2.00	<1,00	4.00	25.00		<1,00
Ga	10.00	16.00	6.00	13.00	13.00	8.00	8.00	10.00	40.00	6.00	96.00	18.00	17.00
In	<0,10	<1,00	<0,10	<0,10	0.60	<0,10	1.00	0.70	1.50	0.10	9.20	<1,00	<0,10
Ge	1.20	1.00	1.50	2.70	2.40	1.10	1.00	12.00	9.00	11.70	52.00	<1,00	1.40
Sn	8.10	<20,00	1.20	11.00	1.60	6.50	<20,00	1.00	<0,50	1.10	<0,50	<20,00	<1,00
Sb	0.40	0.50	1.23	0.40	0.67	0.30	10.80	7.59	27.30	1.10	25.90	<0,10	0.10
Bi	<0,05	<5,00	0.13	0.10	0.13	<0,05	90.00	0.25	0.07	<0,05	0.05	<5,00	<0,06
Br	4.60	34.00	7.00	5.90	20.00	18.00	10.00	4.50	6.60	11.00	40.00	0.80	<0,50
La	6.37	8.00	3.74	9.11	8.20	7.77	1.34	3.02	2.99	3.38	2.86	6.00	5.23
Ce	12.35	<5,00	5.36	16.30	14.70	14.71	1.36	2.66	5.39	4.42	1.36	<5,00	11.00
Pr	1.25		0.66	1.81	1.61	1.52		<0,005	0.64	0.45	0.44		1.50
Nd	6.70		3.65	10.20	8.86	7.79		2.65	2.35	2.38	1.46		7.62
Sm	1.61	2.30	0.81	2.07	1.83	1.80	0.29	0.52	0.35	0.66	0.27	2.50	2.55
Eu	1.30	<1,00	0.46	0.73	0.60	0.70	<1,00	0.26	<0,100	0.40	<0,200	<1,00	0.987
Gd	1.82		0.93	2.51	2.22	1.97		0.60	0.26	0.60	0.40		3.29
Tb	0.35	<0,50	0.15	0.44	0.38	0.35	0.04	0.09	<0,01	0.15	0.05	0.70	0.62
Dy	2.00		0.95	2.52	2.11	1.96		0.48	0.47	0.59	0.14		4.25
Ho	0.43		0.22	0.50	0.43	0.46		0.10	0.10	0.11	0.02		0.88
Er	1.36		0.67	1.70	1.43	1.20		0.32	0.25	0.32	0.06		2.55
Tm	0.19		0.08	0.25	0.20	0.21		0.04	<0,005	<0,005	<0,005		0.427
Yb	1.36	2.00	0.59	1.36	1.25	1.17	0.04	0.30	0.26	0.28	0.01	3.00	2.67

The origin of silica is clear. But in a first approach, we can consider two hypotheses: is it comes from up or down in the seafloor? Is it hydrogenous or hydrothermal?

The first assumption results from the submarine dive observations, where we permanently see falling particles. Is this silica? The studies in the regions of both

hydrothermal fields (Khripounoff *et al.*, 2000 and Khripounoff, pers. communication) reveal very low particle fluxes, and in particular the content in silica is very low. This way, the first proposal is not reasonable.

Considering the second assumption, we tried to compare the Si versus Al weight % concentrations in a diagram used by several authors (Bonatti, 1981; Toth 1980 and Crerar, 1982) (Figure 6.7). Most of the slab samples fall within the field of the hydrothermal precipitates, with a Si/Al ratio greater than 5. The exceptions are samples where basalt fragments dominate, in which Al is higher, and samples with a considerable percentage in clay minerals.

The silica of the *slabs* is a hydrothermal precipitate of a probably low temperature hydrothermal fluid (see next chapter).

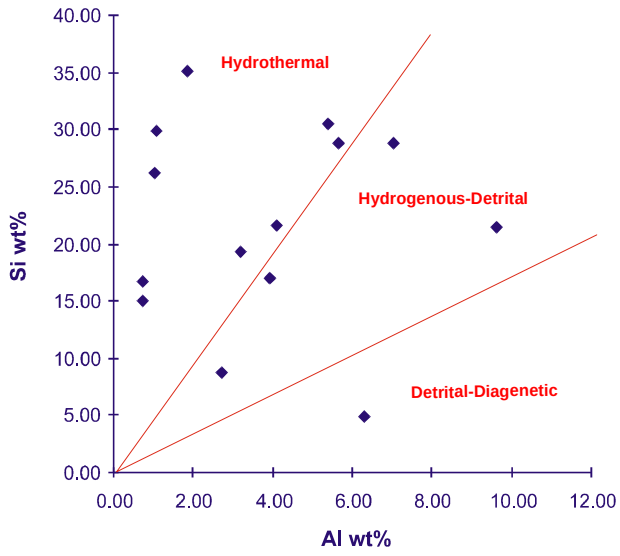

Figure 6.7 – Si vs Al diagram for the hydrothermal crusts from Lucky strike and Menez Gwen.

Trace elements as Sr, Ag, Au and Cr are enriched in *slabs.* Strontium is present in the barite crystal structure, reaching its highest values in samples where this mineral dominates. If we look at the concentration of BaO in some samples of table 6.1 (FL DR-04-02B, DV-3-2 and FL DR-08-04), it is possible to verify a coincidence in the high values of Sr.

Gold is particularly high in samples where the presence of sulphides is important (DV-8-4, FL DR-04-02B and DV-3-2).

6.3.2 RARE-EARTH ELEMENTS GEOCHEMISTRY

The chondrite-normalised Rare Earth Element (REE) distribution patterns of the slab samples are plotted in figure 6.8. All samples are enriched in light REE, which is attributed to the basaltic components of the slab.

The substrate basalt has a MORB-P composition resulting from a enriched mantle source reflected in the REE pattern (the influence of the Azores hot spot), as shown in the diagram by the light REE distribution of the Lucky Strike and Menez Gwen analysed basalts.

Lucky Strike *slabs* generally depict higher absolute concentrations of REE, but with lesser fractionation than most of the MG slabs. This can be explained by a greater hot-spot influence in Menez Gwen, coupled with a dominance of basaltic fragments in LS samples.

Other features are (1) a small negative Ce anomaly; and (2) a marked positive Eu anomaly for many of the samples. Collectively these characteristics do not correspond to any likely fluid, so we conclude that a mixture of fluids is indicated. The positive Eu anomaly is probably related to a hydrothermal fluid. The negative Ce anomaly is typical in the REE sea water pattern, and as the analysed slabs were all collected on the ocean bottom (not underneath) it is reasonable to hypothesise a contribution of this fluid. The presence of this fluid is also expressed in the lower patterns, where it is possible to recognise an inflection upwards in the heaviest REE, typical of the seawater REE distribution.

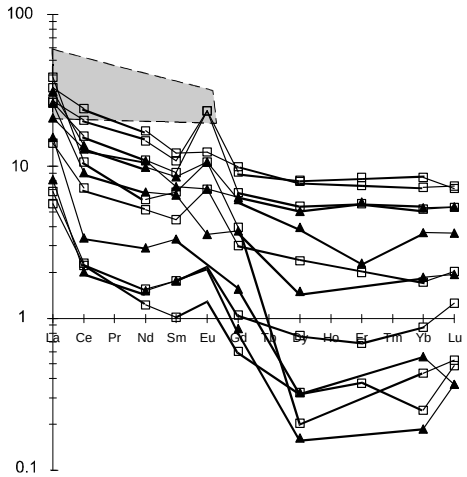

Figure 6.8 – Rare Earth Element distribution in the slabs from Lucky Strike (open squares) and Menez Gwen (triangles). Shaded area – basalts from the same sites (analyses from L. Dosso, 1999).

7. HYDROTHERMAL ALTERATION OF BASALTIC FRAGMENTS

7.1. CHEMICAL AND MINERAL COMPOSITION

The study on the chemical composition of basaltic fragments was mostly based on electron microprobe studies. Spot analyses were carried out not only in the basaltic fragments but also in the infillings of vesicles of these basalts. Additionally, strontium isotope determinations and X-ray diffraction study were carried out in some of the samples.

An initial attempt to dissociate the detrital part from the cement was not completely successful as it was not possible to perform this operation without contamination. The diffractograms obtained are generally not easy to interpret because they correspond to mixtures of several materials, including (dominant) amorphous ones. On the other hand, the common basaltic minerals, also as mixtures, exhibit large peaks, which may hide the ones of less abundant, but more significant minerals.

The petrographic description indicates different stages of alteration in the basaltic fragments. In extreme cases, it is possible to observe complete replacement by pure silica. Systematic microprobe data, in altered samples, in most cases confirms these observations revealing the existence of amorphous (or poorly crystalline) material composed essentially of silica or silica and alumina. Analyses of these fragments, both from Lucky Strike and Menez Gwen *slabs*, can be viewed in Appendix IV.

Other basaltic samples have only the border modified by hydrothermal alteration, also with a gain in silica. A third type is completely unaltered with a basaltic chemical composition very similar to the composition of the basalts from the surrounding regions as confirmed by electron microprobe analysis.

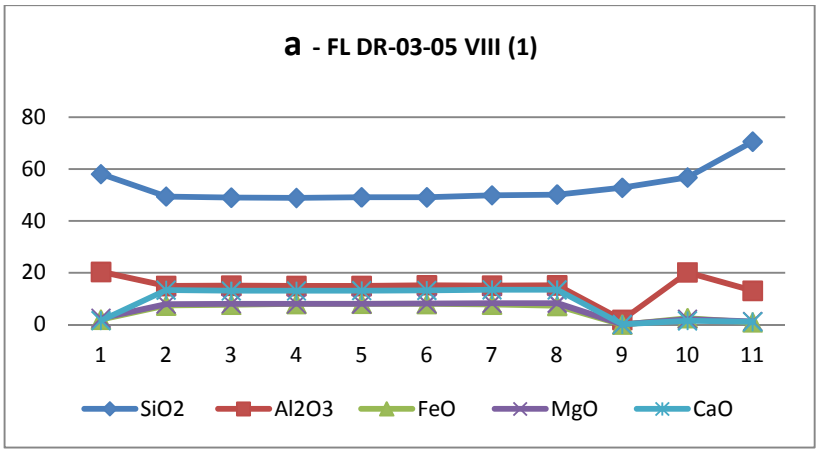

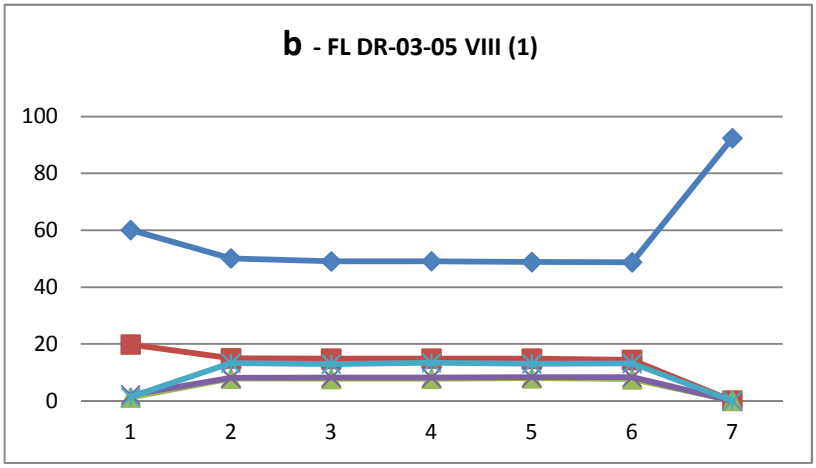

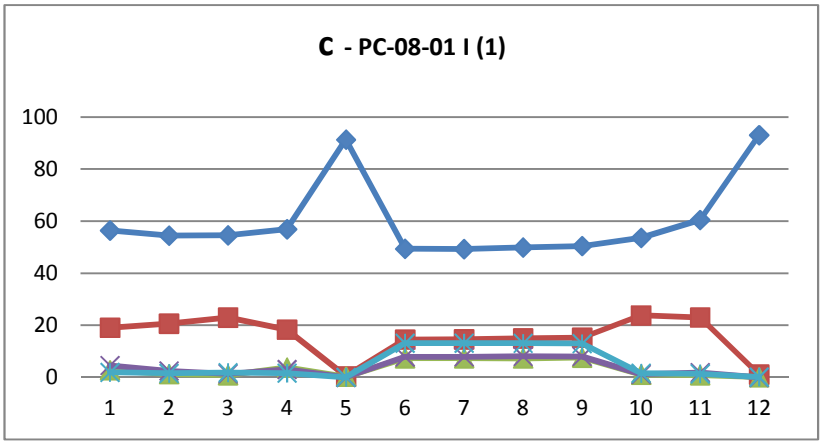

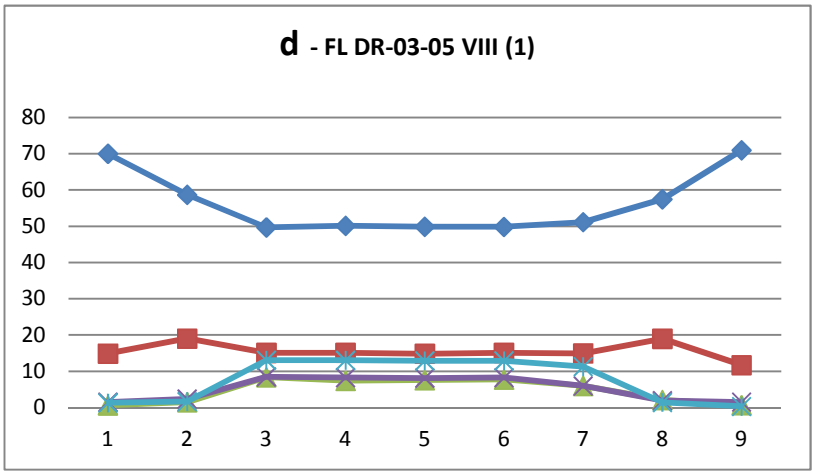

Figure 7.1 – Behaviour of some major components of basaltic glass along a series of points in a straight line, from one border to the other of the basaltic fragment with altered borders. Borders are invariably the more altered regions. Plots **a, b** and **c** are from different fragments of the same sample (FL DR-05-03); plot **d** is from a basaltic fragment from the sample (PC-08-01). See text.

Considering the results of the series of analyses made with the electron microprobe in several fragments fresh in the interior and altered in the border, it is very interesting to analyze the behavior of the chemical elements composing these fragments. In figure 7.1 we can see the result of the analysis performed in several basaltic fragments from Lucky Strike *slab* samples. Silica increases from core to border, while aluminum and the remaining elements considered decrease. This is a direct feature that indicates silicification as a major alteration process. Some points inside the basalts depict a higher content in silica (Fig. 7.1c) which may indicate that the alteration process has expression inside the fragments, probably in the basaltic minerals most susceptible to this chemical alteration.

Aluminum in the altered basaltic fragments is considered remnant of the hydrothermal basaltic alteration, while silica is mainly a result of silicification and in residual amounts may also be a remnant of the original basalt.

Concerning aluminum, Zierenberg *et al.* (1995) explained its important amounts by a phased replacement process of alteration: before the replacement of the basaltic fragments by amorphous silica (explaining the high contents in Si), there is a replacement by smectites. In fact petrographic observations showed relic fibrous textures in our samples. The microprobe study demonstrated the presence of sheet silicates inside the altered fragments of our samples – chlorite/smectite interlayer. Chemical composition of these mixed chlorite/smectite clays are very similar to those analyzed by Zierenberg *et al.* (1995) for the Sea Cliff hydrothermal samples. We use results from two samples, one from Lucky Strike (LS) and another from Menez Gwen (MG), taken on fibrous materials inside the altered clasts and lining the borders to calculate, on a 22-oxygen-formula-unit basis (Table 7.1), their chemical composition and make a comparison with the data of Zierenberg *et al.*. The data are ambiguous concerning the identification of the clay mineral, but the calculation results indicate the presence of interstratified chlorite-smectite, Mg-rich, very similar to some of the material identified in Sea Cliff altered clasts.

Table 7.1 Electron microprobe analyses of interlayered chlorite/smectite from Lucky Strike and Menez Gwen altered basaltic fragments and calculation of unit formula based on 22 oxygens. Values in Weight Percent.

	DV-14-4 (Menez Gwen sample)																SAL-01-01 (Lucky Strike sample)															
SiO2	36,43	38,53	37,66	37,99	38,55	37,24	39,05	39,04	39,58	38,77	36,88	35,22	36,56	38,19	37,08	33,97	37,06	39,07	44,13	38,48	37,64	38,12	41,05	39,53	56,58	50,56	37,92	42,19	57,12	37,56	41,64
TiO2	0,01	0,05	0,00	0,07	0,00	0,02	0,00	0,00	0,00	0,00	0,03	0,00	0,03	0,01	0,03	1,87	0,00	0,01	0,00	0,12	0,00	0,00	0,00	0,00	0,04	0,01	0,05	0,00	0,00	0,01	0,02
Al2O3	12,38	13,81	14,65	12,64	15,39	13,24	13,13	10,02	7,80	7,21	20,92	20,63	15,58	16,31	17,65	14,67	22,79	21,69	20,06	21,90	20,28	22,98	21,08	20,46	15,17	16,15	21,48	19,82	14,78	19,10	19,35
Cr2O3	0,00	0,00	0,13	0,00	0,07	0,08	0,00	0,00	0,03	0,01	0,00	0,00	0,03	0,04	0,00	0,10	0,04	0,03	0,00	0,03	0,00	0,04	0,06	0,01	0,00	0,00	0,00	0,00	0,00	0,02	0,00
Fe2O3	-	-	-	-	-	-	-	-	-	-	-	-	-	-	-	-	-	-	-	-	-	-	-	-	-	-	-	-	-	-	-
FeO	3,83	3,68	3,08	2,59	2,92	4,02	0,96	0,70	0,69	1,43	0,24	0,34	1,03	1,86	0,73	0,79	3,22	3,22	2,61	3,33	4,14	4,21	3,15	3,30	2,50	2,76	3,66	3,30	2,33	4,45	4,48
MnO	0,01	0,15	0,11	0,00	0,00	0,15	0,00	0,06	0,10	0,06	0,00	0,00	0,00	0,00	0,02	0,02	0,14	0,00	0,15	0,21	0,08	0,00	0,13	0,09	0,07	0,05	0,06	0,00	0,01	0,08	0,07
MgO	29,52	29,70	26,94	27,96	26,07	28,53	27,43	28,60	29,59	29,88	22,48	24,27	22,38	23,88	22,89	22,02	22,61	20,74	18,76	22,38	21,73	21,42	20,10	21,96	13,61	16,48	22,44	20,21	13,01	21,74	20,20
CaO	0,07	0,00	0,07	0,05	0,05	0,04	0,04	0,04	0,05	0,04	0,01	0,01	0,02	0,04	0,01	0,07	0,47	0,41	0,40	0,48	0,43	0,42	0,42	0,49	0,58	0,39	0,45	0,51	0,61	0,78	0,74
Na2O	0,16	0,11	0,19	0,14	0,13	0,16	0,19	0,20	0,16	0,16	0,07	0,17	0,20	0,13	0,16	0,19	0,05	0,11	0,14	0,13	0,11	0,11	0,14	0,19	0,26	0,22	0,12	0,14	0,23	0,05	0,15
K2O	0,06	0,04	0,02	0,07	0,05	0,04	0,01	0,00	0,03	0,02	0,19	0,25	0,03	0,06	0,16	0,01	0,17	0,20	0,25	0,14	0,24	0,15	0,18	0,20	0,41	0,30	0,20	0,21	0,41	0,06	0,10
TOTAL	82,46	86,08	82,85	81,49	83,22	83,53	80,81	78,65	78,02	77,58	80,83	80,89	75,87	80,51	78,73	73,69	86,54	85,48	86,50	87,20	84,64	87,46	86,30	86,23	89,22	86,93	86,39	86,38	88,49	83,84	86,74
Oxygens	22	22	22	22	22	22	22	22	22	22	22	22	22	22	22	22	22	22	22	22	22	22	22	22	22	22	22	22	22	22	22
Ions in formula																															
Si	5,64	5,68	5,74	5,87	5,81	5,68	6,00	6,17	6,31	6,26	5,61	5,39	5,95	5,89	5,81	5,72	5,38	5,70	6,27	5,53	5,60	5,48	5,91	5,73	7,61	7,07	5,52	6,06	7,72	5,66	6,01
Al(IV)	2,36	2,32	2,26	2,13	2,19	2,32	2,00	1,83	1,69	1,74	2,39	2,61	2,05	2,11	2,19	2,28	2,62	2,30	1,73	2,47	2,40	2,52	2,09	2,27	0,39	0,93	2,48	1,94	0,28	2,34	1,99
Tot(IV)	**8,00**	**8,00**	**8,00**	**8,00**	**8,00**	**8,00**	**8,00**	**8,00**	**8,00**	**8,00**	**8,00**	**8,00**	**8,00**	**8,00**	**8,00**	**8,00**	**8,00**	**8,00**	**8,00**	**8,00**	**8,00**	**8,00**	**8,00**	**8,00**	**8,00**	**8,00**	**8,00**	**8,00**	**8,00**	**8,00**	**8,00**
Al(VI)	-0,11	0,08	0,36	0,17	0,55	0,06	0,37	0,03	-0,22	-0,37	1,36	1,11	0,94	0,86	1,07	0,64	1,27	1,43	1,64	1,25	1,16	1,37	1,49	1,23	2,01	1,73	1,20	1,42	2,07	1,05	1,30
Ti	0,00	0,01	0,00	0,01	0,00	0,00	0,00	0,00	0,00	0,00	0,00	0,00	0,00	0,00	0,00	0,24	0,00	0,00	0,00	0,01	0,00	0,00	0,00	0,00	0,00	0,00	0,01	0,00	0,00	0,00	0,00
Cr	0,00	0,00	0,02	0,00	0,01	0,01	0,00	0,00	0,00	0,00	0,00	0,00	0,00	0,00	0,00	0,01	0,00	0,00	0,00	0,00	0,00	0,00	0,01	0,00	0,00	0,00	0,00	0,00	0,00	0,00	0,00
Fe3+	-	-	-	-	-	-	-	-	-	-	-	-	-	-	-	-	-	-	-	-	-	-	-	-	-	-	-	-	-	-	-
Fe2+	0,49	0,45	0,39	0,33	0,37	0,51	0,12	0,09	0,09	0,19	0,03	0,04	0,14	0,24	0,10	0,11	0,39	0,39	0,31	0,40	0,52	0,51	0,38	0,40	0,28	0,32	0,45	0,40	0,26	0,56	0,54
Mn	0,00	0,02	0,01	0,00	0,00	0,02	0,00	0,01	0,01	0,01	0,00	0,00	0,00	0,00	0,00	0,00	0,02	0,00	0,02	0,03	0,01	0,00	0,02	0,01	0,01	0,01	0,01	0,00	0,00	0,01	0,01
Mg	6,80	6,53	6,11	6,43	5,86	6,49	6,28	6,73	7,03	7,19	5,09	5,54	5,43	5,49	5,35	5,53	4,89	4,51	3,98	4,80	4,82	4,59	4,31	4,75	2,73	3,43	4,87	4,33	2,62	4,88	4,35
Tot	**7,19**	**7,09**	**6,90**	**6,94**	**6,78**	**7,09**	**6,78**	**6,86**	**6,92**	**7,02**	**6,48**	**6,69**	**6,51**	**6,59**	**6,52**	**6,53**	**6,58**	**6,34**	**5,94**	**6,49**	**6,51**	**6,48**	**6,20**	**6,39**	**5,03**	**5,49**	**6,53**	**6,14**	**4,95**	**6,50**	**6,20**
Ca	0,01	0,00	0,01	0,01	0,01	0,01	0,01	0,01	0,01	0,01	0,00	0,00	0,00	0,01	0,00	0,01	0,07	0,06	0,06	0,07	0,07	0,07	0,06	0,08	0,08	0,06	0,07	0,08	0,09	0,13	0,11
Na	0,05	0,03	0,06	0,04	0,04	0,05	0,06	0,06	0,05	0,05	0,02	0,05	0,06	0,04	0,05	0,06	0,02	0,03	0,04	0,04	0,03	0,03	0,04	0,05	0,07	0,06	0,03	0,04	0,06	0,02	0,04
K	0,01	0,01	0,00	0,01	0,01	0,01	0,00	0,00	0,01	0,00	0,04	0,05	0,01	0,01	0,03	0,00	0,03	0,04	0,04	0,02	0,05	0,03	0,03	0,04	0,07	0,05	0,04	0,04	0,07	0,01	0,02
Tot	**0,07**	**0,04**	**0,07**	**0,06**	**0,05**	**0,06**	**0,07**	**0,07**	**0,06**	**0,06**	**0,06**	**0,10**	**0,07**	**0,06**	**0,08**	**0,08**	**0,12**	**0,13**	**0,14**	**0,14**	**0,15**	**0,12**	**0,14**	**0,17**	**0,22**	**0,17**	**0,14**	**0,16**	**0,22**	**0,15**	**0,17**
Tot(other)	7,27	7,13	6,97	7,00	6,84	7,15	6,84	6,93	6,98	7,08	6,54	6,80	6,59	6,65	6,60	6,61	6,70	6,47	6,09	6,63	6,66	6,60	6,34	6,56	5,26	5,66	6,67	6,30	5,17	6,66	6,37
Total	15,27	15,13	14,97	15,00	14,84	15,15	14,84	14,93	14,98	15,08	14,54	14,80	14,59	14,65	14,60	14,61	14,70	14,47	14,09	14,63	14,66	14,60	14,34	14,56	13,26	13,66	14,67	14,30	13,17	14,66	14,37

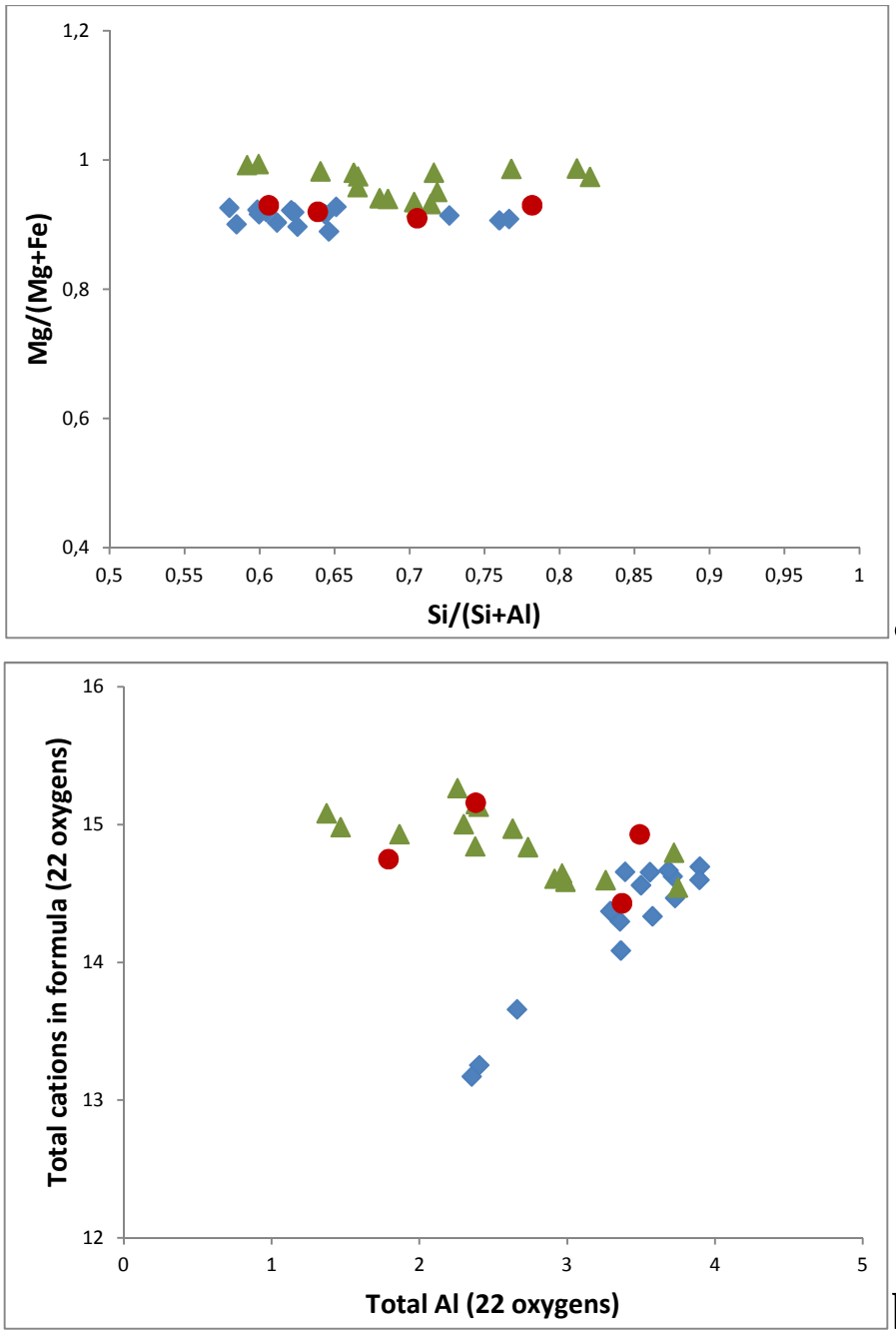

Figure 7.2 – Composition of interstratified chlorite/smectite from Lucky Strike (lozenges) and Menez Gwen (triangles) altered basaltic clasts. (**a**) Si/(Si+Al) versus Mg/(Mg+Fe) ratios. (**b**) Total Al versus total cations in formula (on the basis of 22 oxygen per formula unit). Data from selected samples of the Sea Cliff hydrothermal field (Zierenberg *et al.*, 1995) (circles) are plotted for comparison.

The plots in figure 7.2 relate the total Al content of our fibrous material with sums of tetrahedral+octahedral cations in formula, and the Mg/(Mg+Fe) ratios with the Si/(Si+Al). Note the remarkable similarity of Lucky Strike and Sea Cliff samples, indicative of the presence of identical interstratified chlorite-smectites.

It is possible to identify small differences in the plots for LS and MG. Menez Gwen interlayered smectite/chlorites are richer in Mg when compared with the ones from Lucky Strike. If we analyze figure 7.2b, the LS samples have higher contents in aluminum than MG. The reason for this is probably due to different stages of alteration. The altered basaltic fragments from LS have, in general, higher contents in Si and Al than those from MG (Table 7.1).

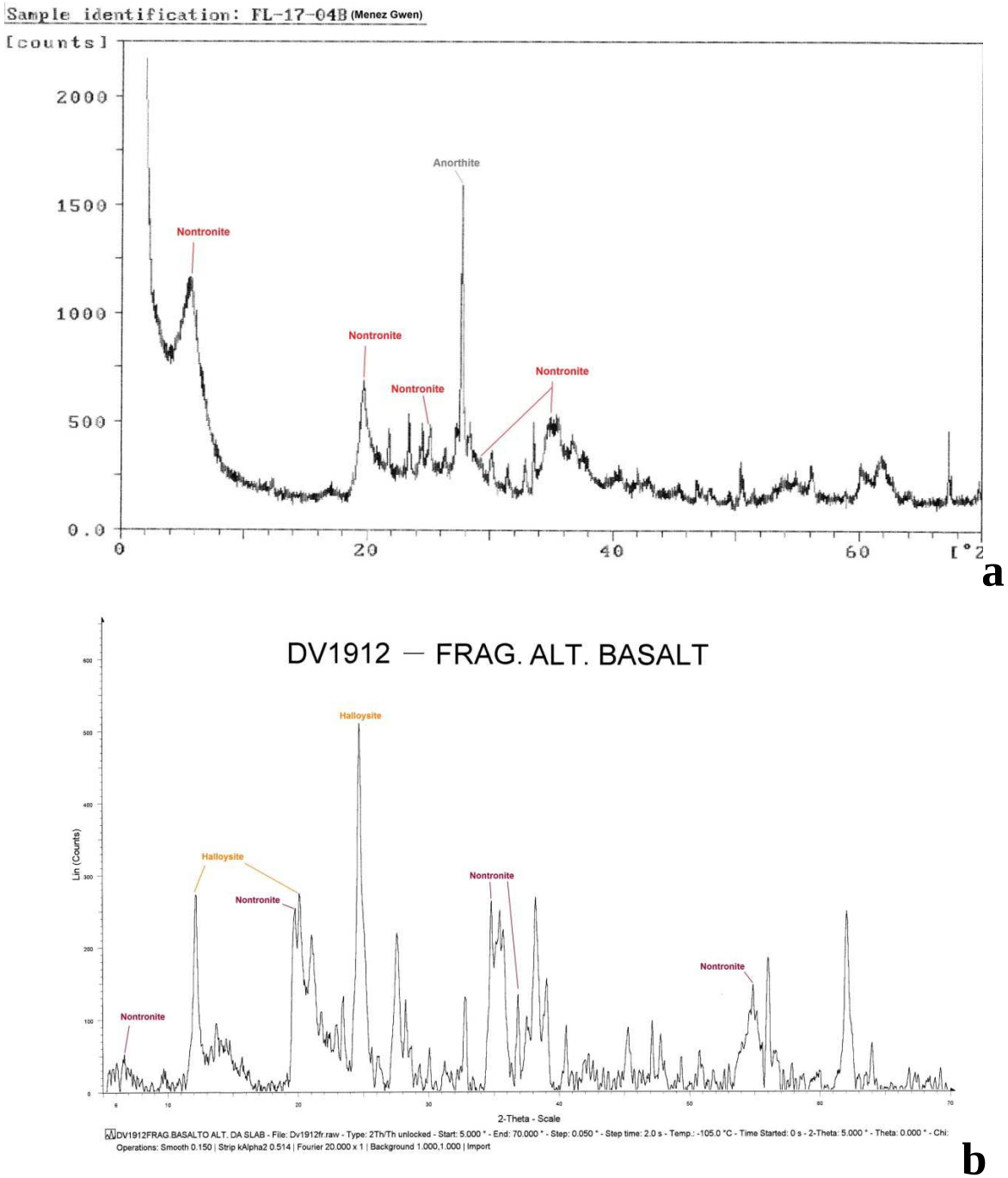

Figure 7.3 – Diffractograms from altered basaltic fragments of *slab* samples from Lucky Strike (**b**) and Menez Gwen (**a**). In both diagrams nontronite was detected. The sample from LS shows also the strong possibility of having halloysite (see text).

X-ray diffraction data confirmed the presence of sheet silicates. Nontronite, an iron- rich Smectite Group clay mineral, was found in samples from LS and MG (Figure 7.3). Nontronite is a weathering product of basalts, which may occur in some hydrothermally altered mineral deposits in mid-ocean ridge basalts.

Halloysite, a hydrated aluminosilicate (Kaolinite Group) was detected in X-ray diffraction of an altered basaltic fragment of LS (Figure 7.3b). This is a mineral found in widely varied environments, including as an alteration product of basaltic rocks. It has an earthy appearance showing extremely fine-grained clayey masses, with bright colors. Possibly this is the light green earthy mineral described in some hand samples.

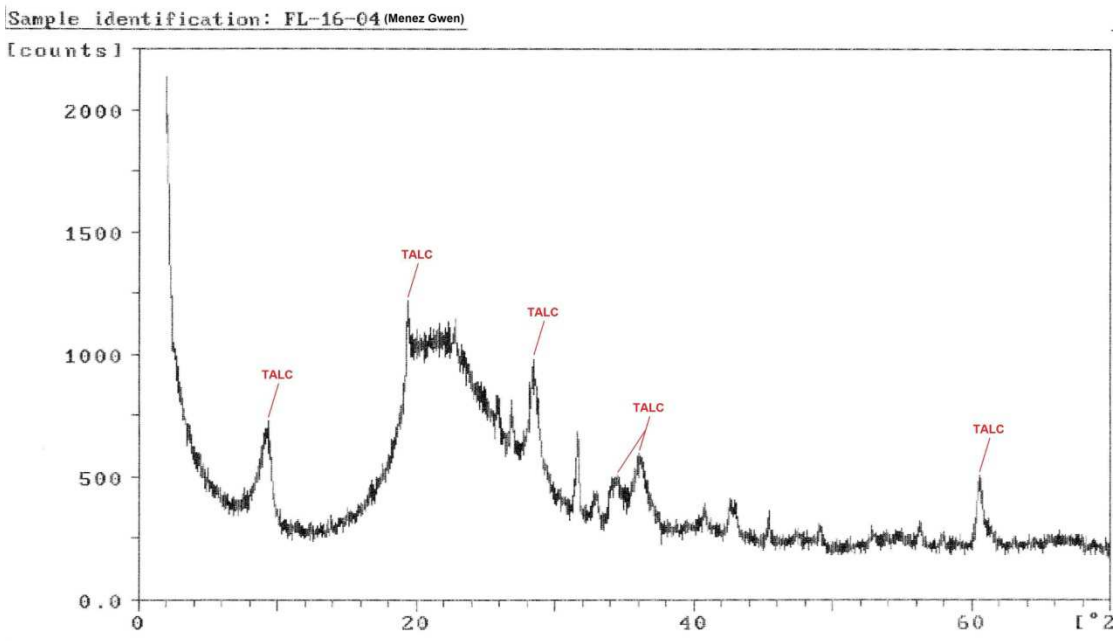

Figure 7.4 – Diffractogram from altered basaltic fragment of a *slab* sample from Menez Gwen where most of the talc peaks were detected.

Talc is another phyllosilicate detected by X-ray diffraction in a piece of basalt from MG (Figure 7.4). This is a secondary mineral formed by the alteration of magnesium silicates, such as olivine, pyroxenes and amphiboles. More often appears in low grade metamorphic rocks and associated with serpentinized ultramafic igneous rocks. It was recently described in several Mid-Atlantic Ridge hydrothermal sites hosted in ultramafic rocks: in Mount Saldanha sediments (Dias & Barriga, 2006) and in Rainbow serpentinites (Costa, 2005). Talc was also

found by electron microprobe studies within a basaltic clast from Sea Cliff hydrothermal field (Zierenberg *et al.*, 1995), replacing an olivine phenocryst.

Another mineral given by X-RD is a recently discovered mineral – motukoreaite (aluminum-magnesium hydrosulfate) (Fig. 7.5). It was found in one of the altered basalt Menez Gwen samples powder (FLDR-09). Motukoreaite apparently forms as a low temperature alteration product during seawater-basaltic glass interaction, and has a widespread occurrence (Zamarreño *et al.*, 1989).

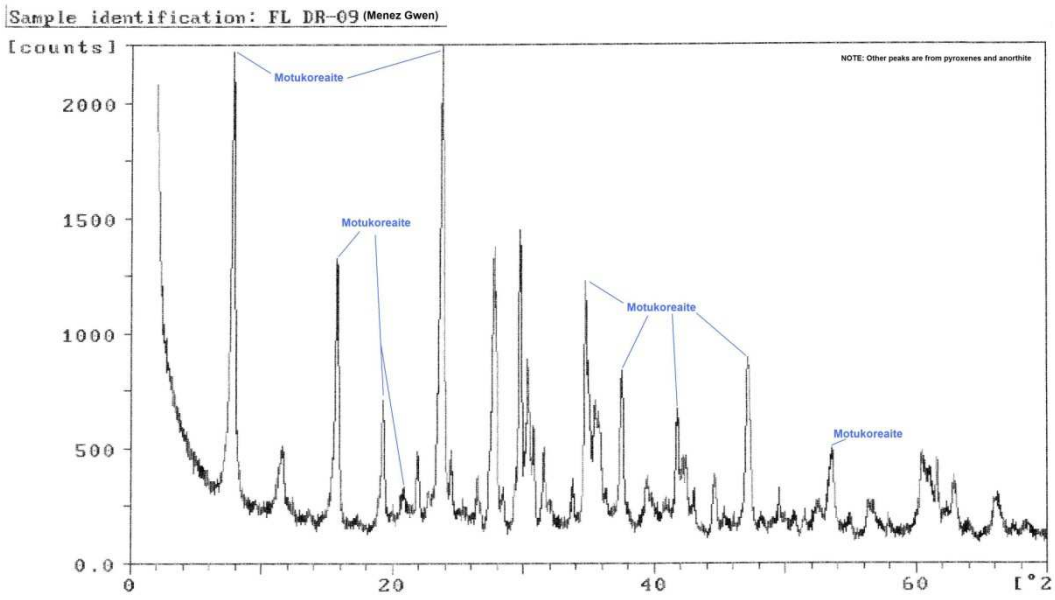

Figure 7.5 – Difractogram from altered basaltic fragment of a *slab* sample from Menez Gwen where a recently identified mineral was detected – motukoreaite.

7.2. MASS-BALANCE ANALYSIS

Mass balance studies using the isocon method (Grant, 1986) were made to determine and confirm the mobility of the elements in basalt during the hydrothermal process that is responsible for the breccia consolidation.

We compared chemical compositions of different basalt fragments both from Lucky Strike and Menez Gwen, in different stages of alteration. Relevant data for major and some trace elements were plotted assuming on one hand that alumina is constant (so we calculate the isocon for "Alconst" fig. 7.6), and on the other hand that the total mass of the fragments is constant (fig. 7.7). This difference is mostly due to the fact that in samples from MG the alumina is not constant.

Elements that have no changes in concentration from the fresh pieces to the altered ones will plot on the on the isocon lines represented in the diagrams. Elements that are enriched relative to the fresh composition will plot above those lines, and depleted elements will plot bellow.

The intermediate cases of alteration show a clear enrichment in silica (SiO_2) and in hydrothermal components as SO_3 and BaO. These ones are certainly related with the high content in barite in the LS and MG *slabs*. Magnesium (MgO), manganese (MnO) and also calcium (CaO) and iron (FeO) are strongly depleted in the altered fragments. This is expressed in the isocon plot of figure 7.6, where alumina (Al_2O_3) and titanium (TiO_2) are relatively immobile.

The results indicate a clear hydrothermal origin for the alteration. There is an important gain in elements like SiO_2, BaO, SO_3, and as well in chalcophilic elements, consistent with the presence of sulphide chimney fragments.

Considering still the intermediate cases of alteration, TiO_2 and Al_2O_3 have been relatively immobile in samples from LS, but in MG samples the later one is enriched. This observation is consistent with what was stated in 7.1 about the raise in aluminum associated with a phased replacement process of alteration where clay minerals, like smectites, are involved (Zierenberg *et al.*, 1995).

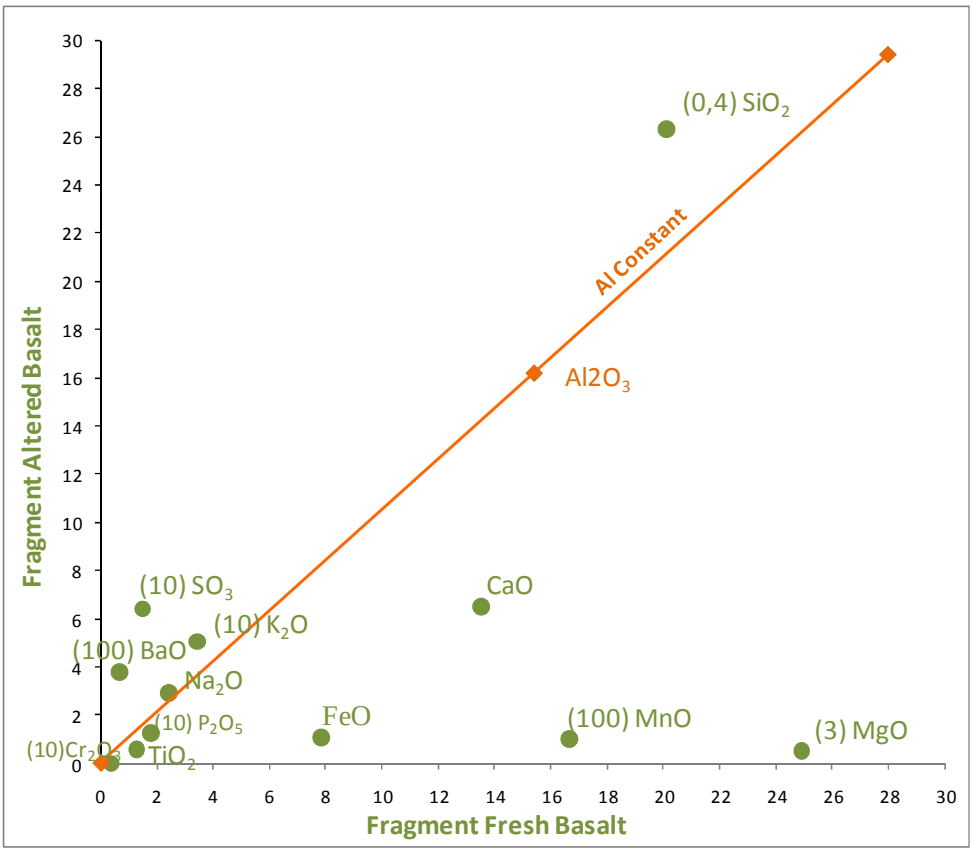

Figure 7.6 – Isocon plot for chemical composition of Lucky Strike basaltic fragments (sample FL DR-03-05). Contents are in weight percent. Some elements are ratioed by factors (in parentheses) to reduce the scale of the plot.

Chromium (Cr_2O_3) and potassium (K_2O) have random behavior in samples of both hydrothermal fields, whereas CaO, MgO, MnO and FeO are strongly depleted in both LS and MG samples.

The extreme cases of basalt alteration, evidenced by the petrography, are confirmed by the mass balance studies, also using Grant's method. We were able to recognize a clear silicification of the basalt fragments. All elements are mobile, even Al_2O_3 and TiO_2 (Fig. 7.8). Some fragments are completely silicified with content in silica higher than 90 wt%.

In fact, petrographic observations clearly indicate addition of silica to the altered basalts by substitution of the basalt mineralogy, by deposition in basalt vesicles and by deposition between basaltic fragments. The mass balance data presented here support the macro and microscopic studies in what seemed a substitution process of silicification, near 100% in extreme cases, where the fragments have a white earthy appearance but retain the original volcanic vesicular texture.

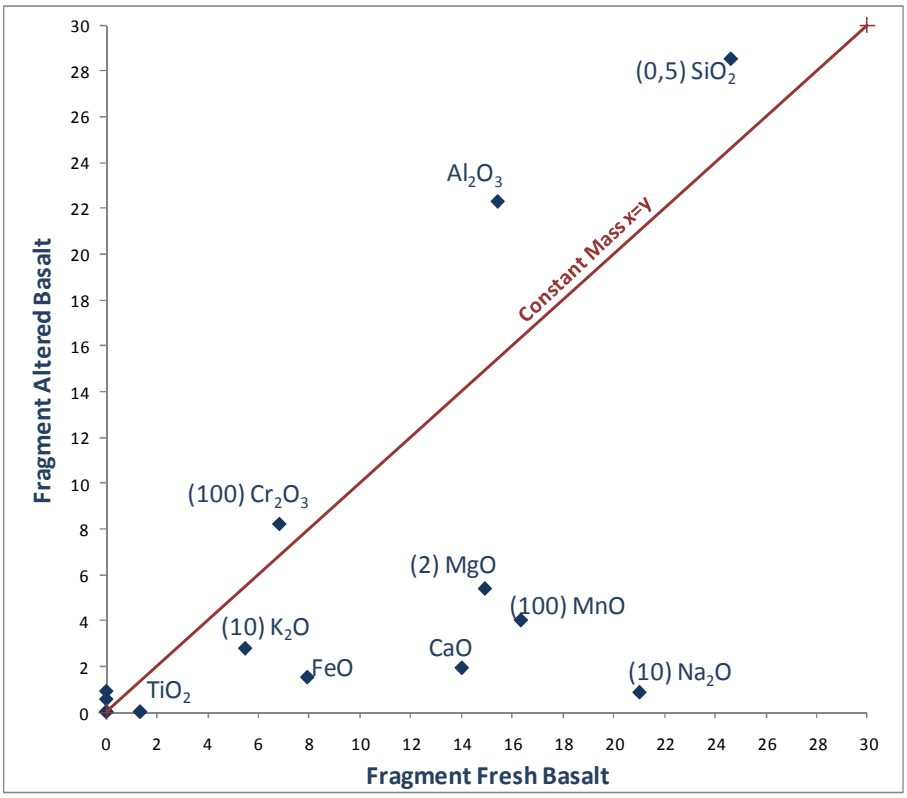

Figure 7.7 – Isocon plot for chemical composition of Menez Gwen basaltic fragments (samples FL-30-03 – fresh and FL-17-06 – altered). Contents are in weight percent. Points near the origin are from minor elements (Cu, Zn, Ag, Co). Some elements are ratioed by factors (in parentheses) to reduce the scale of the plot.

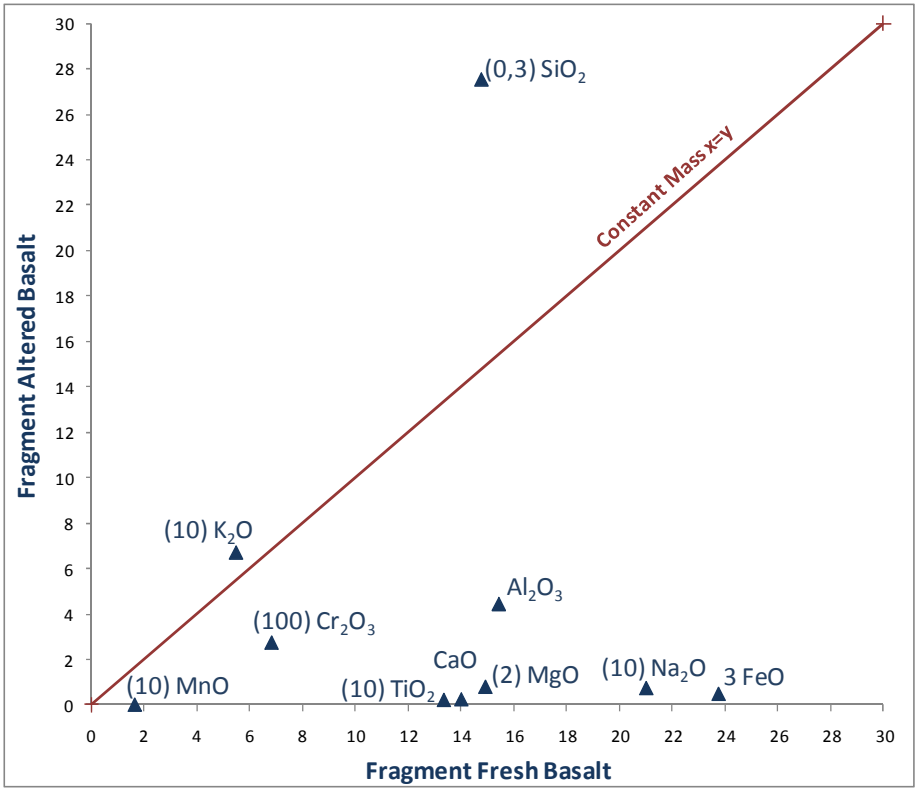

Figure 7.8 – Isocon plot for chemical composition of Menez Gwen basaltic fragments (samples FL-30-03 – fresh and FL-17-06 – altered). Contents are in weight percent. Some elements are ratioed by factors (in parentheses) to reduce the scale of the plot.

7.3. STRONTIUM ISOTOPIC DATA

The purpose of the strontium isotopic analyses was to find a possible origin for the altering hydrothermal fluids. Therefore we decided to study the altered basaltic fragments and also the barite crystals frequently found in some *slabs*. These elements were then carefully separated from the samples and prepared for the method used to determine strontium isotope contents.

Problems that we suppose happened during the chemical preparation of barite samples disabled the use of the data obtained. However, the analysis for the altered basaltic fragments was successful (Table 7.2).

Table 7.2 Strontium isotope composition of altered basaltic fragments from Lucky Strike (LS) and Menez Gwen (MG) samples. Strontium content for the samples where fragments were separated. *Data from Dosso *et al.*, 1999; **Data from Von Damm *et al.*, 1998.

Sample	Site	87Sr/86Sr	Sr (ppm)
FL-29-01	LS	0,70365	367,00
DV-19-12	LS	0,70440	2167,00
FL-17-06	MG	0,70450	301,00
ALV 2608-2-2E	LS	0,70702	435,00
DV2-12	MG	0,70556	6216,00
FL-17-04B	MG	0,70521	301,00
FL-18-08	LS	0,70667	251,00
FL-30-05	MG	0,70805	339,00
Basalt *		0,70313	168,00
Seawater **		0,70900	7,45
Hydrothermal Fluid LS **		0,70378	7,71

The Sr isotope ratios analyzed for the LS and MG altered basaltic fragments were plotted versus inverse Sr content (Fig. 7.9). Compositions of seawater, hydrothermal fluid (Von Damm *et al.*, 1998) and basalt (Dosso *et al.*, 1999) from those sites were used to compare the results. Our samples have Sr isotope compositions intermediate between those of seawater and the hydrothermal fluid indicating mixing of these two types of fluid. However, their content in Sr is high, due to the elevated concentration of this element in the basalts of the region which are rich in barite.

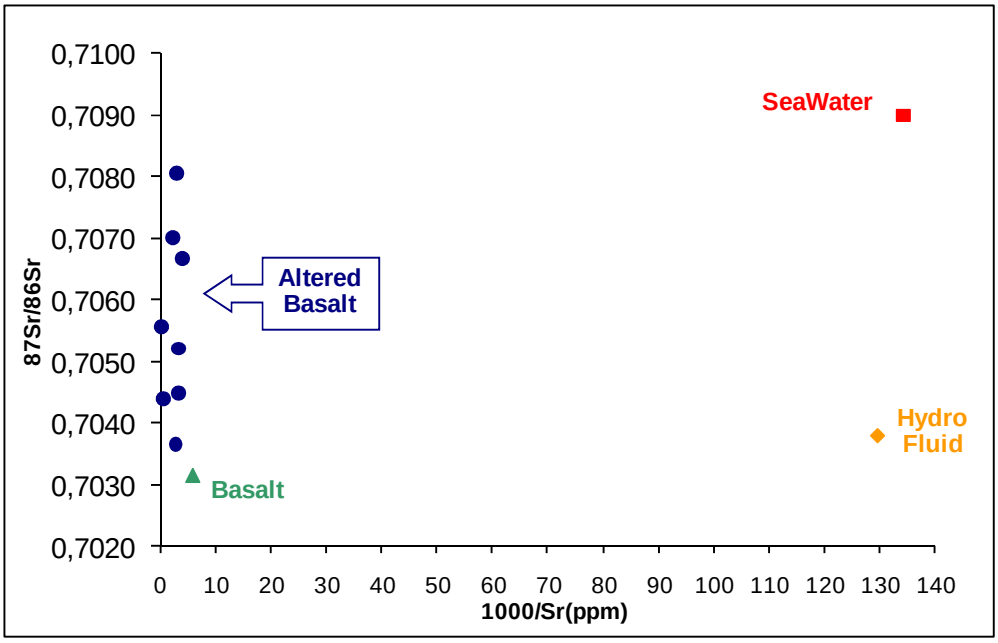

Figure 7.9 – Strontium isotope ratios versus inverse Sr content of the Lucky Strike and Menez Gwen samples where altered basaltic fragments were separated. Compositions for basalt, seawater and hydrothermal (see Table 7.2) were ploted for comparison.

7.4. SILICIFICATION

Silification is the main process resulting from hydrothermal fluid circulation that alters the basaltic components of the *slab*. This alteration process leads, in extreme cases, to the complete replacement by silica, as can be clearly seen in binocular microscope photos (Figure 7.10).

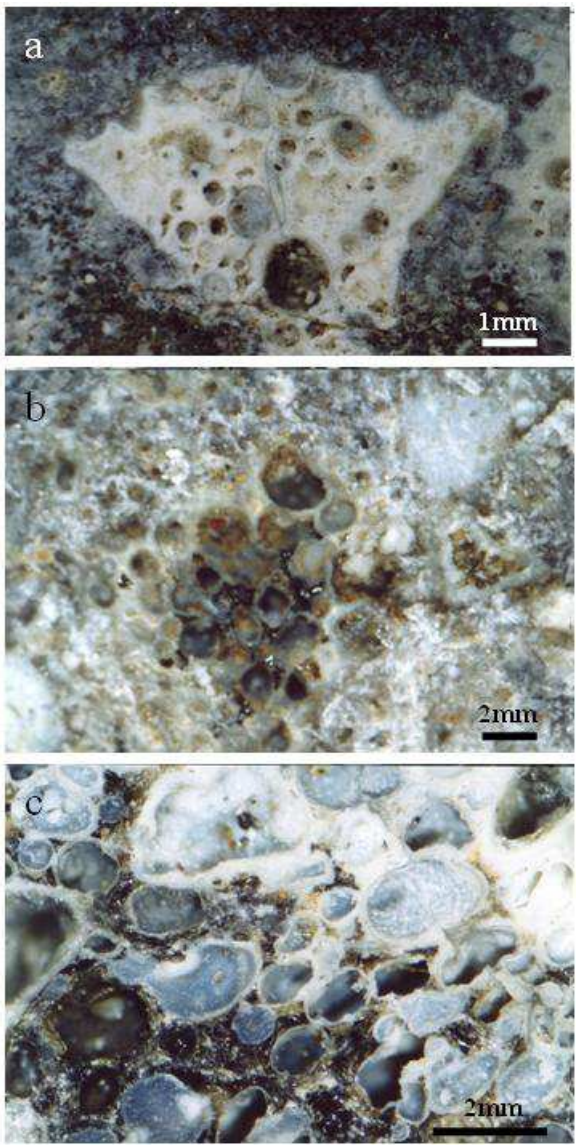

Figure 7.10 – Silica replacement in basaltic fragments from hydrothermal breccias (binocular microscope photos). (**a**) Piece of basalt entirely silicified (**b**) Inner part of nor complete silicified fragment; in the photo centre is it possible to recognize fresh basalt; (**c**) Detail from (b).

The determination of the possible forms of silica in our samples was made initially by petrographic studies, then by x-ray diffraction and by Scanning Electron Microscope (SEM). The first petrographic approach indicates predominant amorphous silica, probably some chalcedony, and rare quartz.

Chalcedony was not confirmed by microprobe points. What appeared to present optical characteristics of this fibrous form of silica is probably the interlayred silicate of smectite/chlorite referred in 7.1 or the amorphous material composed of silica and aluminum.

Quartz was observed in microscopic scale, and confirmed with microprobe, in two dredged samples from Lucky Strike (Fig. 7.11). The rare crystals are inside altered basaltic fragments surrounded by amorphous material composed of silica and aluminum.

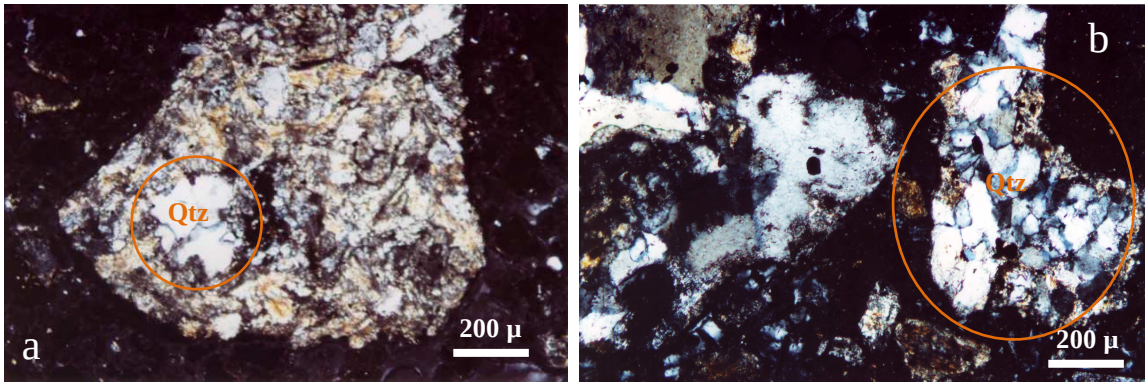

Figure 7.11 – Photomicrographs showing quartz crystals inside altered basaltic fragments in *slab* samples dredged in Lucky Strike. (**a**) Quartz crystals surrounded by amorphous material composed of Si and Al (sample FL DR-04-02; X pol.); (**b**) Quartz crystals in granular texture (sample FL DR-05-03; X pol.).

Opal and cristobalite are two forms of poorly crystalline silica that could not be confirmed by X-ray diffraction. Several of the analyzed difractograms show some of the peaks attributed to those forms of crystalline silica, but the general patterns are from amorphous material, therefore its presence is not certain.

The fine structural details of siliceous products were observed using Scanning Electron Microscopy revealing the presence of silica gel not well crystallized (Fig. 7.12) which is proposed in an experimental study by Oehler (1976). From small poorly developed microspheres (Fig. 7.12a/b/c) to greater and well developed structures (Fig. 7.12d/e), the similarity of the synthetic structures studied by this author and the textures observed in our samples is remarkable. The biggest microspheres show “honeycomb-textured” clearly different from the substrate material. The spheres are sometimes joined locally with this substrate through “bridges” of silica (Fig. 7.12f) as observed also by Oehler. Fractured surfaces of microspheres showing a polygonal network of ridges are observed in one of our samples. Oehler suggests that these features may correspond to anhedral quartz grain boundaries.

The experimental work cited reports formation of synthetic quartz microspheres after silica gel, suggesting that from amorphous silica structures we may evolve to crystalline forms of chalcedony or quartz. Process that can probably explain the presence of quartz in some of the silicified basalt fragments (Figure 7.11).

Ohmoto Rimstidt and Barnes (1980) have shown experimentally that the rate of reaction ($H_4SiO_4(aq) \Rightarrow 2H_2O + SiO_2(qtz)$), for a given mass of fluid, decreases linearly with decreasing surface area of solids (e.g., silicates) on which silica can nucleate, and that the rate decreases also with decreasing temperature. When fluid mixing occurs above the seafloor, the surface area available for the nucleation of quartz is essentially zero, and the cooling rates are very fast; the combined effects, therefore, impede quartz nucleation. This explains why silica is virtually absent in the smokers and sulfide chimneys along the mid-ocean ridges. In fact, the lack of silica in the primitive black ore can be used as evidence that most of the primitive black ore minerals in the Kuroko deposits crystallized from the fluid mixtures above the seafloor.

Precipitation of silica is favored in the stockwork zone, because the highly fractured rocks provide large surface areas for silica to nucleate, and because the cooling rates are slower than in the case of fluid mixing above the seafloor.

Consideration of the kinetics of silica precipitation also leads to the suggestion that the ferruginous chert layers (silica + hematite + barite) that occurs above the massive sulfide ores in many VMSDs were formed by mixing of hydrothermal fluids with cold seawater mostly within unconsolidated sediments, rather than by mixing of fluids above the seafloor; that is, they formed during the early diagenesis of the sediments rather than being truly syngenetic.

Figure 7.11 (next page) – Scanning electron micrographs of silica gel microspheres from *slab* samples collected Menez Gwen (DV2-12 and FL-17-06). (**a**) Overview of the smaller observed microspheres; (**b**) detail from (**a**) where some microspheres are not individualized; (**c**) higher magnification of (**b**); (**d**) well developed microspheres in a cavity, note the different texture of the surrounding materials; (**e**) microsphere in high magnification; (**f**) silica "bridges" joining the microspheres to the amorphous silica matrix; (**g**) "lace-work" amorphous silica matrix; (**h**) silica matrix detail. (All the images were taken using a PHILIPS SEM equipped with an Energy Dispersive X-ray Spectrometer at the Department of Deep Environment of IFREMER, Brest).

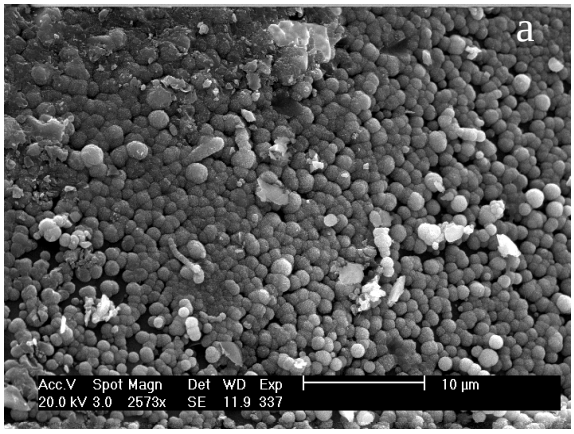
a
Acc.V Spot Magn Det WD Exp
20.0 kV 3.0 2573x SE 11.9 337
10 µm

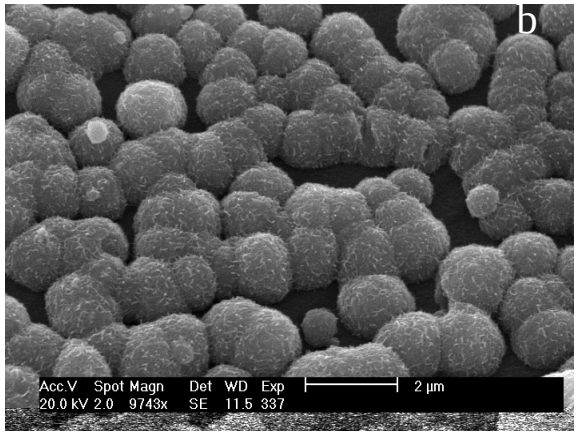
b
Acc.V Spot Magn Det WD Exp
20.0 kV 2.0 9743x SE 11.5 337
2 µm

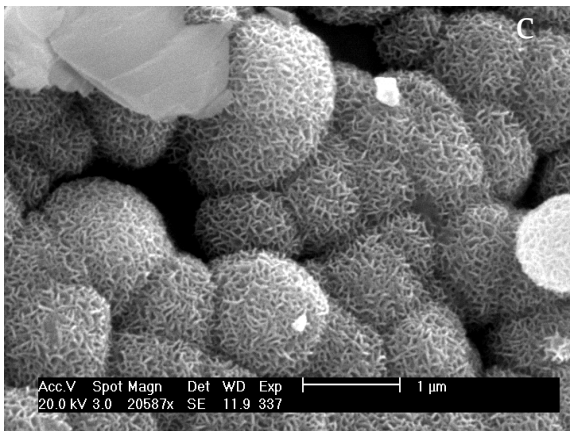
c
Acc.V Spot Magn Det WD Exp
20.0 kV 3.0 20587x SE 11.9 337
1 µm

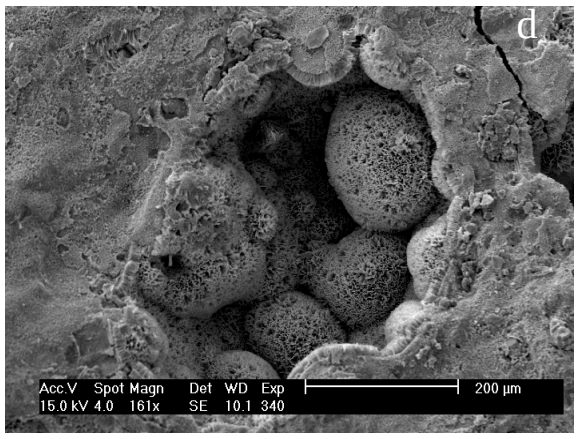
d
Acc.V Spot Magn Det WD Exp
15.0 kV 4.0 161x SE 10.1 340
200 µm

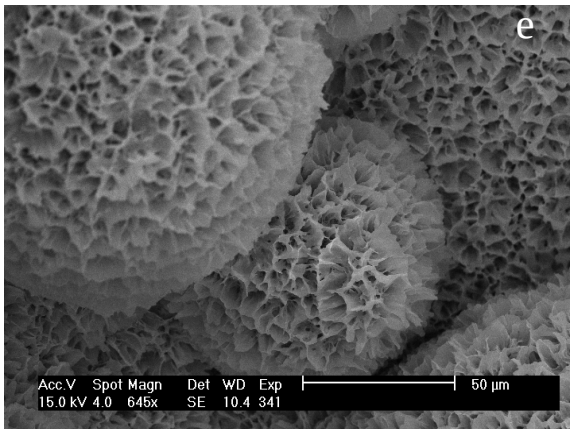
e
Acc.V Spot Magn Det WD Exp
15.0 kV 4.0 645x SE 10.4 341
50 µm

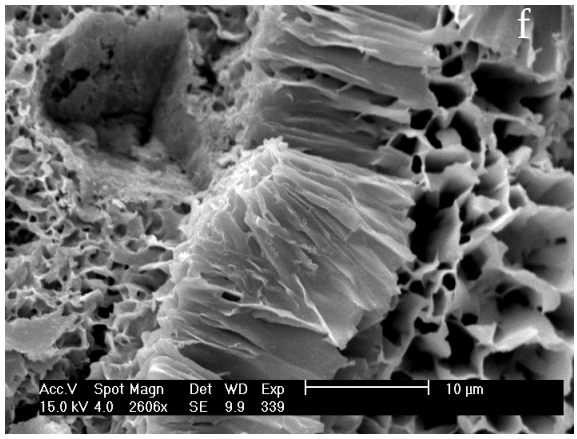
f
Acc.V Spot Magn Det WD Exp
15.0 kV 4.0 2606x SE 9.9 339
10 µm

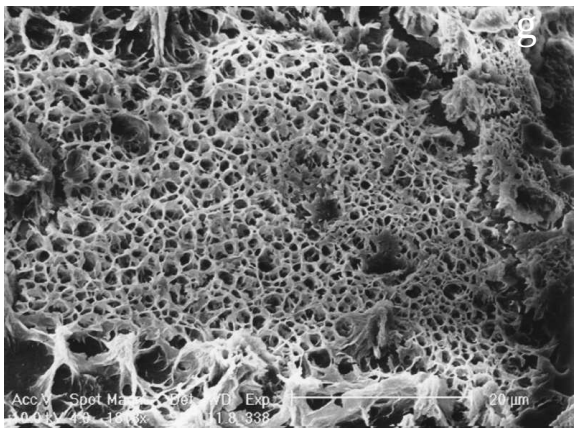
g
20 µm

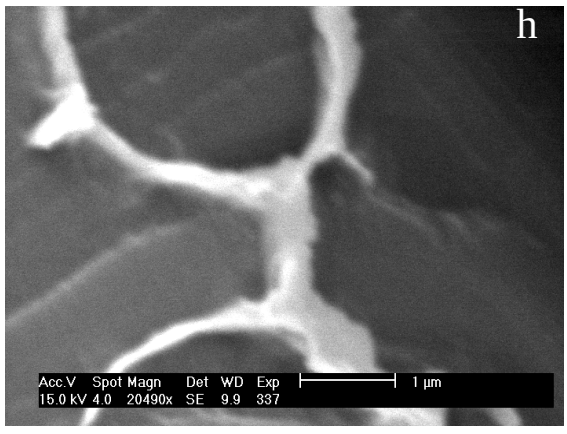
h
Acc.V Spot Magn Det WD Exp
15.0 kV 4.0 20490x SE 9.9 337
1 µm

8. DISCUSSION AND CONCLUSIONS

"*Nada nos pede mais trabalho e arte do que a simplicidade*"

José Tolentino Mendonça – Theologian and Portuguese writer

8.1. ANCIENT EQUIVALENTS FOR THE HYDROTHERMAL BRECCIAS

Since the first discovery and description of recent mineralized submarine hydrothermal deposits, comparison with ancient volcanic massive sulphide deposits is appropriate. Several studies (Barriga & Fyfe, 1988; Zierenberg et al., 1995; Prokin & Buslaev, 1999; Doyle & Allen, 2003; Herrington *et al.*, 2005; Glasby *et al.*, 2008) prove that the processes are very similar, even if the tectonic settings may be slightly different.

On the contrary, studies on ancient analogues to the hydrothermal breccias are scarce.

An introductory statement is necessary concerning the comparisons made here: detailed petrographic, analytical and geochemical studies of similarities between the ancient siliceous sediments and the modern equivalents are required, especially if we consider the amount of data available from the old Iberian Pyritic Belt sulphide deposits. We are going to consider four VMS deposits in different geological settings and with different ages: Turner-Albright deposit, U.S.A., Kuroko deposits, Japan, south Urals deposit, Russia, and the Iberian Pyrite Belt Feitais deposit of Aljustrel, Portugal.

Primarily we are going to consider the study that compares the recent Sea Cliff hydrothermal field and the associated hyaloclastite silicified breccia, with the older Turner-Albright deposit, southern Oregon, U. S. A. (Zierenberg et al., 1995 and references therein). This work was already cited in chapter 7 since the hyaloclastite breccias are very similar to our breccias.

The Turner‐Albright sulfide deposit is part of the Josephine ophiolite and it was formed on and below the seafloor during Late Jurassic volcanism at a back arc spreading center. Metalliferous sediments and massive sulfides in the deposit occur overlying and within basaltic pillow lavas and probably were formed on the seafloor at hydrothermal vents, similar to sulfide‐depositing hot springs on modern spreading centers. Most of the sulfide mineralization formed below the seafloor in the olivine basalt hyaloclastite erupted near the time of mineralization.

Many features referred by these authors for this deposit can be compared with the hydrothermal breccias in the present study: textures of the breccias fragments include clasts

interpreted as devitrified basaltic glass with some fragments retaining chromium spine1 microphenocrysts, just like we found in some of the breccias' basaltic fragments (see chapter 6). The basalts from the Turner-Albright deposit are extensively silicified in part by exhalative processes on the paleoseafloor as we observe in some areas of both hydrothermal fields studied here. In that old deposit other important processes of mineralization are recognized in the shallow subsurface: cementation and replacement of a thick sequence of basaltic hyaloclastites by silica (Zierenberg et al. refer some silicified fragments with textures indicative of deposition as amorphous silica), forming a thin silicified massive sulfide cap over the deposit restricting the flow to the hydrothermal system. Both processes are, as we propose in this study (see next section), taking place in the formation of the hydrothermal breccias. The authors suggest that the high silica concentrations required for deposition of amorphous silica were established by alteration of highly reactive basaltic glass.

Kuroko deposits of the Hokuroku and other districts in Japan are zoned, massive, stratabound, polymetallic sulphide-sulphate deposits concealed under Miocene calc-alkaline lavas and pyroclastics (Hashimoto, 1977). In the hanging wall of the orebodies there is a hydrothermal formation, a ferruginous chert, the "Tetsusekiei bed". In some deposits this chert bed is distributed laterally over an area twice the size of the orebody, and may achieve a thickness of several meters. The Tetsusekiei bed consists of aggregates of cryptocrystalline quartz containing very fine hematite flakes. Barite and some sulphides (mostly pyrite) are also found in this siliceous horizon. Moreover the cherts can occasionally occur in the lower part of the orebody as small discontinuous lenses. These observations (the sulphides and the random location of the cherts near the ore) can support the idea of an original siliceous layer on the seafloor (foraminifera and radiolarian fossils are frequently found in the Tetsusekiei bed) being formed at the same time of the underlying mineralizations, as we propose for Lucky Strike and Menez Gwen.

A schematic model of Kuroko type deposit is presented in figure 8.1 showing a consistent stratigraphical succession of ore and rock types as follows (Evans, 1987): (1) hanging wall – upper volcanic and/or sedimentary formation; (2) ferruginous quartz zone – chiefly hematite and quartz; (3) barite ore zone; (4) Kuroko or black ore zone sphalerite-galena-barite; (5) Oko or yellow ore zone – cupriferous pyrite ores; (6) Keiko or siliceous ore zone – copper bearing, siliceous, disseminated and/or stockwork zone; and (7) footwall – silicified rhyolite and pyroclastic rocks. This structure can be compared with recent hydrothermal mounds emplaced in volcanic rocks where the succession of layers is similar, namely Lucky Strike site (or TAG

hydrothermal mound) in spite of the differences in tectonic setting and also the degree of uncertainty with the subseafloor structure of this mineralized hydrothermal field.

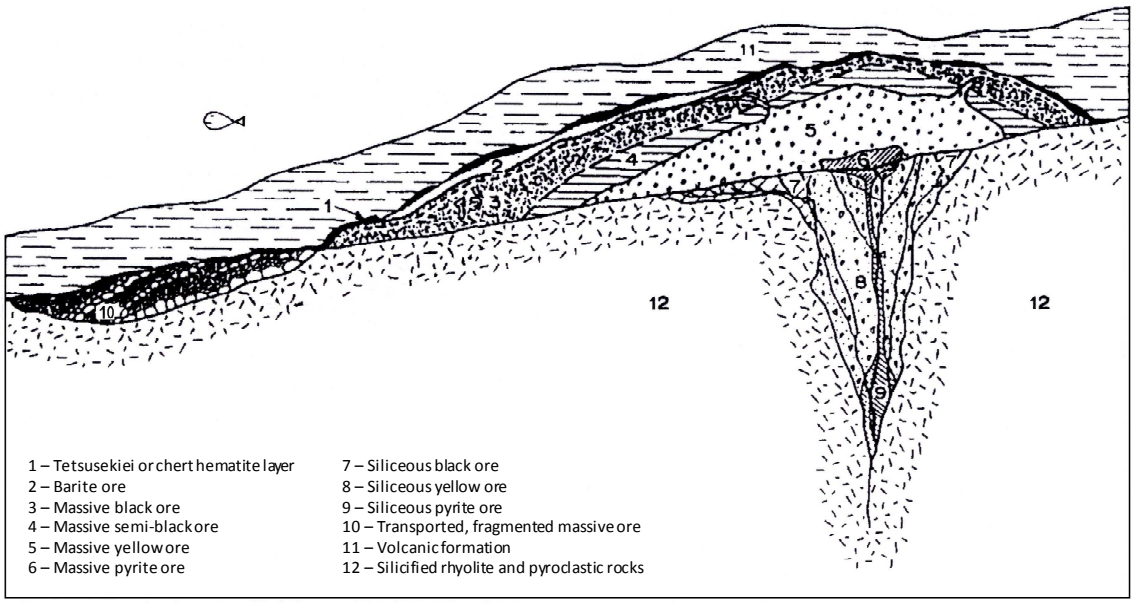

Figure 8.1 – Idealized Kuroko type deposit modified after Ohmoto (1996) and Evans (1987).

VMS deposits of the South Urals depict Paleozoic ages, from Ordovician to Permian, under diverse geotectonic and paleogeographic conditions and within zones of varying deformation and metamorphism (Prokin & Buslaev, 1999). The exceptional degree of preservation in the Urals has permitted the identification of early seafloor clastic and hydrolytic modification to the sulphide assemblages prior to diagenesis (Herrington *et al.*, 2005), meaning that more than 400 Ma ago, if we could dive on the Urals ocean it would probably be possible to sample some hydrothermal breccias. V. Maslennikov identified that early process on the seafloor as halmyrolysis (*in* Herrington *et al.*, 2005) – relating all the pre-diagenetic processes involving seawater and diverse components of all types of seafloor sediments or, in other words, the geochemical reaction of seawater and sediments in an area of little or no sedimentation. In detail, in these deposits, the seafloor reworking can be seen in oxidized layers of clastic sulphide showing secondary sulphides and increased gold contents. It appears that the process can be scaled up to the complete reworking of massive sulphide bodies on the seafloor forming clastic layers of volcanic rocks showing intense interaction with oxidized seawater (Herrington *et al.*, 2005).

Halmyrolysis may lead to complete removal of components from the system and thus may be an ore-forming process itself, while diagenesis typically results in mineralogical change without bulk chemical addition and subtraction. These seafloor effects are potentially important features, particularly in longer-lived seafloor ore systems even though analyses of these effects in ancient VMS systems are difficult, given, in many cases, a relatively high degree of metamorphism, which may obscure early textural features (Herrington *et al.*, 2005 and references therein).

The giant Feitais orebody of Aljustrel (Iberian Pyrite Belt, Portugal) is hosted in rocks depicting clear signs of having been affected by mineralizing fluids. The study made by Barriga & Fyfe (1988) of hanging-wall rocks and alteration above the mineralized deposits shows that the cherts on top of the sulfide deposit result from hydrothermal alteration of laterally equivalent Fe and/or Mn-rich jaspers, which are also products of hydrothermal activity. These siliceous and metalliferous sediments (cherts, jaspers and Mn concentrations) constitute a well-defined horizon immediately above the Aljustrel Volcanics, called by the authors as the Aljustrel Jasper.

The sulfide mineralization occurs associated with later stages of (felsic) explosive volcanism which took place in early Carboniferous times. It is another ancient VMS system where metamorphism may obscure early textural features. Actually, primary textures are obliterated by recrystallization in cherts and jaspers samples, but in the manganiferous recrystallized black cherts sometimes it is possible to observe the original form of globular aggregates (Barriga & Fyfe 1988). This is a very similar texture with the ones we found in the hydrothermal breccias formed at present in the seafloor.

The genetic model initially proposed by Barriga & Fyfe (1988) support that the Aljustrel Jasper formation took place first, and the sulfides formed under a blanket of unconsolidated siliceous sediment. Later on, microscopic studies of some inclusions found at the hanging wall contact of the massive sulphides lens, proved that they are fragments of chert (Barriga & Fyfe, 1991). In fact, we have a siliceous blanket over the mineralization with breccia like textures. Here the sulphide fragments are cement by siliceous and metalliferous precipitates. So, probably this is our closest analogous for the Lucky Strike and Menez Gwen breccias.

This hypothesis needs to be investigated in detail. All the studies indicate that the Feitais big sulphide body has no traces of oxidation or intercalated oxidic facies, meaning that the

ores were not exposed on the ancient ocean floor. But, is there any trace of sulphide material as inclusion in the Aljustrel Jasper?

8.2. GENETIC MODEL FOR HYDROTHERMAL BRECCIAS FORMATION

Hydrothermal breccias explored in this study reveal a two component texture: detrital and hydrothermal cement.

Where do the detrital fragments come from? These have essentially two natures: basaltic and sulphides. Foraminifer fossils were rarely observed.

Pieces of sulphides are not so frequent. They result from *in situ* fragmentation of ancient chimneys due to volcanic and tectonic movements.

Basalt fragments are dominant and the main sources are the surrounding formations – Lava Lake Formation and Volcanic Breccia Formation. Pieces from Lava Lake are basaltic devitrified glass with low vesicularity. The highly vesicular and porphyric fragments belong to Volcanic Breccia. These are probably formed as a result of magmatic explosivity which explains the vesicles abundance and also the presence of shards with extremely elongated and deformed vesicles (Eissen *et al.*, 2003). Local evidences showed that this volcanic activity might have occurred in several episodes repeatedly over relatively long periods of time (more frequently in Menez Gwen than in Lucky Strike) (Fouquet *et al.*, 1998a).

All these types of fragments suffered short transportation (probably due to tectonic movements) from the volcanic hills and would then be grouped resulting in heterogeneous deposits. Here we can find randomly distributed pieces from different explosive events: the older ones may already exhibit hydrothermal alteration and the young ones are fresh. This can explain the presence of basaltic clasts showing different degrees of alteration, in the same sample Hydrothermal activity previously started brings the precipitates responsible for breccia formation.

What is the origin of cement (or groundmass) of the *slabs*? It is a hydrothermal precipitate composed mainly of amorphous silica and sulphides. But the main question deals with the origin of the fluid that brings the hydrothermal minerals. Is it seawater that enters the

sea floor only superficially and doesn't mix with the fluid that circulates under the surface? Is it hydrothermal fluid coming directly from inside the crust? Or is it a mixture of those two types of fluid?

This study tends to indicate the last hypothesis. The model is proposed in Figure 8.2 and is based on the behavior of the silica transported by the hydrothermal fluid. The main component of the breccias groundmass is amorphous silica which tends to precipitate when the fluid is conductive cooled (Fouquet *et al.*, 1998b) (Figure 8.2b). The process evolves gradually from an initial stage where we have just the fragments and circulating seawater – stage 1 in Figure 8.2a. The ascending hydrothermal fluid mixes with the seawater which favors the precipitation of the sulphide components (stage 2 in Figure 8.2a). Sealing of the initially loose fragments begins, the temperature rises below, and the processes of mixing fluid circulation and conductive cooling are simultaneous (stage 3 in Figure 8.2a). At this stage the fluid becomes oversaturated with respect to amorphous silica. This form of silica can precipitate in the open spaces of the porous sulphides and seal the system. Normally this can happen at low temperatures. At this stage the hydrothermal breccias is formed creating an impermeable cap rock at the surface. Once the fluid is trapped under this impermeable layer, conductive cooling is enhanced and mixing with seawater is restricted, making the precipitation of amorphous silica more efficient (stage 4 in Figure 8.2a).

The strontium isotope studies made for the Lucky Strike and Menez Gwen altered basaltic fragments (section 7.3) also support the mixing hypothesis above defended.

REPLACEMENT

Silica in its amorphous form is a major component in the hydrothermal breccias. Part of this silica is originated by chemical precipitation from a fluid as stated before. But petrographic analyses have show that basalt replacement is also an important process for adding silica to the *slab* (section 7.4).

Replacement is defined as a change in composition of a mineral or mineral aggregate, presumably accomplished by diffusion of new material in and old material out, without breakdown of the solid state. This is out might happened with the *slabs´* basaltic fragments and hydrothermal silica, as we recognise fragments almost composed replaced by silica.

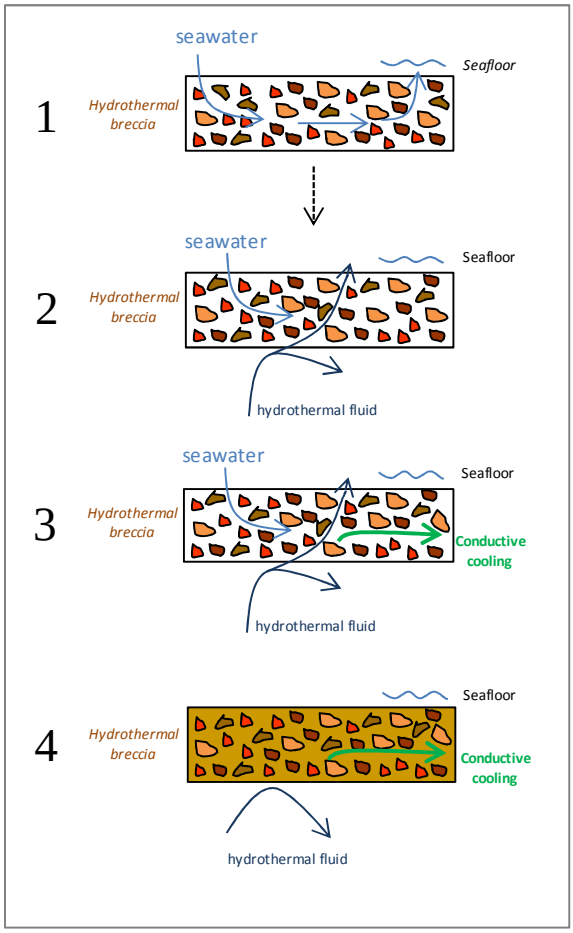

a

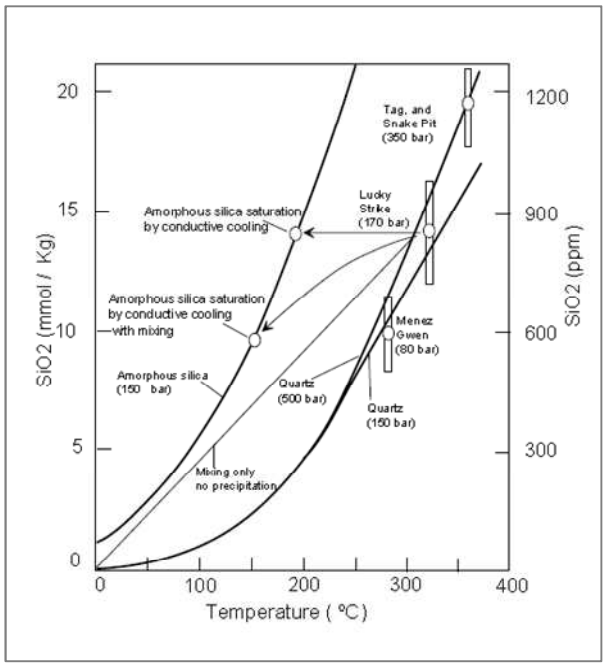

b

Figure 8.2 – Model for the formation of the hydrothermal breccia. (**a**) Sequential processes responsible for sealing the hydrothermal breccias: 1- Circulating seawater – no hydrothermal precipitates; 2 – Mixing fluids (seawater and hydrothermal fluid) – precipitation of sulphides (pyrite/marcasite and sphalerite); 3 – Mixing fluids with simultaneous conductive cooling – beginning of amorphous silica precipitation; 4 – Conductive cooling prevailing – continuous formation of amorphous silica – the hydrothermal breccia is formed . (b) Solubility curve for amorphous silica and quartz (Fournier, 1983 *in* Fouquet *et al.*, 1998b), with silica concentrations from hydrothermal sites at different depths. TAG end-member fluid is close to the saturation of quartz, explaining the quartz enrichment of deepest parts of this mound. Si concentrations in the fluids from Lucky Strike, Menez Gwenn were confirmed from Charlou *et al*. (2000), and TAG from Campbell *et al*. (1988).

Although most of the experimental analyses for basalt alteration indicate that Si (among other elements) is leached form the rock at high temperatures, the opposite elemental exchange trends can be observed (Hajash & Archer, 1980) in the shallow portion of the ocean crust due to low temperature alteration.

In the context of VMS deposits, subsea-floor replacement is also studied (Doyle & Allen, 2003) in a context that can be compared with recent processes in hydrothermal sites, in particular the subject of the present work. These authors refer the precipitation from syn-volcanic hydrothermal solutions, of ore-forming minerals within pre-existing volcanic deposits, meaning that replacement is synchronous with volcanism and diagenesis. The host deposits may be unconsolidated or lithified at the time of replacement. Subsea-floor

replacement in most cases probably includes components of infiltration and precipitation in open spaces (fractures, inter- and intra-particle porosity) as well as replacement of solid materials. They also argue that the replacement in old deposits might took place mainly in the meters of the oceanic crust, where the clastic facies are wet, porous and poorly consolidated.

Furthermore, supporting the similarity of ancient and actual hydrothermal processes in the shallow crust, the same authors sustained mixing between the upwelling hydrothermal fluid and cold seawater as a major cause of sulphide precipitation in VMS systems.

All the four factors that Doyle & Allen (2003) propose to influence subsea-floor replacement in VMS systems – permeability and porosity patterns of host lithofacies; the relative ease of replacement of host lithofacies (especially glassy materials); early formed alteration minerals during hydrothermal attack; and physiochemical characteristics of the hydrothermal fluid – are present in the hydrothermal breccias formation process.

8.3. FUTURE WORK

To enhance the knowledge of hydrothermal breccias associated with recent sulphide deposits and associated processes it is necessary:

- Study of isotope geochemistry – in order to have more assertive and strong conclusions in what concerns the origin of the fluids that forms the breccias it will be very useful to analyze hydrogen and sulphur isotopes;
- Detailed petrographic comparison studies with old analogous hydrothermal deposits - to consolidate the similarities already proved;
- Prepare a scientific drilling program in Lucky Strike hydrothermal site.

A detailed planned scientific program for drilling the sulphide deposit in lucky Strike can be made with minimum damage of the vents community. In the future, if eventually the richness of the deposit is confirmed, the mining industries will not be as careful as scientific groups performing the drilling.

In addition, we point out some of the good scientific reasons to drill Lucky Strike:

- Is one of the largest hydrothermal fields known (Fouquet,1997) – about 1 km in diameter;
- It is located in a slow spreading ridge where the formation of extensive mineralization is favourable;
- Better understand the volcanic and tectonic architecture at Lucky Strike;
- Relationship between magma chemistry (including volatiles), eruptive style and the depth and position on the volcanic complex;
- The nature and extent of hydrothermal alteration under the seafloor in the hydrothermal field;
- Relationship between volcanic evolution and hydrothermal activity – distribution and origin of permeability in explosive volcanic products and the consequences for alteration and mineralization of permeable volcanic materials;
- Determination of the types and spatial mineralization around the lava lake and their vertical extensions;
- Study the relations between the hydrothermal breccias and superficial sulphide with sub-superficial mineralization – confirming the role of hydrothermal breccias as cap rocks;
- Relations between sub-surface mineralization and the fluids expelled by the vents;
- Understanding the types and relations of microbiological communities in hydrothermal areas (deep biosphere and its relation with hydrothermal processes).

APPENDIX I – LUCKY STRIKE AND MENEZ GWEN SITES LOCATION

Lucky Strike and Menez Gwen hydrothermal sites location

Apart from the name, each site has one or more markers, from different cruises: US# - ALVIN 93 cruise (June 1993); DIVA# – DIVA1 cruise (June 1994); PP# – DIVA2(?) cruise (July 1994); Flores# – FLORES (July 1997)

Positioning references:
Zone Number: 25
Lucky Strike: X_0 – 562 000 Y_0 – 4 123 000
Menez Gwen: X_0 – 628 000 Y_0 – 4 185 000

Site/Marker(s)	X	Y	Z (Depth)	Latitude	Longitude
Lucky Strike					
"Statue of Liberty"/US1	2300	4580	1628	37º17,550N	32º16,467W
"Sintra"/US3/Flores15	2275	4517	1622	37º17,517N	32º16,483W
"Y3"/"2608Vent"*/DIVAI/ Flores14	2003	4474	1740	37º17,500N	32º16,667W
"Tour Eiffel"/ DIVAII,IV,V/ Flores16	2247	4160	1685	37º17,317N	32º16,500W
"Marker 4"/US4	2255	4045	1700	37º17,267N	32º16,517W
"Marker 6"/US6	2225	4085	1703	37º17,283N	32º16,517W
"Marker 7"/US7	2210	4090	1698	37º17,283N	32º16,533W
Flores28 (near US4, 6, 7)	2218	4048	1705	37º17,267N	32º16,517W
Flores30 (near US4, 6, 7)	2192	4052	1701	37º17,267N	32º16,533W
"Pipi de souris"/PP3	2069	4281	1687	37º17,396N	32º16,631W
"Isabel"/DIVAVIII/Flores22	2088	4237	1683	37º17,367N	32º16,617W
"Timor"/Flores26 (south *"Isabel")*	2130	4197	1689	37º17,350N	32º16,583W
"Nuno"/ DIVAX/Flores19	1660	4398	1722	37º17,450N	32º16,900W
"Hélène"/Flores17/"Crystal"**	1675	4324	1719	37º17,417N	32º16,883W
Flores18 (near *"Hélène"*)	1685	4355	1719	37º17,433N	32º16,883W
"Pico"	1670	4370	1727	37º17,446N	32º16,900W
"Catedral"	1875	4602	1731	37º17,570N	32º16,761W
"Bairro Alto"/Flores21/PP7/ PP8	1580	4659	1624	37º17,600N	32º16,950W
Flores20 (south *"Bairro Alto")*	1602	4628	1649	37º17,583N	32º16,933W
Flores26 (south *"Bairro Alto")*	1592	4580	1665	37º17,N	32º16,W
"Tony Blair"/Flores23	2127	4255	1686	37º17,367N	32º16,583W
"Mário Soares"/Flores24/ PP4	2126	4360	1677	37º17,433N	32º16,583W
"Elisabeth"/PP12/PP13/"Jason"**	1656	4858	1640	37º17,700N	32º16,900W
Menez Gwen					
"Mogued Gwen"/DIVAVI***	2145	4182	860	37º50,448N	31º31,254W
*Menez Gwen 2****	2445	4536	844	37º50,637N	31º31,046W

* Langmuir et al. (1997)
** Humphris et al. (2002)
*** Coordinates from PICO cruise (July 1998)

APPENDIX II – SAMPLES FROM LUCKY STRIKE AND MENEZ GWEN - LOCATION AND ANALYTICAL METHODS

Samples from Lucky Strike and Menez Gwen – Location and Analyze methods

[Each sample reference is related with the mission in what it was collected: ALV and AII – ALVIN 93 (June 1993); DV – DIVA 1 (June 1994); DV2 – DIVA 2 (July 1994); FL – FLORES (July 1997); PC – PICO (June 1998); SAL – SALDANHA (July 1998)]

	Sample	Type	Local	Petrography	Whole-rock Geoch. data	Chem. Microanaly.	XRD	Sr Isotope data	Latitude	Longitude	Depth(m)	Site
1	ALV2606-6-1	Slab	L. S.	x (2)	x				37º17,418N	32º16,497W	1685	
2	ALV2607	Sediment Core	L. S.						37º17,340N	32º16,518W	1696	St. Liber.(near)
3	ALV2608-2-2B	Slab	L. S.	x	x	x			37º17,267N	32º16,506W	1700	Marker 4
4	ALV2608-2-2E	Slab	L. S.	x (2)	x	x		x	37º17,267N	32º16,506W	1700	Marker 4
5	ALV2608-3-3B	Slab	L. S.	x	x	x (chromite)			37º17,319N	32º16,516W	1685	Tour Eiffel
6	ALV2608-4-1B	Slab	L. S.	x	x				37º17,319N	32º16,516W	1685	Tour Eiffel
7	AII-129-6	Altered Basalt	L. S.	x	x				Dredge			
8	AII-129-6	Fresh Basalt	L. S.	x	x				Dredge			
9	DV-1-6	Slab	L. S.	x	x				37º17,438N	32º16,625W	1700	Le Chimiste
10	DV-3-2	Slab	L. S.	x (2)	x	x (barite)			37º17,423N	32º16,497W	1623	
11	DV-4-9	Slab	L. S.	x					37º17,319N	32º16,516W	1685	Tour Eiffel
12	DV-4-10	Slab	L. S.	x	x				37º17,319N	32º16,516W	1685	Tour Eiffel
13	DV-8-3	Slab	L. S.	x					37º17,597N	32º16,804W	1702	
14	DV-8-4	Slab	L. S.	x (2)	x				37º17,516N	32º16,880W	1728	
15	DV-8-7	Slab	L. S.	x			x		37º17,199N	32º16,355W	1706	
16	DV-8-9	Slab	L. S.						37º17,297N	32º16,509W	1697	
17	DV-13-7	Slab	M. G.	x		x (sul+bar)	x		37º50,271N	31º31,306W	877	
18	DV-14-1	Slab	M. G.	x	x	x (sulph)			37º50,459N	31º31,353W	840	Mogued Gwen
19	DV-14-2	Slab (?)	M. G.	x					80m east of sample 26		856	
20	DV-14-3	Slab	M. G.	x		x (barite)	x		Near the previous samp.		856	
21	DV-14-4	Slab	M. G.	x		x			37º50,459N	31º31,353W	840	Mogued Gwen
22	DV-14-6	Slab	M. G.		x				37º50,459N	31º31,353W	840	Mogued Gwen
23	DV-15-3	Slab	M. G.	x	x				37º49,796N	31º31,084W	1003	
24	DV-16-1	Slab	M. G.	x	x	x			37º50,479N	31º31,202W	840	
25	DV-16-3	Slab	M. G.	x	x				37º50,479N	31º31,202W	840	
26	DV-16-4	Slab	M. G.	x			x		37º50,474N	31º31,250W	846	
27	DV-19-12	Slab	L. S.	x(2)	x		x	x	37º17,651N	32º16,811W	1665	
28	DV2-05A	Fresh Basalt	L. S.		x							Lava Lake
29	DV2-05B	Fresh Basalt	L. S.	x	x				37º17,486N	32º16,876W		Pico
30	DV2-12	Slab	M. G.	x	x			x	37º50,459N	31º31,353W	840	Mogued Gwen
31	FL-16-01	Basalt	M. G.				x		37º50,400N	31º31,410W	880	
32	FL-16-04	Slab	M. G.	x	x		x		37º50,450N	31º31,275W	845	
33	FL-17-04A	Slab (?)	M. G.	x					37º50,445N	31º31,312W	845	
34	FL-17-04B	Slab	M. G.	x			x	x	37º50,445N	31º31,312W	845	
35	FL-17-05	Slab	M. G.	x	x	x	x		37º50,445N	31º31,312W	845	
36	FL-17-06	Basalt/Slab	M. G.	x (10)	x	x	x	x	37º50,445N	31º31,312W	845	
37	FL-17-07	Slab	M. G.	x		x			37º50,445N	31º31,312W	849	
38	FL-17-10	Basalt	M. G.						37º50,970N	31º31,172W	955	
39	FL-17-11	Basalt	M. G.	x	x				37º51,171N	31º31,237W	850	
40	FL-17-12	Basalt	M. G.	x					37º51,063N	31º31,593W	913	
41	FL-17-13	Basalt	M. G.						37º51,018N	31º31,695W	912	
42	FL-18-04	Inact. Chim.(?)	L. S.						37º17,463N	32º16,609W	1675?	
43	FL-18-08	Slab	L. S.	x				x	37º17,314N	32º16,560W	1687?	
44	FL-18-09	Slab	L. S.	x (5)	x	x			37º17,330N	32º16,511W	1680?	
45	FL-19-02	Sediment Core	L. S.	x					37º17,428N	32º16,891W	1714	
46	FL-19-03	Sediment Core	L. S.		x				37º17,428N	32º16,891W	1714	
47	FL-20-02	Slab	L. S.	x (5)	x	x	x		37º17,292N	32º16,536W	1698	
48	FL DR-03-01	Slab	L. S.	x (2)		x			Dredge FL-DR-03			
49	FL DR-03-03	Slab	L. S.						Dredge FL-DR-03			
50	FL DR-03-05	Slab	L. S.	x (9)	x (A, B)	x			Dredge FL-DR-03			
51	FL DR-03-12	Slab	L. S.	x					Dredge FL-DR-03			
52	FL DR-03-13	Slab	L. S.	x	x				Dredge FL-DR-03			
53	FL DR-03-A	Slab	L. S.	x	x				Dredge FL-DR-03			
54	FL DR-04-02	Slab	L. S.	x (8)	x (A, B)	x	x		Dredge FL-DR-04			
55	FL DR-04	Basalt	L. S.		x				Dredge FL-DR-04			
56	FL-22-01	Basalt	L. S.						37º16,250N	32º15,800W	1800	
57	FL-22-02	Basalt	L. S.				x		37º16,300N	32º15,960W	1746	
58	FL-22-03	Basalt	L. S.				x		37º16,450N	32º15,880W	1738	
59	FL-22-04	Basalt	L. S.						37º17,020N	32º16,300W	1690	
60	FL-22-05	Basalt	L. S.	x					37º17,300N	32º16,500W	1703	
61	FL-22-07	Iron Oxides	L. S.						37º17,300N	32º16,500W	1703	

	Sample	Type	Local	Petrography	Whole-rock Geoch. data	Chem. Microanaly.	XRD	Sr Isotope data	Latitude	Longitude	Depth(m)	Site
62	FL-22-08	Basalt	L. S.	x					37º17,120N	32º16,900W	1562	
63	FL DR-05-01	Slab	L. S.	x (2)	x	x	x		Dredge FL-DR-05			
64	FL DR-05-02	Slab	L. S.	x			x		Dredge FL-DR-05			
65	FL DR-05-03	Slab	L. S.	x (3)	x (I, II)	x			Dredge FL-DR-05			
66	FL DR-05-A	Slab	L. S.	x					Dredge FL-DR-05			
67	FL DR-05-B	Slab	L. S.	x(2)	x	x			Dredge FL-DR-05			
68	FL DR-05-C	Slab	L. S.	x	x	x			Dredge FL-DR-05			
69	FL DR-08-02	Altered Basalt	L. S.	x	x				Dredge FL-DR-08			
70	FL DR-08-03	Altered Basalt	L. S.	x(2)	x	x			Dredge FL-DR-08			
71	FL DR-08-04	Slab	L. S.	x	x	x	x		Dredge FL-DR-08			
72	FL DR-08-05	Altered Basalt	L. S.						Dredge FL-DR-08			
73	FL DR-09	Alter Basalt?	M. G.	x	x	x	x		Dredge FL-DR-09			
74	FL-25-01	Slab	L. S.	x		x			37º17,434N	32º16,893W	1735	
75	FL-25-02	Slab	L. S.	x					37º17,434N	32º16,893W	1735	
76	FL-27-07	Basalt	L. S.	x					37º09,750N	32º25,522W	1929	
77	FL-28-01	Slab	M. G.	x (2)					37º50,450N	31º31,275W	845	
78	FL-28-02	Slab	M. G.	x (2)	x (A, B)				37º50,450N	31º31,275W	845	
79	FL-29-01	Slab	L. S.	x (10)	x	x	x	x	37º17,554N	32º16,893W	1723	
80	FL-29-05	Altered Basalt	L. S.	x	x		x		37º17,641N	32º16,987W	1655	
81	FL-29-06	Slab	L. S.	x (2)	x	x	x		37º17,627N	32º16,868W	1660	
82	FL-30-01	Basalt	M. G.				x		37º50,450N	31º31,370W	864	
83	FL-30-03	Basalt/Slab	M. G.	x (4)	x	x			37º50,450N	31º31,350W	843	
84	FL-30-04	Basalt	M. G.		x				37º49,830N	31º30,950W	972	
85	FL-30-05	Altered Basalt	M. G.	x				x	37º49,800N	31º30,870W	885	
86	FL-30-06	Altered Basalt	M. G.	x					37º49,800N	31º30,760W	821	
87	FL-30-07	Basalt	M. G.	x					37º49,470N	31º30,680W	740	
88	FL-30-08	Basalt	M. G.						37º49,350N	31º30,850W	821	
89	PC-08-01	Slab	L. S.	x (2)		x			37º17,319N	32º16,516W	1685	Tour Eiffel
90	SAL-01-01	Slab	L. S.	x		x						

APPENDIX III – WHOLE-ROCK CHEMICAL ANALYSES OF LUCKY STRIKE AND MENEZ GWEN HYDROTHERMAL BRECCIAS AND BASALTS

Whole-rock Chemical Analyses of Lucky Strike and Menez Gwen *slabs* and basalts

Sample Ref.	AII-129-6F	AII-129-6A	DV2-05A	DV2-05B	ALV2608-2-2E	ALV2608-3-3B	ALV2608-4-1B	DV-1-6	DV-3-2	DV-4-10	DV-8-4	DV-14-1	DV-14-6	DV-15-3	DV-16-1
Sample Type	**FreshBas.**	**Alter.Bas.**	**FreshBas.**	**FreshBas.**	**Slab**	**Slab**	**Slab**	**Slab**	**Slab**	**Slab**	**Slab**	**Slab**	**Slab**	**Slab**	**Slab**
Local	LS	LS	LS	LS	LS	LS	LS	LS	LS	LS	LS	MG	MG	MG	MG
Weight percent															
SiO2	49.46	39.96	50.80	50.91	46.13	61.78	65.22	61.62	74.94	46.04	32.23	55.99	63.86	10.57	41.23
Al2O3	14.83	17.35	15.02	14.97	7.77	13.31	10.17	10.70	3.50	18.22	1.38	1.95	2.06	11.87	6.01
Fe2O3(Cal)		4.22				0.65	1.98	1.36	0.65	1.38				1.70	
FeO	8.88	3.67	8.88	8.94	1.10	3.30	2.60	2.00	0.60	4.50	0.96	0.45	0.51	0.45	0.38
MnO	0.21	0.39	0.20	0.21	0.02	0.07	0.09	0.29	0.05	0.29	<0,01	0.01	0.02	0.12	0.01
MgO	9.17	7.65	9.11	9.20	0.35	4.53	4.08	3.23	1.03	6.41	0.06	1.83	0.49	12.25	1.81
CaO	11.80	14.11	11.85	11.86	1.58	7.89	7.40	6.75	1.62	11.7	0.02	0.35	0.08	22.13	0.77
Na2O	1.79	1.67	1.67	1.64	0.65	1.41	1.65	1.22	0.72	2.52	0.07	0.53	0.47	1.25	0.54
K2O	0.20	0.31	0.20	0.20	0.25	0.37	0.43	0.30	0.18	0.53	0.13	0.10	0.14	0.08	0.20
TiO2	1.30	1.50	1.30	1.30	0.31	0.72	0.69	0.49	0.22	1.20	0.11	0.08	0.05	0.70	0.28
P2O5	0.15	0.53	0.11	0.10	< 0,01	0.11	0.15	0.07	0.03	0.25	0.09	<0,03	0.06	0.53	0.04
BaO(Cal)	0.01	0.06	0.02	0.02	2.68	0.46	0.13	2.79	5.92	0.09	1.79		5.92	0.01	21.21
Fe(sulph)(Nor)	0.07	0.04	0.10	0.08	3.11	0.27	0.19	1.05	0.50	0.22	24.53		4.01	1.26	2.52
Cu	0.01	0.05	0.01	0.01	0.35	0.02	0.02	0.03	0.05	0.03	5.10	1.83	2.40	0.01	0.01
Zn	0.02	0.02	0.01	0.01	16.46	0.02	0.00	0.01	0.36	0.01	0.35	1.41	5.50	0.01	0.24
Pb	0.01	0.00	0.00	0.00	0.03	0.00	0.00	0.00	0.16	0.00	0.01	0.01	0.01	0.00	0.01
As	0.00	0.01	0.00	0.00	0.00	0.00	0.00	0.00	0.01	0.00	0.02	0.01	0.01	0.01	0.01
S(sulph)(Cal)	0.10	0.04	0.12	0.09	10.80	0.17	0.18	0.34	-1.08	0.24	27.77		5.45	1.44	-3.63
S(barite)(Cal)	0.00	0.03	0.01	0.01	1.40	0.24	0.07	1.46	3.09	0.04	0.93		3.09	0.01	11.08
CO2	0.05	1.21	0.05	0.05	0.14	< 0,009	0.08	<0,009	<0,009	0.06	0.06	0.05	0.05	16.82	0.05
H2O-	0.02	2.89	0.02	0.03	2.26	1.25	1.79	1.36	2.16	3.57	1.30	1.78	1.78	6.54	3.88
H20+	<0,01	3.23	<0,01	<0,01	0.77	0.54	0.29	2.31	0.50	1.94	0.90	5.99	2.10	9.39	4.35
TOTAL	**98.08**	**98.95**	**99.49**	**99.62**	**96.16**	**97.11**	**97.23**	**97.40**	**95.21**	**99.25**	**97.80**	**72.36**	**98.06**	**97.15**	**91.01**
Fe(Tot)	6.13	5.85	6.4	6.24	2.53	3.29	3.60	3.56	1.42	4.69	23.40	3.66	4.26	2.8	1.61
S (Tot)	0.10	0.07	0.13	0.10	12.20	0.41	0.25	1.80	2.01	0.28	28.70	8.46	8.54	1.45	7.45
Razão Fe	0.53	0.33	0.52	0.53	3.06	0.46	0.37	0.38	0.34	0.44	-1.95	0.09	0.62	0.19	-0.48
Parts per million															
Li	3.00	8.00	3.00	3.00						9.00	<2,00	3.00	<2,00	57.00	10.00
Rb	6.00	6.00	6.00	6.00	6.80	7.99	8.68	6.70	4.44	14.00	4.00	<2,00	4.00	3.00	<2,00
Cs	<0,50	<0,50	<0,50	<0,50	0.21	0.19	0.19	0.18	0.17	<0,50	0.54	0.80	0.25	0.04	0.35
Be					<1,00	<1,00	<1,00	<1,00	<1,00						
Sr	98.00	293.00	101.00	102.00	435.00	346.00	193.00	1166.00	1019.00	201.00	154.00	2544.00	1038.00	390.00	3782.00
Ba (%)	0.01	0.06	0.02	0.01	2.40	0.41	0.12	2.50	5.30	0.08	1.60	>2,00	5.30	0.01	19.00
Sc	38.50	37.70	41.30	40.40	11.00	25.00	21.00	17.00	7.10	30.80	2.10	1.80	1.30	19.00	7.20
Y	20.00	21.00	19.00	21.00	1.20	11.80	12.60	9.00	3.70	14.00	3.00	1.00	2.00	16.00	2.00
Zr	43.00	70.00	41.00	40.00	19.00	40.00	39.00	30.00	16.00	52.00	<5,00	<5,00	<5,00	33.00	12.00
Hf	2.00	2.00	2.00	2.00	0.55	1.19	1.01	0.85	0.80	1.00	0.18	8.00	3.00	1.00	12.00
Th	0.50	3.20	0.40	0.70	0.50	1.07	1.10	0.56	0.35	1.20	0.10	<0,80	0.05	1.50	0.37
V	189.00	185.00	182.00	180.00	122.00	140.00	131.00	129.00	69.00	129.00	<2,00	27.00	29.00	83.00	51.00
Nb	7.00	29.00	7.00	8.00	5.39	11.84	11.96	7.87	3.72	17.00	1.88	<2,00	0.76	14.00	<2,00
Ta	0.60	2.20	0.70	0.60	0.62	0.80	0.83	0.82	<0,5	1.10	0.395	<0,50	<0,50	0.70	<0,50
Cr	65.00	520.00	92.00	84.00	250.00	510.00	360.00	460.00	90.00	660.00	<20,00	110.00	52.00	390.00	88.00
Mo	<1,00	4.00	<1,00	<1,00	130.00	62.00	<1,00	22.00	11.00	9.00	64.00	25.00	101.00	<1,00	29.00
W	<1,00	2.00	<1,00	<1,00	< 2,00	<1,00	<1,00	<1,00	<1,00	<1,00	<1,00	1.00	<1,00	<1,00	<1,00
U	<0,20	3.00	<0,20	0.20	2.95	0.85	2.87	1.55	5.71	1.10	6.40	15.00	13.00	2.20	17.00
Co	42.00	42.00	40.00	40.00	12.00	22.00	19.00	16.00	5.00	24.00	194.00	14.00	14.00	24.00	4.00
Ni	67.00	112.00	68.00	70.00	9.00	44.00	53.00	35.00	9.00	71.00	7.00	9.00	6.00	163.00	18.00
Ag	0.40	0.40	<0,10	0.20	35.00	< 5,00	< 5,00	< 5,00	34.00	0.40	14.70	4.20	7.90	<0,10	4.80
Au (ppb)	<2,00	5.00	<2,00	<2,00	160.00	11.00	< 5,00	26.00	176.00	<2,00	247.00	17.00	92.00	<2,00	76.00
Cd	<5,00	<5,00	<5,00	<5,00						<5,00	24.00	120.00	440.00	<5,00	31.00
Hg					<1,00	2.00	2.00	<1,00	4.00						
Ga	17.00	13.00	18.00	18.00	29.00	10.00	8.00	11.00	6.00	16.00	8.00	13.00	44.00	4.00	8.00
In	<1,00	<1,00	<1,00	<1,00	<0,10	<0,10	<0,10	<0,10	0.10	<1,00	1.00	<1,00	<1,00	<1,00	<1,00
Tl															
Ge	3.00	2.00	<1,00	<1,00	8.30	1.20	1.10	1.00	11.70	1.00	1.00	<1,00	3.00	1.00	1.00
Sn	<20,00	<20,00	<20,00	<20,00	0.80	8.10	6.50	3.90	1.10	<20,00	<20,00	<20,00	1.10	0.70	2.00
Sb	<0,10	1.10	<0,10	<0,10	28.00	0.40	0.30	1.00	1.10	0.50	10.80	6.60	17.80	1.80	7.10
Bi	<5,00	<5,00	<5,00	<5,00	<0,05	<0,05	<0,05	<0,05	<0,05	<5,00	90.00	32.00	30.00	<5,00	<5,00
Se	<5,00	<5,00	<5,00	<5,00	<3,00	<3,00	<3,00	<3,00	<3,00	<5,00	140.00	54.00	60.00	<5,00	<12,00
Br	<0,50	49.00	0.60	0.80	<0,80	4.60	18.00	7.50	11.00	34.00	10.00	4.70	7.50	26.00	6.60
La	5.00	19.00	6.00	6.00	1.62	6.37	7.77	6.23	3.38	8.00	1.34	4.00	1.93	10.00	4.00
Ce	<5,00	29.00	<5,00	<5,00	1.41	12.35	14.71	9.66	4.42	<5,00	1.36	<23,00	1.24	12.00	5.57
Pr					0.12	1.25	1.52	0.93	0.45						
Nd					0.71	6.70	7.79	5.03	2.38						
Sm	2.50	4.20	2.70	2.50	0.26	1.61	1.80	1.34	0.66	2.30	0.29	<0,41	0.26	2.30	<0,43
Eu	<1,00	<1,00	<1,00	<1,00	<0,20	1.30	0.70	1.30	0.40	<1,00	<1,00	<1,00	<1,00	0.40	0.20
Gd					0.21	1.82	1.97	1.34	0.60						
Tb	0.60	1.00	0.90	0.70	0.04	0.35	0.35	0.24	0.15	<0,50	0.04	<0,50	0.05	0.23	0.18
Dy					0.19	2.00	1.96	1.34	0.59						
Ho					0.06	0.43	0.46	0.29	0.11						
Er					0.11	1.36	1.20	0.91	0.32						
Tm					<0,005	0.19	0.21	0.18	<0,005						
Yb	2.00	3.00	3.00	3.00	0.14	1.36	1.17	0.84	0.28	2.00	0.04	<2,00	0.03	0.86	0.30
Lu	<0,20	<0,20	0.30	0.30	0.03	0.18	0.18	0.13	0.05	<0,20	0.01	<0,20	0.01	0.13	0.05
LOI (%)	<0,05	7.33	<0,05	<0,05	10.51	3.80	4.22	<0,01	7.04	5.57	21.35	7.82	8.45	32.75	8.28

Sample Ref.	DV-16-3	DV-19-12	DV-2-12	FL-17-06B	FL-30-03B	FL-17-11	FL-30-04	FL-17-06S	FL-30-03S	FL-DR-08-02	FL-29-05	FL-29-01	FL-16-04	FL-17-05	FL-18-09
Sample Type	**Slab**	**Slab**	**Slab**	**Alter.Bas.**	**Alter.Bas.**	**FreshBas.**	**FreshBas.**	**Slab**	**Slab**	**Alter.Bas.**	**Alter.Bas.**	**Slab**	**Slab**	**Slab**	**Slab**
Local	MG	LS	MG	MG	MG	MG	MG	MG	MG	LS	LS	LS	MG	MG	LS
Weight percent															
SiO2	35.73	18.78	36.34	47.87	47.89	48.61	48.29	50.93	64.54	54.33	48.52	53.60	67.89	78.08	73.88
Al2O3	1.36	5.10	7.44	21.24	20.35	19.17	19.41	4.80	0.50	15.96	19.17	15.68	1.63	4.27	7.24
Fe2O3(Cal)			10.35	1.83	6.12	1.02	0.34			1.10	2.42	1.43	0.09	2.45	0.41
FeO	0.80	1.10	<0,10	2.07	2.25	4.50	5.13	0.86	1.17	3.06	2.03	3.24	0.59	1.17	2.07
MnO	0.04	< 0,01	0.04	0.07	0.06	0.12	0.13	<0,01	0.03	0.09	0.10	0.11	0.01	0.01	0.08
MgO	0.35	0.31	2.57	5.50	5.72	7.16	7.43	0.42	0.19	5.98	6.87	3.92	2.61	0.65	2.31
CaO	0.10	0.67	4.64	13.77	13.33	14.87	14.73	0.23	0.14	12.94	13.06	9.73	0.38	0.18	4.25
Na2O	0.18	0.59	0.87	2.25	2.26	2.26	2.25	0.39	0.37	2.00	2.32	1.84	0.86	0.45	1.06
K2O	0.21	0.19	0.20	0.31	0.40	0.50	0.35	0.29	0.08	0.38	0.61	0.40	0.27	0.24	0.28
TiO2	0.09	0.36	0.38	0.96	1.01	1.09	0.95	0.23	0.02	1.06	1.04	0.79	0.01	0.25	0.47
P2O5	< 0,01	< 0,01	0.04	0.12	0.30	0.21	0.13	<0,01	<0,01	0.10	0.16	0.09	0.03	0.02	0.06
BaO(Cal)	11.60	35.73	17.86	0.11	0.04	0.02	0.02	5.79	9.84	0.32	0.03	1.67	6.81	0.49	1.02
Fe(sulph)(Nor)	17.82	12.27	5.68	0.61	0.60	0.04	0.01	8.34	2.74	0.11	-0.01	0.40	2.86	1.01	0.20
Cu	0.00	0.22	0.03	0.03	0.02	0.01	0.01	0.66	0.72	0.01	0.01	0.07	1.20	0.21	0.02
Zn	1.51	4.20	0.09	0.05	0.02	0.00	0.00	2.53	0.51	0.01	0.02	0.04	0.60	1.75	0.02
Pb	0.01	0.01	0.00	0.00	0.00	0.00	0.00	0.01	0.03	0.00	0.00	0.01	0.00	0.00	0.00
As	0.06	0.06	0.01	0.00	0.00	0.00	0.00	0.02	0.02	0.00	0.00	0.00	0.01	0.01	0.00
S(sulph)(Cal)	17.54	4.95	0.97	0.69	0.69	0.04	0.01	8.99	0.31	0.03	-0.02	0.48	3.58	2.02	0.24
S(barite)(Cal)	6.06	18.65	9.33	0.06	0.02	0.01	0.01	3.03	5.14	0.17	0.02	0.35	1.42	0.10	0.21
CO2	0.01	< 0,009	< 0,009	<0,05	<0,05	<0,05	<0,05	<0,05	0.11	<0,05	<0,05	0.07	0.10	0.15	0.07
H2O-	0.75	2.31	1.20	1.10	1.39	0.08	0.16	2.49	1.53	0.96	1.18	1.93	1.78	2.80	2.30
H20+	1.09	1.11	1.75	1.53	1.01	0.50	0.03	4.26	3.19	1.69	1.35	2.71	5.26	4.81	2.54
TOTAL	**95.31**	**106.61**	**99.81**	**100.17**	**103.49**	**100.21**	**99.39**	**94.26**	**91.17**	**100.31**	**98.88**	**98.57**	**97.99**	**101.12**	**98.73**
Fe(Tot)	17.10	0.97	7.30	3.50	6.63	4.25	4.24	6.88	2.14	3.26	3.26	3.92	3.38	3.63	2.09
S (Tot)	23.60	23.60	10.30	0.75	0.71	0.05	0.02	12.02	5.45	0.20	0.00	0.83	5.00	2.12	0.45
Razão Fe	-6.61	-0.08		0.36	0.22	0.45	0.49	-0.85	2.94	0.43	0.33	0.42	0.47	0.26	0.46
Parts per million															
Li															
Rb	4.41	2.69	6.09	3.70	5.30	11.00	8.00	5.40	1.90	5.40	13.00	6.10	4.20	9.40	7.80
Cs	0.26	0.09	0.20	0.10	0.10	0.20	0.10	0.30	0.20	0.10	0.30	0.10	0.30	0.30	0.30
Be	<1,00	<1,00	<1,00	1.00	1.00	1.00	1.00	<1,00	<1,00	1.00	1.00	<1,00	<1,00	<1,00	<1,00
Sr	4310.00	2167.00	6216.00	301.00	273.00	297.00	238.00	1460.00	3520.00	296.00	274.00	367.00	1390.00	164.00	239.00
Ba (%)	10.39	32.00	16.00	0.10	0.04	0.02	0.02	5.19	8.81	0.29	0.03	1.50	6.10	0.44	0.92
Sc	2.10	13.00	12.00	32.00	34.00	35.00	34.00	7.00	1.00	37.00	35.00	24.00	0.80	9.10	14.00
Y	0.90	1.60	6.40	17.00	17.00	19.00	18.00	1.40	1.40	16.00	18.00	11.00	1.30	0.40	6.80
Zr	11.00	23.00	20.00	57.00	56.00	60.00	51.00	15.00	3.60	60.00	61.00	52.00	3.90	16.00	35.00
Hf	0.58	1.74	1.10	1.60	1.70	1.80	1.30	0.80	1.60	1.80	1.60	1.30	1.60	0.50	0.90
Th	0.10	0.60	0.51	1.55	1.49	1.75	1.34	0.33	0.08	2.09	1.99	0.88	0.11	0.34	0.89
V	27.00	70.00	77.00	158.00	201.00	173.00	191.00	124.00	26.00	185.00	188.00	133.00	29.00	88.00	87.00
Nb	1.45	7.52	6.90	17.00	17.00	20.00	15.00	4.50	0.90	24.00	24.00	15.00	1.10	4.10	8.00
Ta	-	-	-	1.11	1.11	1.31	0.98	1.93	0.08	1.57	1.42	1.06	0.75	0.24	0.36
Cr	33.00	120.00	130.00	264.00	323.00	286.00	560.00	71.00	13.00	357.00	415.00	605.00	11.00	100.00	250.00
Mo	119.00	<1,00	28.00	1.80	1.30	0.80	0.40	112.00	12.00	1.20	0.90	4.80	44.00	56.00	2.70
W	<1,00	<1,00	<1,00	154.00	120.00	356.00	445.00	46.00	2.20	247.00	78.00	136.00	<0,20	3.20	180.00
U	12.02	24.03	9.64	1.45	1.63	0.75	0.37	24.00	3.10	1.22	0.58	16.20	10.10	40.90	1.46
Co	6.00	4.00	11.00	47.00	46.00	62.00	52.00	39.00	7.00	39.00	30.00	52.00	24.00	10.00	35.00
Ni	< 5,00	< 5,00	< 5,00	80.00	121.00	135.00	123.00	<10,00	14.00	65.00	81.00	53.00	<10,00	24.00	39.00
Ag	7.00	85.00	< 5,00	<0,50	<0,50	0.60	<0,50	2.00	0.90	0.60	0.50	<0,50	<0,50	<0,50	0.60
Au (ppb)	154.00	651.00	99.00	3.00	<2,00	<2,00	5.00	136.00	91	<2,00	<2,00	295	40.00	35.00	21.00
Cd															
Hg	62.00	< 2,00	13.00	<1,00	<1,00	<1,00	<1,00	10.00	13.00	<1,00	<1,00	<1,00	3.00	4.00	<1,00
Ga	3.00	36.00	7.00	18.00	16.00	16.00	16.00	12.00	7.00	14.00	16.00	12.00	7.00	16.00	6.00
In	<0,10	2.60	<0,10	<0,10	<0,10	<0,10	<0,10	0.10	<0,10	<0,10	<0,10	0.10	0.20	<0,10	<0,10
Tl				0.27	0.32	0.05	<0,05	6.55	7.15	0.11	<5,00	0.90	1.76	4.37	0.94
Ge	4.90	31.00	1.00	1.20	1.10	1.40	1.20	25.00	17.00	1.60	1.40	1.60	1.10	10.00	1.50
Sn	<0,20	0.80	1.30	0.60	0.60	2.20	1.20	<0,50	<0,50	1.50	0.90	0.70	1.70	1.00	1.20
Sb	31.00	200.00	6.30	0.33	0.23	0.19	<0,05	16.50	5.13	0.25	0.16	0.52	6.47	6.06	1.23
Bi	<0,05	<0,05	<0,05	<0,05	<0,05	0.05	0.06	<0,05	0.05	<0,05	<0,05	0.05	0.08	0.07	0.13
Se	20.00	<4,00	16.00	<3,00	<3,00	<3,00	<3,00	150.00	31.00	<3,00	<3,00	<3,00	52.00	20.00	<3,00
Br	<0,60	8.50	11.00	9.80	13.00	7.30	4.60	5.70	27.00	8.40	3.80	10.00	30.00	14.00	7.00
La	3.68	9.13	7.37	9.92	10.30	11.40	8.86	3.73	4.23	9.39	12.20	6.99	1.43	0.24	3.74
Ce	2.08	6.56	8.43	19.00	19.50	21.80	16.50	3.16	2.78	19.80	22.20	10.10	<0,005	<0,005	5.36
Pr	0.16	0.36	0.74	1.87	1.88	2.09	1.66	0.22	0.20	1.92	2.05	0.99	<0,005	<0,005	0.66
Nd	1.33	2.77	4.52	8.73	8.97	9.86	7.95	0.66	0.96	8.91	9.41	5.07	0.80	0.33	3.65
Sm	0.49	1.00	1.27	2.69	2.80	2.95	2.52	0.23	0.32	2.77	2.63	1.06	0.18	0.08	0.81
Eu	<0,20	0.60	0.60	0.90	0.94	0.93	0.84	<0,005	<0,005	1.30	0.86	0.81	0.30	0.08	0.46
Gd	0.31	0.79	1.20	2.75	2.88	2.96	2.76	0.33	0.56	2.91	2.78	1.61	0.24	0.08	0.93
Tb	0.08	0.23	0.28	0.49	0.52	0.52	0.49	<0,01	<0,01	0.52	0.48	0.25	0.04	0.01	0.15
Dy	0.08	0.05	0.98	2.84	3.02	3.09	2.97	0.13	0.12	3.03	2.86	1.81	0.14	0.09	0.95
Ho	0.02	0.01	0.20	0.57	0.60	0.61	0.60	0.02	0.02	0.59	0.58	0.37	0.02	0.02	0.22
Er	<0,01	<0,01	0.37	1.64	1.71	1.73	1.70	0.08	0.06	1.68	1.66	1.06	0.07	0.06	0.67
Tm	<0,005	<0,005	<0,005	0.24	0.25	0.26	0.26	0.01	0.01	0.25	0.25	0.16	<0,005	0.01	0.08
Yb	0.09	0.07	0.59	1.51	1.63	1.64	1.57	0.09	0.06	1.62	1.59	1.01	0.06	0.10	0.59
Lu	0.01	0.01	0.09	0.23	0.23	0.24	0.24	0.01	<0,002	0.24	0.24	0.15	<0,002	0.02	0.10
LOI (%)	17.25	9.08	7.98	3.26	3.72	0.18	0.02	13.09	6.32	2.92	2.90	5.19	9.47	9.43	6.11

Sample Ref.	FL-19-03	FL-20-02	FL-DR-03-05 A	FL-DR-03-05 B	FL-DR-03-13	FL-DR-03A	FL-DR-04-02 A	FL-DR-04-02 B	FL-DR-04	FL-DR-04-V1	FL-DR-04-V2
Sample Type	**Sed. core**	**Slab**	**Slab**	**Slab**	**Slab**	**Slab**	**Slab**	**Slab**	**Alter.Glass**	**Fresh Glass**	**Fresh Glass**
Local	LS	LS	LS	LS	LS	LS	LS	LS	LS	LS	LS
Weight percent											
SiO2	46.73	79.10	56.19	64.80	71.51	26.61	78.10	53.40	47.98	51.22	51.26
Al2O3	13.07	3.85	2.72	8.37	5.12	2.82	3.28	2.00	22.22	14.37	14.55
Fe2O3(Cal)	7.29	1.56			0.26		0.00		0.23	1.15	0.28
FeO	1.94	0.36	1.76	3.84	1.71	0.41	1.31	1.26	2.79	8.47	9.29
MnO	0.06	0.56	<0,01	0.05	0.03	<0,01	0.01	<0,01	0.09	0.18	0.18
MgO	4.78	1.19	0.35	2.83	1.58	0.04	0.81	0.21	5.24	8.22	8.17
CaO	2.75	1.69	0.36	5.32	2.44	0.02	1.37	0.29	14.99	12.51	12.29
Na2O	2.18	1.40	0.33	0.98	0.66	0.23	0.48	0.32	1.92	2.22	2.24
K2O	0.64	0.29	0.08	0.25	0.19	0.04	0.20	0.18	0.16	0.19	0.21
TiO2	0.73	0.27	0.31	0.49	0.39	0.21	0.19	0.13	0.83	1.04	1.05
P2O5	0.17	0.08	<0,01	0.05	0.03	<0,01	0.05	0.04	0.09	0.12	0.13
BaO(Cal)	2.42	0.57	10.50	5.15	6.75	0.16	4.25	13.17	0.02	0.01	0.01
Fe(sulph)(Nor)	0.72	0.16	2.36	1.38	0.99	33.06	0.61	4.94	0.92	0.08	0.08
Cu	0.06	0.03	0.25	0.04	0.06	0.57	0.07	0.35	0.01	0.01	0.01
Zn	0.02	0.01	8.96	0.69	0.59	0.02	0.88	3.82	0.01	0.01	0.01
Pb	0.00	0.00	0.05	0.01	0.02	0.01	0.02	0.01	0.00	0.00	0.00
As	0.01	0.00	0.02	0.00	0.00	0.04	0.01	0.01	0.00	0.90	1.10
S(sulph)(Cal)	0.84	0.19	7.11	1.92	1.43	37.97	1.13	7.55	1.05	0.10	0.10
S(barite)(Cal)	0.51	0.12	2.19	1.08	1.41	0.03	0.89	2.75	0.01	0.00	0.00
CO2	0.26	0.14	<0,05	0.15	0.16	0.17	0.12	<0,05	<0,05	0.18	0.07
H2O-	5.30	2.59	1.35	1.05	1.27	0.81	2.29	1.12	0.44	Not Analysed	Not Analysed
H20+	7.02	3.97	3.13	4.14	3.14	19.62	2.94	4.35	1.08	Not Analysed	Not Analysed
TOTAL	**97.50**	**98.13**	**98.01**	**102.59**	**99.75**	**122.83**	**99.01**	**95.90**	**100.07**	**100.97**	**101.02**
Fe(Tot)	7.33	1.53	2.02	3.22	2.50	29.10	1.63	4.84	3.25	7.47	7.50
S (Tot)	1.35	0.31	9.30	3.00	2.84	38.00	2.02	10.30	1.06	0.10	0.10
Razão Fe	0.19	0.17	1.32	0.62	0.47	-0.09	0.50	1.11	0.48	0.47	0.49
Parts per million											
Li											
Rb	10.00	6.70	3.40	6.10	7.80	2.60	7.00	5.60	1.90	5.00	4.00
Cs	0.10	0.20	0.10	0.10	0.20	0.10	0.20	0.10	<0,10	<0,10	<0,10
Be	<1,00	<1,00	<1,00	<1,00	<1,00	<1,00	<1,00	<1,00	1.00	<1.00	<1.00
Sr	456.00	253.00	848.00	430.00	492.00	12.90	355.00	941.00	208.00	109.00	102.00
Ba (%)	2.17	0.51	9.40	4.61	6.05	0.14	3.81	11.80	0.01	0.01	0.01
Sc	23.00	7.00	6.90	15.00	11.00	1.90	6.40	4.60	29.00	40.40	42.60
Y	12.00	5.90	4.70	8.40	6.40	0.10	3.30	2.70	12.00	23.00	22.00
Zr	49.00	25.00	23.00	28.00	27.00	16.00	14.00	11.00	44.00	60.00	57.00
Hf	1.50	0.70	2.30	1.30	1.50	0.40	1.00	2.70	1.30	1.70	1.60
Th	1.19	0.90	0.38	0.67	0.57	0.27	0.52	0.29	1.11	0.61	0.60
V	227.00	101.00	48.00	108.00	94.00	48.00	126.00	75.00	145.00	278.00	263.00
Nb	16.00	5.50	6.30	8.50	7.00	4.30	5.40	3.70	13.00	7.50	6.90
Ta	0.40	0.29	0.45	0.11	0.29	0.15	0.47	0.33	0.85	0.50	0.50
Cr	450.00	130.00	110.00	270.00	200.00	110.00	83.00	59.00	760.00	79.00	82.00
Mo	5.70	17.00	29.00	13.00	12.00	69.00	18.00	25.00	2.20	<1,00	<1,00
W	3.60	1.10	190.00	251.00	4.20	1.90	260.00	231.00	309.00	338.00	333.00
U	4.70	2.71	1.94	1.35	3.33	1.61	4.98	4.72	1.94	0.37	0.34
Co	13.00	8.00	57.00	60.00	11.00	12.00	62.00	95.00	50.00	77.00	69.00
Ni	43.00	24.00	25.00	45.00	29.00	23.00	22.00	16.00	130.00	69.00	68.00
Ag	0.70	<0,50	100.00	5.50	25.00	96.00	40.00	67.00	<0,50	<0,50	<0,50
Au (ppb)	56.00	13.00	420.00	152.00	148.00	891.00	78.00	298.00	<2,00	<2,00	<2,00
Cd											
Hg	<1,00	<1,00	6.00	2.00	3.00	8.00	2.00	<1,00	<1,00	<1,00	<1,00
Ga	14.00	4.00	16.00	8.00	9.00	8.00	10.00	40.00	15.00	17.00	16.00
In	0.40	0.10	0.20	<0,10	0.20	0.70	0.70	1.50	<0,10	<0,10	<0,10
Tl	<0,05	0.35	2.33	1.47	2.57	2.41	1.32	1.41	0.05	<0,05	<0,05
Ge	3.70	1.70	68.00	3.40	6.00	3.70	12.00	9.00	0.90	1.40	1.30
Sn	1.60	4.30	<0,50	<0,50	<0,50	0.70	1.00	<0,50	3.30	<1,00	<1,00
Sb	2.97	0.70	54.50	2.73	6.73	71.40	7.59	27.30	0.11	0.10	<0,10
Bi	0.14	0.12	<0,05	<0,05	0.13	0.09	0.25	0.07	0.06	<0,06	<0,06
Se	<3,00	<3,00	<3,00	<3,00	5.00	96.00	<3,00	<3,00	<3,00	<3,00	<3,00
Br	62.00	39.00	3.70	4.20	6.70	18.00	4.50	6.60	10.00	<0,50	<0,50
La	7.97	3.80	3.18	6.39	4.05	1.44	3.02	2.99	6.35	5.23	4.97
Ce	13.70	5.29	2.79	8.38	7.64	2.74	2.66	5.39	12.40	11.00	11.00
Pr	1.57	0.64	0.28	1.25	0.87	0.33	<0,005	0.64	1.23	1.50	1.48
Nd	6.21	3.75	1.07	5.10	3.40	1.14	2.65	2.35	5.79	7.62	7.38
Sm	1.64	0.85	0.31	1.12	0.73	0.15	0.52	0.35	1.84	2.55	2.50
Eu	0.76	0.37	<0,100	0.78	0.70	0.11	0.26	<0,100	0.65	0.987	0.965
Gd	1.96	0.88	0.44	1.28	0.82	0.10	0.60	0.26	1.94	3.29	3.21
Tb	0.34	0.15	0.10	0.21	0.14	<0,01	0.09	<0,01	0.35	0.62	0.61
Dy	2.07	0.98	0.59	1.29	0.95	0.04	0.48	0.47	2.11	4.25	4.01
Ho	0.42	0.21	0.12	0.26	0.19	<0,01	0.10	0.10	0.42	0.88	0.86
Er	1.32	0.58	0.38	0.86	0.62	0.03	0.32	0.25	1.21	2.55	2.46
Tm	0.23	0.07	0.06	0.11	0.08	<0,005	0.04	<0,005	0.18	0.427	0.412
Yb	1.26	0.57	0.34	0.72	0.50	0.02	0.30	0.26	1.20	2.67	2.53
Lu	0.20	0.09	0.05	0.11	0.08	0.00	0.05	0.04	0.18	0.389	0.392
LOI (%)	14.35	7.94	10.70	5.51	5.64	27.94	7.67	11.19	1.91	-0.53	-0.64

Sample Ref.	FL-DR-05-01	FL-DR-05-03 I	FL-DR-05 B	FL-DR-05 C	FL-DR-08-03	FL-DR-09	FL-28-02 A	FL-29-06	FL-DR-05-03 II	FL-DR-08-04	FL-28-02 B
Sample Type	**Slab**	**Slab**	**Slab**	**Slab**	**Slab**	**Slab**	**Slab**	**Slab**	**Slab**	**Slab**	**Slab**
Local	LS	LS	LS	LS	LS	MG	MG	LS	LS	LS	MG
Weight percent											
SiO2	56.17	64.57	57.80	55.68	53.58	14.18	58.12	59.08	33.27	31.41	52.90
Al2O3	13.89	4.79	13.85	13.86	16.39	14.47	4.38	12.22	12.43	1.31	2.71
Fe2O3(Cal)	0.32	2.16	0.54	1.43		1.68		0.83			
FeO	4.95	1.04	5.09	4.46	5.63	0.45	0.81	3.38	1.98	1.49	1.08
MnO	0.10	0.34	0.10	0.10	0.11	0.10	0.01	0.08	0.10	<0,01	0.01
MgO	6.44	1.66	5.98	6.09	5.78	11.02	1.58	4.12	4.52	0.08	1.83
CaO	11.36	2.06	11.01	10.63	11.50	20.37	0.10	7.31	1.72	0.05	0.09
Na2O	1.91	0.82	1.83	1.95	2.04	0.90	0.60	1.86	1.19	0.35	0.47
K2O	0.50	0.22	0.38	0.50	0.45	0.10	0.53	0.51	0.46	0.04	0.23
TiO2	0.90	0.26	0.87	0.91	0.98	0.57	0.22	0.82	0.68	0.35	0.14
P2O5	0.17	0.04	0.16	0.14	0.20	0.28	<0,01	0.13	0.05	0.03	0.01
BaO(Cal)	0.14	9.04	0.04	0.09	0.09	0.00	1.64	1.15	2.08	24.90	2.29
Fe(sulph)(Nor)	0.18	1.29	0.06	0.20	0.09	1.35	8.70	0.12	11.35	4.43	9.43
Cu	0.02	0.05	0.02	0.02	0.02	0.01	3.65	0.04	1.88	2.43	5.98
Zn	0.02	0.05	0.01	0.00	0.01	0.00	1.56	0.01	0.08	9.59	3.86
Pb	0.00	0.01	0.00	0.00	0.00	0.00	0.00	0.00	0.00	0.00	0.01
As	0.00	0.00	0.00	0.00	0.00	0.01	0.01	0.00	0.01	0.06	0.01
S(sulph)(Cal)	0.21	1.51	0.07	0.23	0.11	1.55	10.76	0.15	13.07	9.79	12.72
S(barite)(Cal)	0.03	1.89	0.01	0.02	0.02	0.00	0.34	0.24	0.43	5.21	0.48
CO2	0.08	0.18	0.07	0.08	0.12	0.22	0.05	0.18	<0,05	0.07	<0,05
H2O-	0.78	1.28	0.85	1.35	0.41	3.44	1.75	2.72	6.57	0.67	1.64
H20+	0.51	4.74	0.57	1.22	1.52	10.11	7.79	3.88	9.52	2.80	5.46
TOTAL	**98.68**	**97.99**	**99.31**	**98.97**	**99.05**	**80.80**	**102.61**	**98.84**	**101.38**	**95.06**	**101.34**
Fe(Tot)	4.25	3.61	4.39	4.67	4.26	2.87	8.10	3.33	12.80	2.98	8.75
S (Tot)	0.24	3.40	0.08	0.25	0.13	1.55	11.10	0.39	13.50	15.00	13.20
Razão Fe	0.49	0.26	0.48	0.44	0.51	0.19	22.96	0.45	0.51	-3.92	5.29
Parts per million											
Li											
Rb	13.00	8.20	12.00	15.00	15.00	5.70	15.00	9.60	7.40	5.10	6.20
Cs	0.20	0.10	0.10	0.30	0.90	0.10	0.90	0.10	0.20	0.40	0.30
Be	<1,00	<1,00	<1,00	1.00	<1,00	<1,00	<1,00	<1,00	1.00	<1,00	<1,00
Sr	256.00	1380.00	207.00	251.00	226.00	339.00	297.00	357.00	295.00	1660.00	459.00
Ba (%)	0.13	8.10	0.03	0.08	0.08	0.00	1.47	1.03	1.86	22.30	2.05
Sc	29.00	7.70	28.00	27.00	31.00	17.00	3.50	24.00	23.00	3.20	2.50
Y	15.00	5.80	15.00	14.00	16.00	14.00	0.90	13.00	9.70	3.10	0.70
Zr	73.00	21.00	65.00	51.00	58.00	19.00	19.00	52.00	46.00	26.00	12.00
Hf	1.70	1.40	1.60	1.50	1.50	0.60	0.50	1.40	1.10	3.50	0.60
Th	1.45	0.56	1.39	1.29	1.09	0.89	0.30	1.10	1.00	0.48	0.23
V	165.00	98.00	170.00	156.00	163.00	81.00	98.00	138.00	155.00	167.00	69.00
Nb	18.00	5.10	17.00	18.00	16.00	10.00	5.20	15.00	13.00	6.40	3.40
Ta	0.96	<0,01	0.95	1.00	0.84	0.52	0.11	0.74	0.34	<0,01	0.11
Cr	410.00	130.00	390.00	380.00	470.00	260.00	62.00	320.00	400.00	140.00	40.00
Mo	1.60	16.00	1.70	1.30	1.30	0.80	175.00	2.40	26.00	14.00	101.00
W	3.80	147.00	2.80	0.60	244.00	25.00	62.00	17.00	0.70	96.00	96.00
U	0.58	2.31	0.61	0.71	1.98	1.74	34.30	3.07	14.70	23.00	23.50
Co	25.00	37.00	26.00	22.00	49.00	19.00	52.00	19.00	64.00	22.00	53.00
Ni	69.00	26.00	72.00	50.00	67.00	66.00	14.00	52.00	39.00	26.00	15.00
Ag	7.80	3.00	1.80	1.30	0.70	<0,50	<0,50	<0,50	6.00	32.00	0.50
Au (ppb)	5.00	68.00	<2,00	<2,00	<2,00	<2,00	50.00	14.00	45.00	74.00	46.00
Cd											
Hg	<1,00	4.00	<1,00	<1,00	<1,00	<1,00	4.00	<1,00	2.00	25.00	5.00
Ga	12.00	6.00	13.00	10.00	13.00	6.00	15.00	13.00	14.00	96.00	24.00
In	<0,10	0.10	<0,10	<0,10	0.10	<0,10	0.50	0.60	0.50	9.20	0.90
Tl	0.19	<0,05	0.16	0.08	0.07	0.06	7.35	<0,05	0.76	<0,05	5.62
Ge	1.90	4.30	2.70	2.40	1.20	0.50	18.00	2.40	5.40	52.00	16.00
Sn	10.00	4.30	11.00	7.20	18.00	<0,50	1.40	1.60	3.10	<0,50	2.80
Sb	1.99	3.23	0.40	0.58	0.25	1.30	6.70	0.67	1.67	25.90	5.44
Bi	<0,05	0.08	0.10	<0,05	0.10	<0,05	0.12	0.13	0.05	0.05	0.16
Se	<3,00	<3,00	<3,00	<3,00	<3,00	<3,00	160.00	<3,00	68.00	5.00	200.00
Br	6.30	17.00	5.90	8.60	2.80	23.00	12.00	20.00	12.00	40.00	15.00
La	9.21	5.01	9.11	10.70	8.43	8.36	0.61	8.20	7.50	2.86	0.67
Ce	17.30	5.05	16.30	19.80	16.40	14.70	0.98	14.70	14.30	1.36	1.09
Pr	1.93	0.87	1.81	2.65	1.84	2.28	0.14	1.61	1.72	0.44	0.14
Nd	10.10	3.19	10.20	9.95	9.59	9.04	0.56	8.86	7.47	1.46	0.70
Sm	2.01	0.75	2.07	2.18	2.15	1.95	0.11	1.83	1.44	0.27	0.13
Eu	0.77	0.50	0.73	0.81	0.80	0.72	0.50	0.60	0.62	<0,200	0.19
Gd	2.63	0.66	2.51	2.63	2.55	2.20	0.12	2.22	1.55	0.40	0.09
Tb	0.42	0.12	0.44	0.44	0.46	0.39	0.03	0.38	0.29	0.05	0.01
Dy	2.27	0.85	2.52	2.44	2.61	2.25	0.14	2.11	1.67	0.14	0.10
Ho	0.49	0.18	0.50	0.52	0.57	0.47	0.03	0.43	0.32	0.02	0.02
Er	1.62	0.57	1.70	1.65	1.86	1.54	0.10	1.43	1.05	0.06	0.09
Tm	0.23	0.09	0.25	0.24	0.26	0.22	0.02	0.20	0.15	<0,005	<0,005
Yb	1.24	0.62	1.36	1.39	1.56	1.26	0.15	1.25	0.97	0.01	0.10
Lu	0.21	0.09	0.22	0.22	0.25	0.19	0.02	0.18	0.14	<0,002	0.01
LOI (%)	1.43	8.41	1.48	2.89	1.97	28.24	12.19	6.96	20.62	11.34	12.95

Notes:
Cal – calculated value; Nor – normative value; LOI – mass lost on ignition
The negative values of Fe2O3 (Cal) are not show. Fe2O3 of the DV-2-12 sample was not calculated, but determined by Whole-rock analyses.
The Ir values are not detected (< 50.00 ppm) for all samples.
Sample DV-14-1 has a high content in Ba that was not determined. The blank spaces are dependent on this value.

APPENDIX IV – MINERAL CHEMISTRY DATA (ELECTRON MICROPROBE)

Mineral Chemistry Data

Plagioclase Feldspar

Sample Ref.		FL-17-06S			FL DR-05-03 I			FL DR-05-03 II			FL DR-05 B		
Sample Type		Slab			Slab			Slab			Slab		
SiO2		45.456	46.331	46.134	44.493	46.124	45.390	46.254	45.028	45.612	45.875	45.991	46.263	45.300
TiO2		0.000	0.000	0.018	0.000	0.000	0.000	0.020	0.007	0.000	0.075	0.000	0.005	0.000
Al2O3		32.326	32.927	33.183	33.183	33.230	32.975	33.559	32.661	33.500	33.196	33.394	33.305	32.937
Cr2O3		0.181	0.000	0.083	0.000	0.000	0.000	0.028	0.178	0.082	0.000	0.000	0.000	0.000
FeO		0.140	0.302	0.246	0.407	0.347	0.259	0.428	0.394	0.408	0.325	0.306	0.472	0.260
MnO		0.021	0.075	0.083	0.148	0.056	0.074	0.027	0.000	0.000	0.000	0.009	0.058	0.063
MgO		0.234	0.214	0.220	0.194	0.214	0.194	0.217	0.194	0.204	0.204	0.216	0.240	0.206
CaO		18.493	17.950	18.096	18.425	17.988	18.345	18.816	18.108	18.468	18.418	18.478	18.446	18.681
Na2O		1.388	1.391	1.363	1.452	1.337	1.147	1.307	1.287	1.228	1.165	1.201	1.258	1.221
K2O		0.022	0.000	0.013	0.000	0.000	0.002	0.000	0.000	0.000	0.000	0.000	0.000	0.000
TOTAL		98.26	99.19	99.44	98.30	99.30	98.39	100.66	97.86	99.50	99.26	99.60	100.05	98.67
Number of ions on the basis of 32 oxygens														
Si		8.560	8.615	8.564	8.397	8.570	8.523	8.505	8.512	8.478	8.535	8.528	8.548	8.497
Al		7.174	7.216	7.260	7.381	7.277	7.298	7.273	7.276	7.338	7.279	7.298	7.252	7.281
Ti		0.000	0.000	0.003	0.000	0.000	0.000	0.003	0.001	0.000	0.010	0.000	0.001	0.000
Cr		0.027	0.000	0.012	0.000	0.000	0.000	0.004	0.027	0.012	0.000	0.000	0.000	0.000
Fe2+ e Fe3+		0.022	0.047	0.038	0.064	0.054	0.041	0.066	0.062	0.063	0.051	0.047	0.073	0.041
Mn		0.003	0.012	0.013	0.024	0.009	0.012	0.004	0.000	0.000	0.000	0.001	0.009	0.010
Mg		0.066	0.059	0.061	0.055	0.059	0.054	0.059	0.055	0.057	0.057	0.060	0.066	0.058
Ca		3.731	3.576	3.599	3.726	3.581	3.691	3.707	3.667	3.678	3.672	3.671	3.652	3.754
Na		0.507	0.502	0.491	0.531	0.482	0.418	0.466	0.472	0.443	0.420	0.432	0.451	0.444
K		0.005	0.000	0.003	0.000	0.000	0.000	0.000	0.000	0.000	0.000	0.000	0.000	0.000
	Ab	11.943	12.299	11.986	12.481	11.856	10.163	11.166	11.396	10.740	10.271	10.524	10.986	10.577
Moles %	An	87.932	87.701	87.939	87.519	88.144	89.825	88.834	88.604	89.260	89.729	89.476	89.014	89.423
	Or	0.125	0.000	0.075	0.000	0.000	0.012	0.000	0.000	0.000	0.000	0.000	0.000	0.000

Altered Plagioclase Feldspar (Lucky Strike)

Sample Ref.	FL DR-03-01 I					FL DR-03-05 I 2				
Sample Type	Slab					Slab				
SiO2	89,578	86,894	92,290	84,050	83,930	85,126	88,979	86,571	87,459	90,342
TiO2	0,410	0,265	0,240	0,070	0,025	0,000	0,030	0,008	0,013	0,000
Al2O3	0,108	0,149	0,270	0,404	0,263	1,952	0,469	0,539	0,584	1,535
Cr2O3	0,000	0,003	0,038	0,000	0,000	0,050	0,000	0,000	0,039	0,000
FeO	0,000	0,000	0,000	0,000	0,000	0,024	0,000	0,000	0,000	0,000
MnO	0,019	0,022	0,000	0,000	0,000	0,000	0,000	0,000	0,000	0,000
MgO	0,035	0,003	0,000	0,002	0,000	0,007	0,000	0,000	0,028	0,002
CaO	0,024	0,000	0,027	0,000	0,025	0,036	0,028	0,060	0,004	0,004
Na2O	0,159	0,097	0,140	0,338	0,297	0,050	0,062	0,042	0,031	0,249
K2O	0,023	0,007	0,039	0,053	0,001	0,082	0,033	0,051	0,030	0,173
P2O5	0,032	0,000	0,011	0,000	0,011	0,039	0,055	0,000	0,000	0,000
BaO	0,003	0,000	0,000	0,000	0,000	0,015	0,000	0,000	0,000	0,040
SO3	0,000	0,030	0,035	0,000	0,012	0,005	0,040	0,025	0,000	0,000
TOTAL	90,391	87,470	93,090	84,917	84,564	87,386	89,696	87,296	88,188	92,345

Piroxenes

Sample Ref.	FL-20-02 I (1)		ALV 2608-2-2 II (1)					
Sample Type	Slab		Slab					
SiO2	53,68	53,72	52,36	52,74	51,82	51,62	51,60	51,22
TiO2	0,42	0,32	0,47	0,37	0,43	0,58	0,56	0,48
Al2O3	2,26	2,46	4,22	3,82	4,40	4,16	4,22	4,67
Cr2O3	0,14	0,16	1,22	1,04	1,40	1,36	1,69	1,78
FeO	4,95	4,89	2,62	2,58	2,64	2,79	2,68	2,69
MnO	0,12	0,00	0,06	0,07	0,19	0,06	0,04	0,00
MgO	18,70	17,89	16,82	16,90	16,68	16,78	16,44	16,66
CaO	20,72	20,91	22,41	22,77	22,56	22,52	22,64	22,89
Na2O	0,21	0,16	0,24	0,22	0,24	0,18	0,20	0,30
K2O	0,03	0,00	0,00	0,00	0,00	0,00	0,01	0,00
TOTAL	101,22	100,52	100,42	100,50	100,34	100,05	100,06	100,68
Number of ions on the basis of 6 oxygens								
Si	1,932	1,944	1,894	1,906	1,880	1,880	1,879	1,858
Al(IV)	0,068	0,056	0,106	0,094	0,120	0,120	0,121	0,142
Tot(IV)	**2**	**2**	**2**	**2**	**2**	**2**	**2**	**2**
Al(VI)	0,028	0,049	0,074	0,069	0,069	0,058	0,061	0,057
Ti	0,011	0,009	0,013	0,010	0,012	0,016	0,015	0,013
Cr	0,004	0,004	0,035	0,030	0,040	0,039	0,049	0,051
Fe3+	-	-	-	-	-	-	-	-
Fe2+ e Fe3+	0,149	0,148	0,079	0,078	0,080	0,085	0,082	0,082
Mn	0,004	0,000	0,002	0,002	0,006	0,002	0,001	0,000
Mg	1,003	0,965	0,907	0,910	0,902	0,911	0,893	0,901
Tot	**1,199**	**1,176**	**1,109**	**1,099**	**1,108**	**1,111**	**1,100**	**1,104**
Ca	0,799	0,811	0,868	0,882	0,877	0,879	0,883	0,890
Na	0,015	0,011	0,017	0,015	0,017	0,012	0,014	0,021
K	0,001	0,000	0,000	0,000	0,000	0,000	0,001	0,000

$Ca_{0,8\ -\ 0,9}(Mg, Fe)_{1,1\ -\ 1,2}(Si, Al)_2O_6$ – **Augite**

Olivine

Sample Ref.	FL DR-05 C (1)
Sample Type	Slab
SiO2	40,449
TiO2	0,000
Al2O3	0,096
Cr2O3	0,056
FeO	9,839
MnO	0,229
MgO	47,683
CaO	0,369
Na2O	0,034
K2O	0,005
TOTAL	98,76
Number of ions on the basis of 4 oxygens	
Si	1,005
Al	0,000
Ti	0,003
Cr	0,001
Fe2+ e Fe3+	0,204
Mn	0,005
Mg	1,765
Ca	0,010
Na	0,002
K	0,000
Tot	**1,990**
Atomic Percentages	
Fe	10,4
Mg	89,6

$(Mg_{1,774}Fe_{,205}Mn_{,005})SiO_4$
Forsterite ($Fo_{89,6}$)

Chromite

Sample Ref.	ALV2608-3-3B		FL-20-02 II	
Sample Type	Slab		Slab	
SiO2	0,09	0,04	0,00	0,07
TiO2	0,57	0,53	0,59	0,58
Al2O3	27,22	29,54	29,52	29,25
Cr2O3	44,70	36,76	38,02	38,08
FeO	14,84	14,39	14,29	15,08
MnO	0,21	0,15	0,17	0,13
MgO	16,06	16,48	17,00	16,68
CaO	0,04	0,01	0,00	0,04
Na2O	0,00	0,00	0,00	0,04
K2O	0,00	0,00	0,00	0,00
TOTAL	103,73	97,91	99,61	99,96
Number of ions on the basis of 32 oxygens				
Si	0,02	0,01	0,00	0,02
Al	7,40	8,35	8,21	8,14
Cr	8,15	6,97	7,09	7,11
Fe3+	-	-	-	-
Ti	0,10	0,10	0,11	0,10
Tot	**15,67**	**15,42**	**15,41**	**15,37**
Mg	5,52	5,89	5,98	5,87
Fe2+	2,86	2,89	2,82	2,98
Mn	0,04	0,03	0,03	0,03
Ca	0,01	0,00	0,00	0,01
Tot	**8,44**	**8,81**	**8,83**	**8,88**

Smectites (Saponite, smectite-chlorite?)

	DV-14-4 (1)				**SAL-01-01 (1)**											
SiO2	36.43	38.53	37.66	37.99	38.55	37.24	37.06	39.07	44.13	38.48	37.64	38.12	41.05	39.53	56.58	50.56
TiO2	0.01	0.05	0.00	0.07	0.00	0.02	0.00	0.01	0.00	0.12	0.00	0.00	0.00	0.00	0.04	0.01
Al2O3	12.38	13.81	14.65	12.64	15.39	13.24	22.79	21.69	20.06	21.90	20.28	22.98	21.08	20.46	15.17	16.15
Cr2O3	0.00	0.00	0.13	0.00	0.07	0.08	0.04	0.03	0.00	0.03	0.00	0.04	0.06	0.01	0.00	0.00
Fe2O3	-	-	-	-	-	-	-	-	-	-	-	-	-	-	-	-
FeO	3.83	3.68	3.08	2.59	2.92	4.02	3.22	3.22	2.61	3.33	4.14	4.21	3.15	3.30	2.50	2.76
MnO	0.01	0.15	0.11	0.00	0.00	0.15	0.14	0.00	0.15	0.21	0.08	0.00	0.13	0.09	0.07	0.05
MgO	29.52	29.70	26.94	27.96	26.07	28.53	22.61	20.74	18.76	22.38	21.73	21.42	20.10	21.96	13.61	16.48
CaO	0.07	0.00	0.07	0.05	0.05	0.04	0.47	0.41	0.40	0.48	0.43	0.42	0.42	0.49	0.58	0.39
Na2O	0.16	0.11	0.19	0.14	0.13	0.16	0.05	0.11	0.14	0.13	0.11	0.11	0.14	0.19	0.26	0.22
K2O	0.06	0.04	0.02	0.07	0.05	0.04	0.17	0.20	0.25	0.14	0.24	0.15	0.18	0.20	0.41	0.30
TOTAL	82.46	86.08	82.85	81.49	83.22	83.53	86.54	85.48	86.50	87.20	84.64	87.46	86.30	86.23	89.22	86.93
Oxygens	22	22	22	22	22	22	22	22	22	22	22	22	22	22	22	22
Ions in formula																
Si	5.64	5.68	5.74	5.87	5.81	5.68	5.38	5.70	6.27	5.53	5.60	5.48	5.91	5.73	7.61	7.07
Al(IV)	2.36	2.32	2.26	2.13	2.19	2.32	2.62	2.30	1.73	2.47	2.40	2.52	2.09	2.27	0.39	0.93
Tot(IV)	**8.00**	**8.00**	**8.00**	**8.00**	**8.00**	**8.00**	**8.00**	**8.00**	**8.00**	**8.00**	**8.00**	**8.00**	**8.00**	**8.00**	**8.00**	**8.00**
Al(VI)	-0.11	0.08	0.36	0.17	0.55	0.06	1.27	1.43	1.64	1.25	1.16	1.37	1.49	1.23	2.01	1.73
Ti	0.00	0.01	0.00	0.01	0.00	0.00	0.00	0.00	0.00	0.01	0.00	0.00	0.00	0.00	0.00	0.00
Cr	0.00	0.00	0.02	0.00	0.01	0.01	0.00	0.00	0.00	0.00	0.00	0.00	0.01	0.00	0.00	0.00
Fe3+	-	-	-	-	-	-	-	-	-	-	-	-	-	-	-	-
Fe2+	0.49	0.45	0.39	0.33	0.37	0.51	0.39	0.39	0.31	0.40	0.52	0.51	0.38	0.40	0.28	0.32
Mn	0.00	0.02	0.01	0.00	0.00	0.02	0.02	0.00	0.02	0.03	0.01	0.00	0.02	0.01	0.01	0.01
Mg	6.80	6.53	6.11	6.43	5.86	6.49	4.89	4.51	3.98	4.80	4.82	4.59	4.31	4.75	2.73	3.43
Tot	**7.19**	**7.09**	**6.90**	**6.94**	**6.78**	**7.09**	**6.58**	**6.34**	**5.94**	**6.49**	**6.51**	**6.48**	**6.20**	**6.39**	**5.03**	**5.49**
Ca	0.01	0.00	0.01	0.01	0.01	0.01	0.07	0.06	0.06	0.07	0.07	0.07	0.06	0.08	0.08	0.06
Na	0.05	0.03	0.06	0.04	0.04	0.05	0.02	0.03	0.04	0.04	0.03	0.03	0.04	0.05	0.07	0.06
K	0.01	0.01	0.00	0.01	0.01	0.01	0.03	0.04	0.04	0.02	0.05	0.03	0.03	0.04	0.07	0.05
Tot	**0.07**	**0.04**	**0.07**	**0.06**	**0.05**	**0.06**	**0.12**	**0.13**	**0.14**	**0.14**	**0.15**	**0.12**	**0.14**	**0.17**	**0.22**	**0.17**
Tot(other)	7.27	7.13	6.97	7.00	6.84	7.15	6.70	6.47	6.09	6.63	6.66	6.60	6.34	6.56	5.26	5.66
Total	15.27	15.13	14.97	15.00	14.84	15.15	14.70	14.47	14.09	14.63	14.66	14.60	14.34	14.56	13.26	13.66

	SAL-01-01				DV-14-4										
SiO2	37.92	42.19	57.12	37.56	41.64	39.05	39.04	39.58	38.77	36.88	35.22	36.56	38.19	37.08	33.97
TiO2	0.05	0.00	0.00	0.01	0.02	0.00	0.00	0.00	0.00	0.03	0.00	0.03	0.01	0.03	1.87
Al2O3	21.48	19.82	14.78	19.10	19.35	13.13	10.02	7.80	7.21	20.92	20.63	15.58	16.31	17.65	14.67
Cr2O3	0.00	0.00	0.00	0.02	0.00	0.00	0.00	0.03	0.01	0.00	0.00	0.03	0.04	0.00	0.10
Fe2O3	-	-	-	-	-	-	-	-	-	-	-	-	-	-	-
FeO	3.66	3.30	2.33	4.45	4.48	0.96	0.70	0.69	1.43	0.24	0.34	1.03	1.86	0.73	0.79
MnO	0.06	0.00	0.01	0.08	0.07	0.00	0.06	0.10	0.06	0.00	0.00	0.00	0.00	0.02	0.02
MgO	22.44	20.21	13.01	21.74	20.20	27.43	28.60	29.59	29.88	22.48	24.27	22.38	23.88	22.89	22.02
CaO	0.45	0.51	0.61	0.78	0.74	0.04	0.04	0.05	0.04	0.01	0.01	0.02	0.04	0.01	0.07
Na2O	0.12	0.14	0.23	0.05	0.15	0.19	0.20	0.16	0.16	0.07	0.17	0.20	0.13	0.16	0.19
K2O	0.20	0.21	0.41	0.06	0.10	0.01	0.00	0.03	0.02	0.19	0.25	0.03	0.06	0.16	0.01
TOTAL	86.39	86.38	88.49	83.84	86.74	80.81	78.65	78.02	77.58	80.83	80.89	75.87	80.51	78.73	73.69
Oxygens	22	22	22	22	22	22	22	22	22	22	22	22	22	22	22
Ions in formula															
Si	5.52	6.06	7.72	5.66	6.01	6.00	6.17	6.31	6.26	5.61	5.39	5.95	5.89	5.81	5.72
Al(IV)	2.48	1.94	0.28	2.34	1.99	2.00	1.83	1.69	1.74	2.39	2.61	2.05	2.11	2.19	2.28
Tot(IV)	**8.00**	**8.00**	**8.00**	**8.00**	**8.00**	**8.00**	**8.00**	**8.00**	**8.00**	**8.00**	**8.00**	**8.00**	**8.00**	**8.00**	**8.00**
Al(VI)	1.20	1.42	2.07	1.05	1.30	0.37	0.03	-0.22	-0.37	1.36	1.11	0.94	0.86	1.07	0.64
Ti	0.01	0.00	0.00	0.00	0.00	0.00	0.00	0.00	0.00	0.00	0.00	0.00	0.00	0.00	0.24
Cr	0.00	0.00	0.00	0.00	0.00	0.00	0.00	0.00	0.00	0.00	0.00	0.00	0.00	0.00	0.01
Fe3+	-	-	-	-	-	-	-	-	-	-	-	-	-	-	-
Fe2+	0.45	0.40	0.26	0.56	0.54	0.12	0.09	0.09	0.19	0.03	0.04	0.14	0.24	0.10	0.11
Mn	0.01	0.00	0.00	0.01	0.01	0.00	0.01	0.01	0.01	0.00	0.00	0.00	0.00	0.00	0.00
Mg	4.87	4.33	2.62	4.88	4.35	6.28	6.73	7.03	7.19	5.09	5.54	5.43	5.49	5.35	5.53
Tot	**6.53**	**6.14**	**4.95**	**6.50**	**6.20**	**6.78**	**6.86**	**6.92**	**7.02**	**6.48**	**6.69**	**6.51**	**6.59**	**6.52**	**6.53**
Ca	0.07	0.08	0.09	0.13	0.11	0.01	0.01	0.01	0.01	0.00	0.00	0.00	0.01	0.00	0.01
Na	0.03	0.04	0.06	0.02	0.04	0.06	0.06	0.05	0.05	0.02	0.05	0.06	0.04	0.05	0.06
K	0.04	0.04	0.07	0.01	0.02	0.00	0.00	0.01	0.00	0.04	0.05	0.01	0.01	0.03	0.00
Tot	**0.14**	**0.16**	**0.22**	**0.15**	**0.17**	**0.07**	**0.07**	**0.06**	**0.06**	**0.06**	**0.10**	**0.07**	**0.06**	**0.08**	**0.08**
Tot(other)	6.67	6.30	5.17	6.66	6.37	6.84	6.93	6.98	7.08	6.54	6.80	6.59	6.65	6.60	6.61
Total	14.67	14.30	13.17	14.66	14.37	14.84	14.93	14.98	15.08	14.54	14.80	14.59	14.65	14.60	14.61

REFERENCES

Alt, J C (1995). Subseafloor processes in Mid-Ocean Ridge hydrothermal systems. In: Seafloor Hydrothermal Systems: physical, Chemical, Biological, and Geological Interactions. S. Humphries, R. Zierenberg, L. Mullineaux and R. Thomson (eds.). Geophysical Monograph, 91: 85-114. American Geophysical Union, Washington, DC.

Arcyana (1975). Transform fault and rift valley from bathyscaph and diving saucer. Science, 190 (4210): 108-116.

Ballard, R D; Brian, W B; Heirtzler, J R; Keller, G; Moore, J G & Van Andel, Tj (1975). Manned submersible observations in the FAMOUS area: Mid-Atlantic Ridge. Science, 190 (4210): 103-108.

Barriga, F J A S & Fyfe, W.S. (1988). Giant pyritic base-metal deposits: the example of Feitais (Aljustrel, Portugal). Chemical Geology, 69: 331-343.

Barriga, F J A S & Fyfe, W.S. (1991). Giant pyritic base-metal deposits: the example of Feitais (Aljustrel, Portugal) – a Reply. Chemical Geology, 90: 349-352.

Barriga, F J A S; Fouquet Y; Almeida, A; Biscoito, M; Charlou, J L; Costa, R L P; Dias, A; Marques, A M S F; Miranda, J M A; Olu, K; Porteiro, F & Queiroz, M G (1998). Discovery of the Saldanha Hydrothermal Field on the FAMOUS Segment of the MAR (36º30'N). AGU Fall Meeting 1998, EOS, Transactions 79 (45): F67.

Beaulieu, S E; Joyce, K & Soule, S A (2010). InterRidge Global Database of Active Submarine Hydrothermal Vent Fields: prepared for InterRidge, Version 2.0. World Wide Web electronic publication retrieved from http://www.interridge.org/IRvents

Beaulieu, S E; Baker, E T & German, C R (2012). On the global distribution of hydrothermal vent fields: one decade later. Ocean Sciences Meeting, February 20-24, Salt Lake City, UT, USA. Abstract Book: 28 (ID 11235).

Bertine, K K & Keene, J B (1975). Submarine Barite-Opal Rocks of Hydrothermal Origin. Science, 188 (4184): 150-152.

Bischoff, J L & Rosenbauer, R J (1984). The critical point and two-phase boundary of seawater, 200–500°C. Earth and Planetary Science Letters, 68 (1): 172–180.

Bonatti, E; Guerstein-Honnorez, B M & Honnorez, J (1976a). Copper-iron sulfide mineralizations from the equatorial Mid-Atlantic Ridge. Economic Geology, 71 (1299): 1515-1525.

Bonatti, E; Guerstein-Honnorez, B M & Honnorez, J (1976b). Hydrothermal pyrite concretions from the Romanche Trench (Equat. Atl.). Metallogenesis in oceanic fracture zones. Earth and Planetary Science Letters, 32 (1100): 1-10.

Bonatti, E (1981). Metal deposits in the oceanic lithosphere. In: C Emiliani (Ed), The sea, v. 7. John Wiley & Sons, New York, p 639-686.

Campbell, A C; Palmer, M R; Klinkhammer, G P; Bowers, T S; Edmond, J M; Lawrence, J L; Casey, J F; Thompson, G; Humphris, S; Rona, P & Karson, J A (19889. Chemistry of hot springs on the Mid-Atlantic Ridge. Nature, 335, 514-519.

Cannat, M; Briais, A; Deplus, C; Escartín, J; Georgen, J; Lin, J; Mercouriev, S; Meyzen, C; Muller, M; Pouliquen, G; Rabain, A & da Silva, P (1999). Mid-Atlantic Ridge - Azores hotspot interactions: along axis migration of a hotspot-derived event of enhanced magmatism 10 to 4 Ma ago. Earth and Planetary Science Letters, 173: 257-269.

Charlou, J L; Bougault, H; Donval, J P; Pellé, H; Langmuir, C & F S Team (1993). Seawater CH4 concentration over the Mid-Atlantic Ridge from the Hayes F.Z. to the Azores triple junction. EOS, American Geophysical Union Transactions, 74: 380.

Charlou J L; Donval J P; Douville, E; Jean-Baptiste, P; Radford-Knoery, J; Fouquet, Y; Dapoigny, A & Stievenard, M (2000). Compared geochemical signatures and the evolution of Menez Gwen (37º50'N) and Lucky Strike (37º17'N) hydrothermal fluids, south of the Azores Triple Junction on the Mid-Atlantic Ridge. Chemical Geology, 171: 49–75.

Colodner, D; Lin, J; Von Damm, K; Buttermore, L; Kozlowski, R; Charlou, J L; Donval,J P; Wilson, C; & The Lucky Strike Team (1993). Chemistry of Lucky Strike hydrothermal fluids: initial results. EOS, American Geophysical Union Transactions, 74: 99.

Cooper, M J; Elderfield, H & Schultz, A (2000). Diffuse hydrothermal fluids from Lucky Strike hydrothermal vent field: Evidence for a shallow conductively heated system. Journal of Geophysical Research, 105: 19369-19375.

Corliss, J B; Lyle, M; Dymond, J & Crane, K (1979). Submarine thermal springs on the Galapagos rift. Science, 203: 1073-1083.

Costa, I A (1995). Estudo dos processos de alteração associados aos sistemas hidrotermais Lucky Strike e Menez Gwen (Crista médio-Atlântica, Mar dos Açores). MSc. Thesis. Universidade de Lisboa, pp131.

Costa, I; Barriga, F J A S & Fouquet, Y (1997). “Slabs” from Lucky Strike and Menez Gwen (Mid-Atlantic Ridge): mineralogy and preliminary geochemistry. SEG Neves Corvo Field Conference, May 11-14, Lisbon, Portugal. Abstracts and Program: 26.

Costa, I M R (2005). Serpentinization on the Mid-Atlantic Ridge: the Rainbow, Saldanha and Menez Hom sites. PhD. Thesis. Universidade de Lisboa, pp444.

Crerar, D A; Namson, J; So Chyi, M; Williams, L & Feigenson, M (1982). Manganiferous cherts of the Franciscan assemblage: I. General geology, ancient and modern analogues, and implications for hydrothermal convection at oceanic spreading centers. Economic Geology, 77: 519-540.

Desbruyeres, D et équipe scientifique PICO (1998). Compte rendu de la Campagne PICO (25 Juin – 11 Juillet 1998).

Dias, A S & Barriga, F J A S (2006). Mineralogy and geochemistry of hydrothermal sediments from the serpentinite-hosted Saldanha hydrothermal field (36°34′N; 33°26′W) at Mid-Atlantic Ridge. Marine Geology, 225: 157-175.

Donnelly, K; Goldstein, S; Langmuir, C & Spiegelman, M. (2004). Origin of enriched ocean ridge basalts and implications for mantle dynamics. Earth Planet. Sci. Lett., 226, 347-366.

Dosso, L; Bougault, H; Langmuir, C; Bollinger, C; Bonnier, O & Etoubleau, J (1999). The age and distribution of mantle heterogeneity along the Mid-Atlantic Ridge (31-41ºN). Earth and Planetary Science Letters, 170: 269-286.

Doyle, M G, & Allen, R L (2003). Subsea-floor replacement in volcanic-hosted massive sulfide deposits. Ore Geology Reviews, 23: 183–22.

Équipe scientifique DIVA 1 (Y Fouquet; J L Charlou; J P Donval; J Radford-Knoery; H Pellé; H Ondréas; M Segonzac; I Costa; N Lourenço; M Tivey) (1994). Rapport de campagne DIVA 1 (5 Mai - 29 Mai 1994). (Unpublished)

Équipe scientifique DIVA 2 (A M Alayse; E Antoine; G Barbier; F Barriga; M Biscoito; P Briand; J P Brulport; T Comtet; L Cornec; P Crassous; P Dando; D Desbruyeres; M C Fabri; H Felbeck; F Lallier; A Fiala; J Gonçalves; F Menard; J Kerdoncuff; J Patching; L Saldanha; P M Sarradin; D Semac) (1994). Rapport de campagne DIVA (31 Mai - 4 Jul 1994). (Unpublished)

Équipe scientifique FLORES (Y Fouquet; J L Charlou; J P Donval; J Radford-Knoery; H Ondréas; E Douville; R Apprioual; P Cambon; H Pellé; J Y Landure; A Normand; E Ponsevera; C German; L Parson; F Barriga; I Costa; J Relvas; A Ribeiro; H Santana; H Elderfield; A Schultz; M Stephan & S Riches) (1997). Rapport de campagne FLORES (7 Juillet - 9 Août 1997). (Unpublished)

Eissen, J-P; Fouquet, Y; Hardy, D & Ondréas, H (2013). Recent MORB Volcaniclastic Explosive Deposits Formed Between 500 and 1750 m.b.s.l. on the Axis of the Mid-Atlantic Ridge, South of the Azores, in Explosive Subaqueous Volcanism (eds J. D.L. White, J. L. Smellie and D. A. Clague). American Geophysical Union, Washington, D. C.. doi: 10.1029/140GM09, 143-166.

Evans, A M (1987). An introduction to ore geology. Second Edition, Blackwell Scientific Publications, pp 358.

FAZAR Scientific team (C Langmuir; G Klinkhamer; H Bougault; B Bourdon; J L Charlou; C Chin; B Conrad; D Desonie; J P Donval; E Ferguson; K Hirose; G Mandal; R Margolin; J Monteith; C Moser; Y L Niu; H Pellé; T Plank; J Reynolds; D Stuart; M Tatcher; C Wilson; S Corey; S Gleason; J Miller; K Brooksforce; C German; P Kalk; R Keller) (1992). Evaluation of the relationships among segmentation, hydrothermal activity and petrological diversity on the Mid-Atlantic Ridge (cruise report - 29 Aug-20 Oct). (Unpublished)

Fouquet, Y; Charlou, J L; Donval, J P; Radford-Knoery, J; Pellé, H; Ondréas, H; Segonzac, M; Costa, I; Lourenço, N; Tivey, M (1994a). Geological setting and comparison of

the Menez Gwen and Lucky Strike vent fields at 37*17'N and 37º50'N on the Mid-Atlantic Ridge. Preliminary results of the DIVA 1 diving cruise with Nautile. EOS, American Geophysical Union Transactions, 75: 313.

Fouquet, Y; Charlou, J L; Costa, I; Donval, J P; Radford-Knoery, J; Pellé, H; Ondréas, H; Lourenço, N; Segonzac, M & Tivey, M (1994b). A detailed study of the Lucky Strike hydrothermal site and discovery of a new hydrothermal site: Menez Gwen; preliminary results of the DIVA1 cruise (5-29 May, 1994). InterRidge News, 3(2): 14-17.

Fouquet, Y; Ondréas, H; Charlou, J L; Donval, J P; Radford-Knoery, J; Costa, I; Lourenço, N; Tivey, M (1995a). Atlantic lava lakes and hot vents. Nature, 377 (6546): 201.

Fouquet, Y; Charlou, J L; Donval, J P; Radford-Knoery, J; Pellé, H; Ondréas, H; Segonzac, M; Costa, I; Lourenço, N & Tivey, M (1995b). DIVA 1 cruise. Geological control and composition of hydrothermal deposits near the Azores Triple Junction - TERRA abstracts. Abstract supplement no. 1 to TERRA nova, v. 7, p. 211.

Fouquet, Y (1997). Where are the large hydrothermal sulphide deposits in the oceans? Phil. Trans. R. Soc. Lond. A, 355: 427-441.

Fouquet, Y; Eissen, J P; Ondréas, H; Barriga, F; Batiza, R & Danyushevsky, L (1998a). Extensive volcaniclastic deposits at the Mid-Atlantic Ridge axis: results of the deep-water basaltic explosive volcanic activity? TERRA nova, v. 10 (5): 280-286.

Fouquet, Y; Henry, K; Knott, R & Cambon P (1998b). Geochemical section of the TAG hydrothermal mound. In: Herzig PM, Humphris SE, Miller DJ, Zierenberg RA (eds) Proc Ocean Drilling Program, Scientific Results 158, College Station, Texas, pp 363-385.

Fournier, R O (1985). The behaviour of silica in hydrothermal solutions. In Berger, B R & Bethke, P M, Eds., Geology and geochemistry of epithermal systems. Society of Economic Geologists, Reviews in Economic Geology, 2: 45-61.

Francheteau, J; Juteau, T & Ragin, C (1979). Basaltic pillars in collapsed lava-pools on the deep ocean floor. Nature, 281 (5728): 209-211.

German, C R & Von Damm, K L (2003). Hydrothermal processes. In: Treatise On Geochemistry, Volume 6: The Oceans and MarineGeochemistry. H. D. Holland and K. K. Turekian (eds.). Pergamon, Oxford: 181–222.

Glasby, G; Iizasa, K; Hannington, M; Kubota, H & Notsu, K (2008). Mineralogy and composition of Kuroko deposits from northeastern Honshu and their possible modern analogues from the Izu-Ogasawara (Bonin) Arc south of Japan: Implications for mode of formation. Ore Geology Reviews 34: 547–560.

Grant, J A, 1986. The isocon diagram – a simple solution to Gresens equation for metasomatic alteration. Economic Geology, 81: 1976-1982.

Hajash, A & Archer, P (1980). Experimental seawater/basalt interactions: Effects of cooling. Contributions to Mineralogy and Petrology, 75: 1-13.

Hashimoto, K, (1977). The Kuroko deposits of Japan – geology and exploration strategies. XII Convencion National Asociation de Ingenieros de Minas e Metalurgistas Y Geologos de Mexico, October 16-20, Acapulco, Mexico.

Hannington, M D; Jonasson, I R; Herzig, P M & Petersen, S (1995). Physical and Chemical Processes of Seafloor Mineralization at Mid-Ocean Ridges. In: Seafloor Hydrothermal Systems: physical, Chemical, Biological, and Geological Interactions. S. Humphries, R. Zierenberg, L. Mullineaux and R. Thomson (eds.). Geophysical Monograph, 91: 115-157. American Geophysical Union, Washington, DC.

Haymon, R M (1983). Growth history of hydrothermal black smoker chimneys. Nature, 301 (5902): 695-698.

Hekinian, R; Moore, J G & Bryan, W B (1976). Volcanic rocks and processes of the Mid-Atlantic Ridge rift valley near 36º49'N. Contributions to Mineralogy and Petrology, 58: 83-110.

Herrington, R; Maslennikov, V; Zaykov, V; Seravkin, I; Kosarev, A; Buschmann, B; Orgeval, J J; Holland, N; Tesalina, S; Nimis, P & Armstrong, R (2005). 6: Classification of VMS deposits: Lessons from the South Uralides. Ore Geology Reviews, 27: 203–237.

Hoffert, M; Person, A; Courtois, C; Karpoff, A M & Trauth, D (1980). Sedimentology, mineralogy, and geochemistry of hydrothermal deposits from holes 424, 424A, 424B, and 424C (Galapagos Spreading Centre), in Deep Sea Drilling Project, Initial Reports, pp. 339-376.

Humphris, S; Tivey, M; Fouquet, Y & The Lucky Strike Team (1993). Comparison of hydrothermal deposits at the Lucky Strike vent field with other mid-ocean ridge vent sites. EOS, American Geophysical Union Transactions, 74: 100.

Humphris, S; Fornari, D; Scheirer, D; German, C & Parson, L (2002). Geotectonic setting of hydrothermal activity on the summit of Lucky Strike Seamount (37º17'N, Mid-Atlantic Ridge). G3- Geochemistry, Geophysics, Geosystems – an electronic journal of the earth sciences, 3 (8): 1-24.

Hutchinson, R W (1973). Volcanogenic sulfide deposits and their metallogenic significance. Economic Geology, 68 (8): 1223-1246.

Kamenetsky, V S; Crawford, A J & Meffre, S (2001). Factors Controlling Chemistry of Magmatic Spinel: an Empirical Study of Associated Olivine, Cr-spinel and Melt Inclusions from Primitive Rocks. Journal of Petrology, 42 (4): 655-671.

Keen, J B (1983). Chalcedonic quartz and occurrence of quartzine (length-slow chalcedony) in pelagic sediments. Sedimentology, 30: 449-454.

Khripounoff, A; Comtet, T; Vangriesheim, A & Crassous, P (2000). Near-bottom biological and mineral particle flux in the Lucky Strike hydrothermal vent area (Mid-Atlantic Ridge). Journal of Marine Systems, 25: 101-118.

Langmuir, C H; Charlou, J L; Colodner, D; Corey, S; Costa, I; Desbruyeres, D; Desonie, D; Emerson, T; Fornari, D; Fouquet, Y; Humphris, S; Fiala-Medioni, A; Saldanha, L; Sours-Page, R; Tatcher, M; Tivey, M; Van Dover, C; Von Damm, K; Wiese, K & Wilson, C (Lucky Strike Team) (1993a). Lucky Strike: a newly discovered hydrothermal site on the Azores platform, Ridge Events, 4: 3-5.

Langmuir, C H; Fornari, D; Colodner, D; Charlou, J L; Corey, S; Costa, I; Desbruyeres, D; Desonie, D; Emerson, T; Medioni, A F; Fouquet, Y; Humphris, S; Saldanha, L; Sours-Page, R; Tatcher, M; Tivey, M; Van Dover, C; Von Damm, K; Wiese, K & Wilson, C (Lucky Strike Team) (1993b). Geological setting and characteristics of the Lucky Strike vent field at 37º17'N on the Mid-Atlantic Ridge. EOS, American Geophysical Union Transactions, 74: 99.

Langmuir, C H; Humphris, S; Fornari, D; Van Dover, C; Von Damm, K; Tivey, M; Colodner, D; Charlou, J L; Desonie, D; Wilson, C; Fouquet, Y; Klinkhammer, G & Bougault,

H (1997). Hydrothermal vents near a mantle hot spot: the Lucky Strike vent field at 37ºN on the Mid-Atlantic Ridge. Earth and Planetary Science Letters, 148: 69-91.

Lydon, J W (1988). Volcanogenic massive sulphide deposits. Part 2: Genetic models. Geoscience Canada, 15 (1), in Ore deposit models. Eds: R G Roberts e P A Sheahan. Reprint Series 3. pp 194.

Luís, J F; Miranda, J M; Galdeano, A; Patriat, P; Rossignol, J C & Mendes Victor, L A (1994). The Azores triple junction evolution since 10 Ma from an aeromagnetic survey of the Mid-Atlantic Ridge. Earth and Planetary Science Letters, 125: 439-459.

Marques, A F A; Scott, S D; Gorton, M P; Barriga, F J A S & Fouquet, Y (2009). Pre-eruption history of enriched MORB from the Menez Gwen (37°50′N) and Lucky Strike (37°17′N) hydrothermal systems, Mid-Atlantic Ridge. Lithos, 112(1):18-39.

Mcphie, J; Doyle, M and Allen, R L (1993). Volcanic textures: a guide to the interpretation of textures in volcanic rocks. Hobart, University of Tasmania, Center for Ore Deposit and exploration Studies, pp189.

Moore, J G (1970). Water content of basalt erupted on the ocean floor. Contributions to Mineralogy and Petrology, 28: 272-279.

Oheler, J H (1976). Hydrothermal crystallization of silica gel. Geological Society of America Bulletin, 87: 1143-1152.

Ohmoto, H (1996). Formation of volcanogenic massive sulfide deposits: The Kuroko Perspective. Ore Geology Reviews 10: 135-177.

Ondréas, H; Fouquet, Y; Voisset, M & Radford-Knoery, J (1997). Detailed study of three contiguous segments of the Mid-Atlantic Ridge, south of the Azores (37ºN to 38º30'N), using acoustic imaging coupled with submersible observations. Marine Geophysical Researches, 19: 231-255.

Parson, L; Gràcia, E; Coller, D; German, C & Needham, D (2000). Second-order segmentation: the relationship between volcanism and tectonism at the MAR, 38ºN-35º40'N. Earth and Planetary Science Letters, 178: 231-251.

Prokin, V A & Buslaev, F P (1999). Massive copper–zinc sulphide deposits in the Urals. Ore Geology Reviews 14: 1–69.

Relvas, J M R S (2000). Geology and metallogenesis at the Neves Corvo Deposit, Portugal. PhD. Thesis. Universidade de Lisboa, pp319.

Rona, P A; Harbinson, R N; Bassinger, B G; Scott, R B & Nalwalk, A J (1976). Tectonic fabric and hydrothermal activity of Mid-Atlantic Ridge crest (lat 26ºN). Geological Society of America Bulletin, 87 (1439): 661-674.

Rona, P A; Klinkhammer, G; Nelson, TA; Trefry, J H & Elderfield, H., (1986). Black smokers, massive sulfides and vent biota on the Mid-Atlantic Ridge. Nature, 321: 33-37.

Scott, R B; Rona, P A; McGregor, B A & Scott, M R (1974). The TAG hydrothermal field. Nature, 251: 301-302.

Searle, R C (1976). Lithospheric Structure of the Azores Plateau from Rayleigh-wave dispersion. Geophysics Journal of Research Astronomy Society, 44: 537-546.

Spiess, F N & RISE Project Group (1980). East Pacific Rise: hot springs and geophysical experiments. Science, 207: 1421-1433.

Stein, C A; Stein, S & Pelayo, A M (1995). Heat flow and hydrothermal circulation. In: Seafloor Hydrothermal Systems: physical, Chemical, Biological, and Geological Interactions. S. Humphries, R. Zierenberg, L. Mullineaux and R. Thomson (eds.). Geophysical Mongraph, 91: 425-445. American Geophysical Union, Washington, DC.

Sun, S & McDonough, W F (1989). Chemical and isotopic systematics of oceanic basalts: implications for mantle composition and processes. In: Saunders, A D & Norry, M J (Eds.), Magmatism in the Ocean Basins: Geological Society Special Publication, 42, pp 313-345.

Thompson, G; Humphris, S E; Schroeder, B; Sulanowska, M & Rona, P A (1988). Active vents and massive sulfides at 26ºN (TAG) and 23ºN (Snake Pit) on the Mid-Atlantic Ridge. Canadian Mineralogist, 26: 697-711.

Tivey, M K (2007). Generation of seafloor hydrothermal vent fluids and associated mineral deposits. In: Oceanography, 20: 50-65. The Oceanography Society, USA.

Toth, J R (1980). Deposition of submarine crusts rich in manganese and iron. Geological Society of America Bulletin, 91: 44-54.

Von Damm K L (1995). Controls on the chemistry and temporal variability of seafloor hydrothermal fluids. In: Seafloor Hydrothermal Systems: physical, Chemical, Biological, and Geological Interactions. S. Humphries, R. Zierenberg, L. Mullineaux and R. Thomson (eds.). Geophysical Monograph, 91: 222-247. American Geophysical Union, Washington, DC.

Von Damm, K L; Bray, A M; Buttermore, L G & Ooosting, S E (1998). The geochemical controls on vent fluids from the Lucky Strike vent field, Mid-Atlantic Ridge. Earth and Planetary Science Letters, 160: 521-536.

Zamarreño, I; Plana, F; Vazquez, A & Clague, D A (1989). Motukoreaite: a common alteration product in submarine basalts. American Mineralogist, 74: 1054-1058.

Zierenberg, R A; Schiffman, P; Jonasson, I R; Tosdal, R; Pickthorn, W & McClain, J (1995). Alteration of basalt hyaloclastite at the off-axis Sea Cliff hydrothermal field, Gorda Ridge. Chemical Geology, 126: 77-99.

"What goes up must come down."

Isaac Newton – English physicist and mathematician who is widely regarded as one of the most influential scientists of all time.